Stony Brook University

Sequence to Topography Relationship in Membrane-Inserted Hydrophobic Helices

A Dissertation Presented

by

Shyam S. Krishnakumar

to

The Graduate School

In Partial Fulfillment of the Requirements

For the Degree of

Doctor of Philosophy

in

Biochemistry and Structural Biology

Stony Brook University

December 2007

Stony Brook University

The Graduate School

Shyam S. Krishnakumar

We, the dissertation committee for the above candidate for the
Doctor of Philosophy degree,
hereby recommend acceptance of this dissertation

Dr**.** Erwin London, Ph.D. Professor
Department of Biochemistry and Cell Biology
Dissertation Advisor

Dr**.** Robert Haltiwanger, Ph.D. Professor
Department of Biochemistry and Cell Biology
Chairperson of Dissertation Committee

Dr. Steven O. Smith, Ph.D. Professor,
Department of Biochemistry and Cell Biology

Dr. James B. Konopka, Ph.D. Professor,
Department of Molecular Genetics and Microbiology

This dissertation is accepted by the Graduate School

Lawrence Martin
Dean of the Graduate School

Abstract of the Dissertation

Sequence to Topography Relationship in Membrane-Inserted Hydrophobic Helices

by

Shyam S. Krishnakumar

Doctor of Philosophy

in

Biochemistry and Structural Biology

Stony Brook University

2007

Hydrophobic α-helices have been widely used to study membrane protein sequence-structure relationships in model membranes. Our lab has developed fluorescence methods to determine the topography of membrane-inserted hydrophobic helices, and to understand the equilibria describing their topographic stability. Using this model membrane system, the minimum hydrophobic length necessary to form a transmembrane (TM) helix in membranes was investigated. Sequences with 13 consecutive hydrophobic residues were found to be the minimum necessary to form a predominantly TM state in a bilayer with a biologically relevant width. The ability of these short hydrophobic sequences to form TM helices in the presence of substantial negative mismatch (~10 Å) implied that lipid bilayers have a considerable ability to adjust to hydrophobic mismatch. In addition, the ability of hydrophilic residues to shift the transverse position of the TM helices within the bilayer was studied. Hydrophilic residues at some positions within

hydrophobic helices induced transverse shifts in TM helix position such that the polar residue moved closer to the bilayer surface. The extent of shift depended on the identity of the hydrophilic residue. The shift was controlled by the combination of amino acid hydrophilicity, ionization state and the ability of the side chains to position the polar groups near the bilayer surface (snorkeling). Furthermore, the structural consequence of pathogenic hydrophilic mutations in the TM domain of neu/ErbB2 receptor was investigated. Hydrophilic mutations in the TM domain were found to alter the membrane position of the TM helix and thus redefine the transmembrane boundary. This suggested a new mode of receptor upregulation in the neu/ErbB2 oncogene. Finally, in collaboration with Dr. Eckard Wimmer, Department of Molecular Genetic and Microbiology, the membrane topography of poliovirus proteins 3A and 3AB was characterized. Fluorescence studies showed that the hydrophobic domain forms a stable TM structure in mature 3A protein, but adopts a non-TM surface topography in context of the precursor 3AB protein. The hydrophobic sequence could insert in a TM form, only when the C-termini 3B domain was removed. Furthermore, a shortened C-terminal part of the putative hydrophobic segment (16 residues rather than 22 residues) was found to span the lipid bilayer.

To Mom and Dad

Table of Contents

List of Abbreviations

TM Helix	Transmembrane Helix
SDS-PAGE	Sodium Dodecyl Sulfate Polyacrylamide Gel Electrophoresis
FRET	Fluorescence Resonance Energy Transfer
pL	poly Leucine Peptide
pLA	poly Leucine-Alanine Peptide
HPLC	High Performance Liquid Chromatography
MALDI-TOF	Matrix Assisted Laser Desorption Ionization Time of Flight
CD	Circular Dichroism
DOPC	Dioleoylphosphatidylcholine
DEuPC	Dierucoylphosphatidylcholine
DEiPC	Dieicoseonylphosphatidylcholine
SUV	Small Unilamellar Vesicles
λmax	Fluorescence Emission Maxima
$L_{TM\ eff}$	Effective Transmembrane Length
10-DN	10-Doxyl Nonadecane
Q-ratio	Quenching ratio
WT	Wild type
DMSO	Dimethylsulfoxide
PV	Poliovirus

List of Figures

List of Tables

Acknowledgement

First of all, I wish to thank my advisor, Dr. Erwin London, for giving me the opportunity to work on this exciting project. He was a tireless and a very accommodating mentor, who was enormously helpful in guiding me through this project. I am deeply grateful to him for always being there to listen and sort out the myriad problems that arose during this project.

I would also like to thank everyone in London lab, past and present, for their support and for creating a wonderful environment in the lab. Few individuals must be singled out for particular thanks - Greg Caputo, who showed me the ropes when I started out in the lab and has been a great collaborator ever since and Khurshida Shahidullah, who helped me out with numerous aspects of this project.

I would also like to thank my thesis committee, Dr. Robert Haltiwanger, Dr. Steve Smith, Dr. William Lennarz and Dr. James Konopka for their inputs and critical comments on the project, and for being very accommodative with my requests.

I had a wonderful time working with our collaborators, Dr. Kentaro Fujita, Dr. Aniko Paul and Dr. Eckard Wimmer and would like to thank them for walking this novice through the complex field of Poliovirus replication.

I wish to thank Suresh and Sheela for opening up their home to me and creating a sanctuary for timely retreats from the monotony of the graduate student life. Also, I like to thank all my friends, in Stony brook and around the globe, for being there whenever I needed them.

None of this would have been possible without the sacrifices and constant support from my parents. So, for this and much more, this work is dedicated to them.

CHAPTER 1

INTRODUCTION

Integral Membrane Proteins

It has been estimated that nearly 30% of a genome encodes for integral membrane proteins (1). The majority of the TM proteins have α-helical segments, typically of 15-25 amino acid residues in length, spanning the membrane bilayer. Structurally, α-helical membrane proteins can be either monotopic (single α-helix spanning the membrane bilayer) or polytopic (multiple α-helices spanning the membrane bilayer).

Integral membrane proteins, which perform a variety of important biological functions, fall into two major classes. Many transmembrane proteins associated with the cell plasma membrane function as receptors. This class of membrane proteins acts as sensors of external signals, transferring information across the membrane and allowing the cell to change its behavior in response to environmental cues. This is typically achieved through conformational (allosteric) change in the receptor with response to ligand binding. There is a large variety in receptor proteins, each responding to particular ligand or a family of ligands. Another class of membrane proteins functions as transporters. The membrane bilayer forms a barrier around the cell that is impermeable to essential molecules and ions and these membrane proteins drive the transmembrane movement of select solute either in an energy independent manner (channels), or in an energy dependent manner (pumps). The transmembrane channels form channels through which the molecule can pass down its concentration gradient (i.e. facilitated diffusion), while transmembrane pumps force ions or small molecules through the membrane against their concentration gradient.

Techniques for Examining TM Helix Structure and Function

Techniques like X-ray crystallography and NMR spectroscopy, which are widely used to obtain high resolution structures of soluble proteins, are not easily applied to membrane proteins (2-4). A number of issues, including solubility of membrane proteins, expression in large quantities, and reconstitution into membrane or membrane-like environments complicate structure determination. Recent advancements in experimental design and techniques have allowed for a growing number of high resolution structures to be obtained for membrane proteins (5-8). Nevertheless, a number of other techniques have been developed to examine the structure and behavior of TM α-helices.

An elegant assay to monitor the structure and behavior of TM α-helices is the glycosylation mapping technique developed by von Heijne and colleagues (9). This method relies on the fact that the oligosaccharyl transferase complex on the luminal side of the ER can only glycosylate residues, in a consensus sequence, if it is 12 residues away (minimum glycosylation distance) from the membrane surface. By varying the number of residues between the glycosylation site and putative TM segment (α-helix) and measuring the glycosylation level, the membrane boundary of the TM helix could be identified (Figure 1). This approach is powerful and gives biologically relevant results, but there are a number of caveats, including the lack of control over pH and lipid composition and that the TM helix boundary could be influenced by interactions within the translocon. Recently, a different glycosylation assay was developed to quantify the efficiency of membrane integration of hydrophobic TM segments into rough microsome membranes (10). In this assay, the hydrophobic sequence is engineered to be flanked by two acceptor sites for N-linked glycosylation and the degree of membrane integration is quantified by the fraction of singly glycosylated versus doubly glycosylated acceptor sites (Figure 2). A limitation of this technique is that the decision to form a TM helix might reflect the kinetic events in the translocon, rather than a true thermodynamic equilibrium.

Another important aspect of transmembrane protein structure is the oligomerization state of the TM helices. The non-covalent association of transmembrane α-helices is a fundamental event in the folding of helical membrane proteins. The TOXCAT assay is a cell based system developed to study helix-helix interactions in natural membrane environments (11). This assay uses a chimeric construct composed of the N-terminal DNA binding domain of ToxR (a dimerization-dependent transcriptional activator) fused to a transmembrane domain of interest and a monomeric periplasmic anchor (the maltose binding protein). Association of the TM helix results in the ToxR-mediated activation of a reporter gene encoding chloramphenicol (CAT). The level of CAT expression indicates the strength of TM association (11). Another useful assay to investigate the oligomeric state of TM helices is analytical ultracentrifugation. The basis for this method is that protein or protein complexes sediment differently depending on the molecular weight of the protein or the complex. As a result, TM helices will sediment

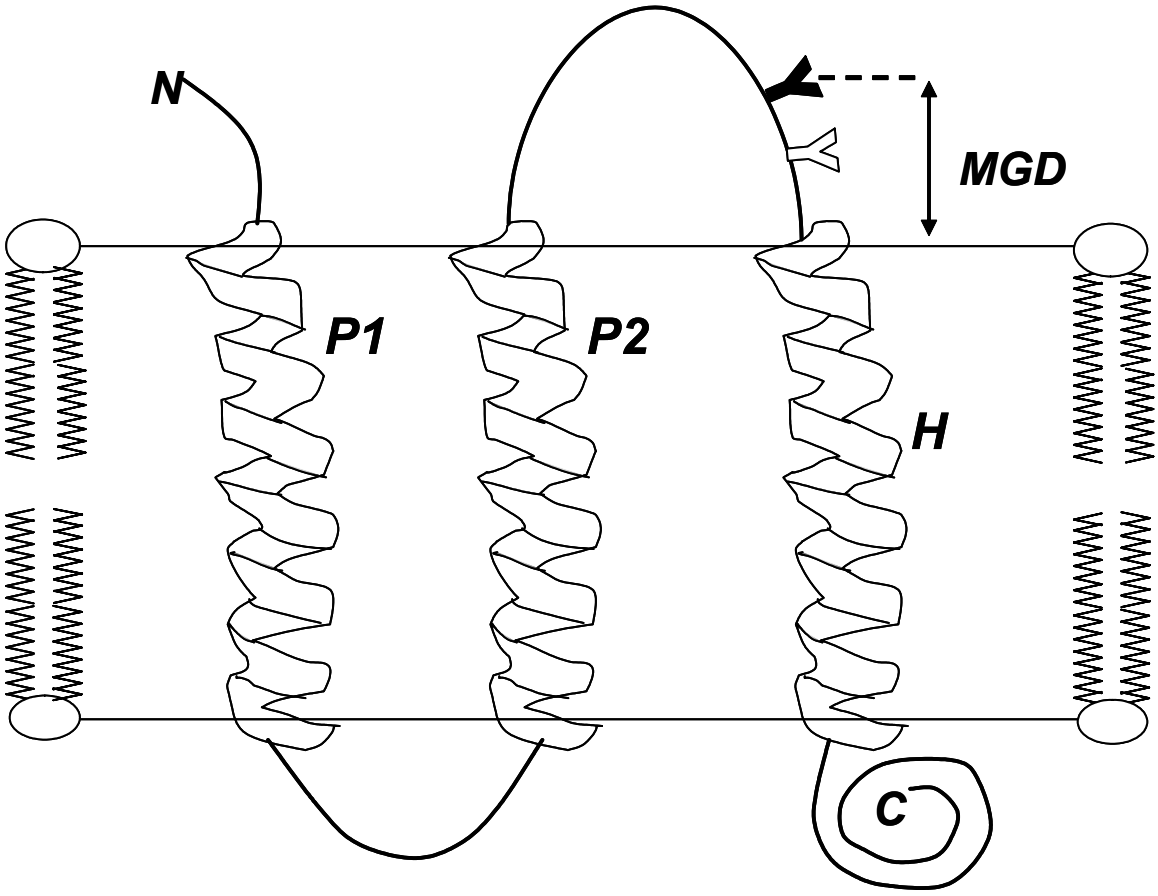

Figure 1. Glycosylation mapping method developed by von Heijne and colleagues (9). The glycosylation mapping mutants are derived from leader peptidase (Lep), with the TM segment of interest (H) inserted into the construct. The modification of luminal glycosylation acceptor site (engineered at different distances with respect to the H-segment) by the oligosaccharyl transference complex depends on the distance of the acceptor site from the membrane. Sites very close to the membrane are not glycosylated (open Y), while sites that extend sufficiently far from the membrane are efficiently glycosylated (bold Y). The minimum glycosylation distance (MGD) is the distance between the end of the H-segment and the first site that is glycosylated 50 % or higher. Adapted from Nilsson et al. 1998 (9).

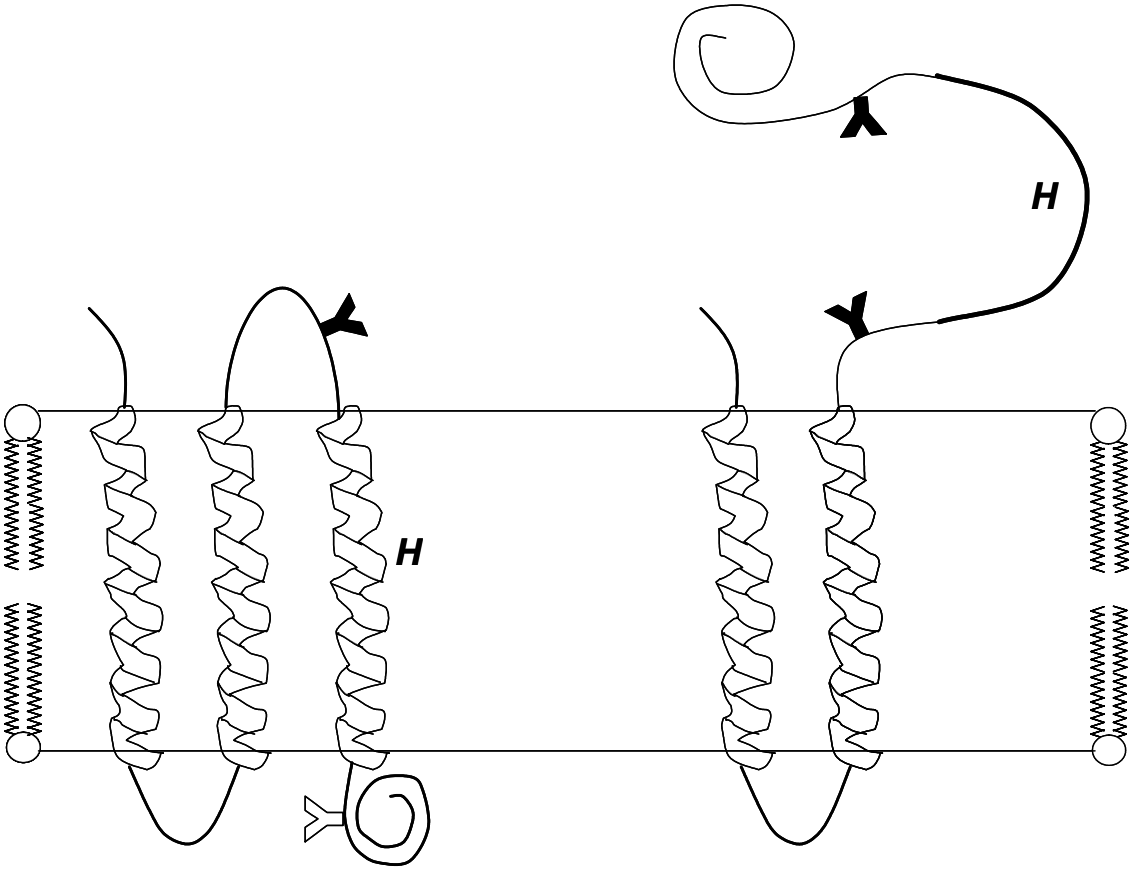

Figure 2. Glycosylation assay for determining fractional integration of putative hydrophobic segments. Integration of the hydrophobic segment (H) leaves one glycosylation site in the cytoplasm and thus un-glycosylated (open Y). But translocation of the sequence allows both sites to be glycosylated (bold Y). Unmodified, singly and doubly modified sites can be resolved using SDS-PAGE and quantified. Adapted from Hessa et al. (2005) (10).

differently depending on their oligomeric state. By fitting the sedimentation profile to mathematical equations, the number of helices in an oligomer can be determined (12). A downside for this method is that the sedimentation analysis is done in detergent micelles and not in lipid bilayers. Also, SDS-PAGE (Sodium Dodecyl Sulfate Polyacrylamide Gel Electrophoresis) analysis has been widely used to assess the degree of association in TM helices (13, 14). TM helices migrate on SDS-polyacrylamide gels with an apparent molecular weight approximately equal to the oligomeric state. Different mobilities of the oligomeric state can be used to identify the number of helices in the oligomeric state. This is a simple and effective technique, but it works only in case of strong oligomers as weak oligomer structures tend to break up under the denaturing conditions.

Another widely used technique, which has been useful in examining various aspects of TM helix behavior, is fluorescence spectroscopy. There are a variety of *in vitro* and *in vivo* fluorescence-based assays that use intrinsic or covalently-linked fluorescent probes to examine helix behavior. Polarity-sensitive fluorescent probes are routinely used to determine location and orientation of TM helices within the membrane bilayer (15-17). Fluorescent properties of these probes (fluorescence intensity and/or wavelength maxima) change in response to the polarity of local environment and this is used to assess helix behavior. Oligomerization of TM helices has been widely studied by FRET (Fluorescence Resonance Energy Transfer), which is the distance dependent transfer of electronic excitation energy between two fluorophores (18, 19). To monitor oligomerization between TM helices, one helix is labeled with a donor fluorophore and the other with an acceptor fluorophore. In absence of helix-helix interaction, donor fluorescence is high. But when the donor and acceptor are in proximity due to helix-helix interaction, then the energy transfer is significant and the donor fluorescence intensity decreases with a concomitant rise in acceptor fluorescence. This is a very sensitive technique, with excellent resolution (18, 19). Fluorescence quenching is another fluorescence phenomenon used to examine TM helix association and other aspects of helix behavior (20-22). Quenching is a loss of fluorescence intensity of fluorophore in a close proximity of the quencher molecule due to decrease in the quantum yield of the fluorophore. Quenching based assays have been used to determine membrane topography of TM proteins, orientation of TM helices and TM helix-helix association (16, 23-25).

Amino Acid Composition of Transmembrane α-Helices

Primary sequence is one of the major factors in determining the topography of the TM helix, its position within the membrane bilayer and its interaction with other membrane-inserted helices. TM helices are primarily composed of hydrophobic residues (Leu, Ile, Val) as they tend to stabilize the TM structure because of the favorable energetics arising from loss of exposure of hydrophobic side chains to water. Conversely, polar and ionizable (charged) residues are less abundant in TM segments because of the energetic cost involved in burying a hydrophilic residue in the nonpolar environment of the bilayer (26-28).

However, there are many instances of hydrophilic residues within the TM domain of membrane proteins. The ability of polar and ionizable residues to deeply bury in a lipid bilayer was shown by work done in our lab (29, 30). Studies with model hydrophobic peptides (polyLeu peptides), showed that a single polar (Ser, Pro, His) or ionizable (Lys, Asp) residue in the middle of hydrophobic sequence could be tolerated and the entire sequence can adopt a stable TM structure (29, 30). This shows the ability of ionizable residues to adopt an uncharged state to minimize the cost of burial in the membrane bilayer. Consequently, a putative TM segment containing an internal polar or ionizable residue should still be able to adopt a stable TM structure if the other residues are sufficiently hydrophobic.

Another way by which membrane proteins tend to overcome the energetic barrier of burial of polar residues in a membrane is oligomerization. Hydrophilic residues reduce the energetic cost of their insertion into membranes by forming hydrogen bonds (31, 32), which drives helix association. Work from the DeGrado and Engelman labs have shown that a single hydrophilic residue in a hydrophobic TM sequences can drive self-association of these TM sequence (31-37). FRET measurements of designed host peptides, SDS-PAGE analysis and TOXCAT assays of chimeric proteins have shown that ionizable and strongly polar residues like Asp, Glu, Asn and Gln tend to promote oligomerization (32, 33, 36, 37). Also, weakly polar side chains have been shown to drive TM domain self-association by favorable H-bonding interactions. TOXCAT analysis of a randomized library showed that motifs involving Ser and Thr (SxxSSxxT or SxxxSSxxT)

have high self-association properties and are regularly found in TM proteins that homo-dimerize (35).

Recent studies have shown that the position and sequence context within which the polar residue resides affects its oligomerization property (34, 38). Systematic Asn substitutions in a host peptide system has demonstrated that Asn at positions close to the middle of the TM domain strongly stabilized oligomers, but Asn close to the membrane interface did not (38). Also, recent work wherein an Asp or Asn were introduced in the TM segment of M13 bacteriophage coat protein showed that while an appropriately placed polar residue could stabilize TM helix–helix interactions, the strongly polar residue was not sufficient in most cases to enhance association (34). Thus, the overall amino acid context plays a significant role in determining whether or not a TM segment would oligomerize, as the sequences flanking the polar residue could either provide unique packing interactions or prevent close approach by steric factors. This is best illustrated by the work of Russ et al. (39) who identified the GxxxG motif as the most significant feature of more than 100 highly dimeric transmembrane domains. The small side chain of Gly is thought to allow close packing of helices in a dimer (40, 41).

Inappropriate inter-helical hydrogen bond formation by polar side chains introduced by mutations may be a molecular basis for disease states. Deber and colleagues have shown that a mutation (Val232Asp) in the TM domain of the cystic fibrosis transmembrane regulator chloride channel (CFTR) affects the regular function of the receptor by altering the normal structure of the CFTR due to a strong hydrogen bonding interaction introduced by Asp 232 (42, 43). An inappropriate hydrogen bond introduced by Val664Glu mutation in TM domain of neu/ErbB2 receptor has been proposed to cause deregulation of tyrosine kinase activity. Inter-helical hydrogen bonding between uncharged Glu side-chains in the membrane is believed to stabilize the receptor dimers, resulting in constitutive activation of the receptor (44).

Charged residues in TM segments could also form intra-helical salt bridges to reduce the energetic cost of burial in the lipid bilayer (45). Glycosylation mapping has shown that a hydrophobic segment with an Asp and a Lys residue placed on the same side of the helix one turn part could adopt a stable TM structure, due to salt bridge interaction between the oppositely charged Lys and Asp residues. However, if the

residues were placed on the opposite face of the α-helix, such that they cannot form a salt bridge, then they disrupt insertion of the hydrophobic sequence in the membrane to a greater degree (45).

A hydrophilic residue within a TM helix can also affect the position of the helix within the membrane bilayer (9, 46-48). Using the glycosylation assay, von Heijne and colleagues have shown that a polar residue within the hydrophobic sequence could alter its transmembrane boundary. They showed that TM segments with polar residues could reposition within the membrane, such that the hydrophilic residue locates closer to the bilayer surface. In addition, they found a strong positional dependence for the membrane-repositioning effect of the polar residue. Mutations located in the first turn of the α-helix had a greater effect in shifting TM helix position compared to mutations that lie deep within the TM segment (47, 48). A similar result was obtained by a recent study in our lab, examining the effect of charge and position of Asp residue on hydrophobic helix behavior (49). In physiologically relevant bilayer widths under pH conditions, wherein the Asp was charged, the Asp residue could not be buried in the bilayer and so either a truncated TM state or non-TM surface state was formed, depending on the position of the Asp in the sequence. A shifted orientation was favored over the non-TM state when the hydrophobic sequence beyond the Asp substitution was long enough to form a truncated TM sequence (49).

Hydrophobicity and Sequence Length

A noted before, strong hydrophobicity is a key characteristic of TM segments. So how hydrophobic does a sequence have to be to incorporate into bilayers as a TM domain? Studies with model peptides have shown that poly-Alanine sequences (18-23 residues) are at the threshold for transmembrane integration (10, 50, 51). Glycosylation mapping studies have shown that for a transmembrane segment of typical length (19 residues) composed of only Leu and Ala residues, a minimum of 5 Leu residues are required for stable membrane insertion (10). This threshold appears to be close to what is predicted using the Wimley-White octanol scale (52). Stable membrane insertion of a hydrophobic sequence is also affected by residues flanking the hydrophobic sequence (see below). This raises the question of what is the minimum length a hydrophobic

sequence must have to function as TM domain in biologically systems? Both *in vivo* and *in vitro* studies have shown that the sequence length depends on the hydrophobicity of the sequence. Very short sequences, as short as 11 residues, can form TM domains if they are very hydrophobic (53-56). The formation and behavior of short TM helices are poorly characterized. Short TM helices may be more common than generally thought because the length of the TM segment may be smaller than that based on naïve hydrophobicity calculations.

Hydrophobic Mismatch

From an energetic point of view, the length of the hydrophobic TM segment is expected to be approximately equal to the hydrophobic thickness of the lipid bilayer. However, membrane proteins are found with a wide range in TM helix length (between 15 – 24 residues) (26, 27, 57). Also, membrane proteins encounter bilayers of different thickness. For example, all plasma membrane proteins are initially fully integrated into endoplasmic reticulum (ER) membranes upon synthesis on ribosomes but the plasma membrane is generally thicker than membranes of ER, partially due to higher cholesterol content (58). These observations raise the question of hydrophobic mismatch. Hydrophobic mismatch can be defined as the difference in hydrophobic thickness of a lipid bilayer and the hydrophobic length of the TM helix. There are two types of hydrophobic mismatch that can occur: positive mismatch results when the hydrophobic TM segment is longer than the hydrophobic thickness of the lipid bilayer. Conversely, negative mismatch occurs when the hydrophobic TM segment is shorter than the hydrophobic thickness of the bilayer (59, 60).

The energetic constraints imposed by hydrophobic mismatch could be relieved in a number of ways (summarized in Figure 3). In case of positive mismatch, the protein or peptide might oligomerize or aggregate to minimize exposed hydrophobic area and/or the helix could tilt to reduce the effective TM length. Lipid in turn could modulate membrane thickness by stretching and ordering their acyl chains. If negative mismatch occurs, then the protein or peptide may aggregate in membrane, or adopt a surface or shallowly located conformation. Lipids could decrease the bilayer thickness by acyl chain disordering or disrupt bilayer organization (59, 60).

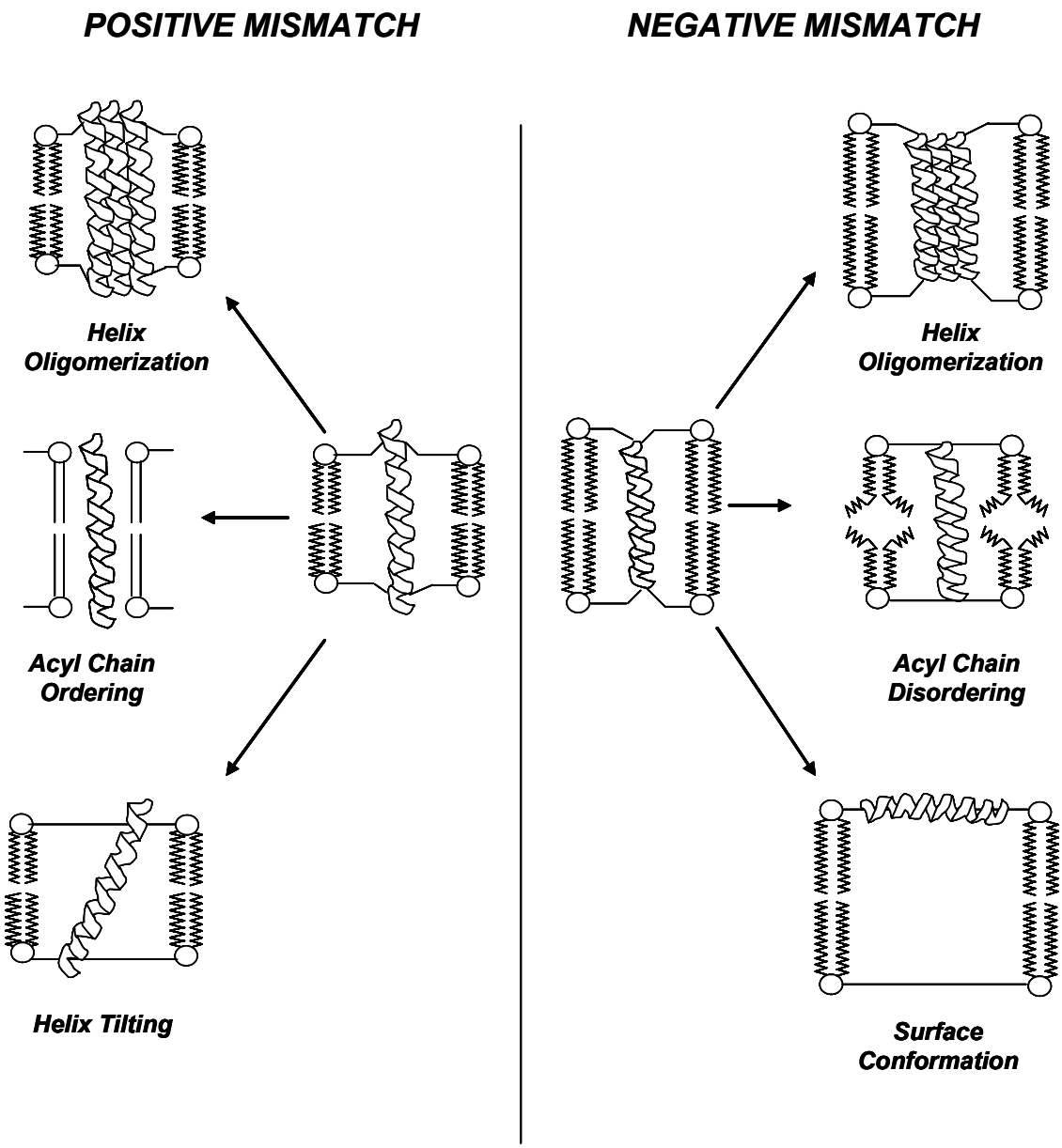

Figure 3. Schematic representation of some possible consequences of hydrophobic mismatch when the hydrophobic segment is longer (left) or smaller (right) than the hydrophobic bilayer thickness. Adapted from Killian 1998 (60).

Ren et al. (24) have shown, using lipids of various acyl chain lengths and model

peptides, that hydrophobic sequences could interconvert between a surface non-TM conformation and a TM structure in response to hydrophobic mismatch and cholesterol content. A short hydrophobic stretch of 11 leucine residues was shown to be surface associated (non-TM conformation) in a moderately thick membrane (DOPC bilayers), while sequences with 15, 19 and 23 Leu were capable of adopting a stable TM structure (16). They also found that the 11, 15 and 19 pL sequences were largely monomeric, but the 23 residue pL sequence had a higher tendency to associate, especially under conditions of positive mismatch (16). Thus, hydrophobic mismatch could significantly affect the energy of the TM structure, resulting in either a non-TM conformation or in helix-helix association.

Tilts in TM helices in response to positive mismatch have been demonstrated in several studies (59, 61-65). NMR studies with the TM domain of virus protein 'u' (Vpu) have shown that it tilts in response to positive hydrophobic mismatch. The Vpu TM domain tilts from 18º in bilayers having 18 carbon acyl chain length to 27º, 35º and 51º in bilayers with 14, 12 and 10 carbon acyl chain lengths (65), close to what would be expected if the entire hydrophobic segment were to be buried within the hydrophobic core of the bilayer. Contrasting data have been obtained for other systems, wherein tilt changes have been reported to be rather small (66).

The activity of several membrane proteins have been found to be sensitive to mismatch (67-69). For example, the enzyme activity of mitochondrial cytochrome *c* oxidase has been shown to be optimal in lipid bilayers with 18 carbon acyl chains. Positive or negative mismatch was found to decrease the enzymatic activity of the protein (68). On the contrary, several studies have shown that membrane proteins can maintain native structure and function to a significant degree in the presence of mismatch. This suggests that in these cases, the lipid bilayers adjust their hydrocarbon thickness to match the length of the hydrophobic surface of the protein to allow normal functioning of the protein (70-72). For example, X-ray lamellar diffraction measurements of bilayer thickness showed that the membrane bilayer could expand or contract (~ 4Å), to match the hydrophobic length of the gramicidin peptide (73). Theoretical quantitative analysis showed that this experimental data can be understood in terms of a simple elasticity theory of membrane deformation (74).

Effect of Residues Flanking the Hydrophobic Segment on TM Structure and Behavior

It has been suggested that residues flanking the hydrophobic segment act as anchors, i.e. they fix the position of the edge of the hydrophobic segment of a helix relative to the bilayer (75). Typically, TM segments are flanked by charged residues (Lys and Asp), which have favorable interactions with the aqueous solution and interfacial region of the bilayer and thus stabilize the TM state (59, 75). However, strong anchoring is not characteristic of all charged residues, as Arg does not have good anchoring ability (59). In addition to anchoring TM segments, positively charged flanking residues (Lys and Arg) have been proposed to act as topological determinants of TM helix orientation (76). This gives rise to the 'positive inside rule', which states that positive charged residues are frequently found on the cytoplasmic side of the membrane (76).

In addition, aromatic residues (Trp and Tyr) assist in anchoring TM segments in the membrane as these aromatic residues preferentially locate at the membrane interfacial region (59, 75). The preference of Trp and Tyr to locate at the bilayer interface was shown by a glycosylation mapping study (46). In this study, Braun and von Heijne (46) examined the effect of Trp placed either in the core of the TM segment or in the region flanking the TM segment. Trp was found to pull the TM helix towards the bilayer interface when located in the core of the TM segment or to push the TM helix towards the bilayer core when located in the region flanking the TM segment. These aromatic residues were found to have their lowest energy state at the polar/nonpolar interfacial region, which makes them good anchoring residues.

The effects of flanking residues on TM helix behavior have been investigated by many groups (59, 66, 77-80). Lew et al. (78) noted the role of flanking charges in inducing or preventing helix association. Hydrophobic pL peptides flanked with $LysAsp_3$ or LysAsp were found to associate under physiological pH conditions due to electrostatic interactions of the flanking residues. This lateral association was reduced under low pH conditions, wherein the Asp residue is protonated, and the electrostatic repulsion between positively charged flanking Lys residues lowers helix association. This showed that the ionic interactions of the flanking charges could promote or prevent TM helix association.

Both aromatic and charged flanking residues have significant effects on TM helix

behavior under conditions of mismatch. In work with model peptides, Killian and colleagues showed that Trp-flanked and Lys-flanked peptides behave somewhat differently in response to mismatch (59, 66, 77, 80). Under conditions of positive mismatch the Trp-flanked peptides showed less tilting (< 8º) compared to Lys-flanked peptides (~12º) suggesting that the Trp anchors the peptide differently from Lys (66, 79, 80). Also, Trp was found to induce lipid distortion (non-lamellar lipid phases) under conditions of less negative mismatch compared to Lys (59, 81). The Lys-flanked peptides are thought to adapt to mismatch more easily due to the flexibility of its Lys side chains. The ability of Lys side chain to 'snorkel' can help peptide compensate for mismatch (75).

Goal of this work – Understanding Sequence to Topography Relationship in TM Helices

As noted above, primary sequence is one major factor determining the topography and TM stability of membrane-inserted helices. Understanding the dependence of their behavior upon sequence would vastly improve our ability to predict membrane protein structure, folding and function from amino acid sequence. The goal of this work was to understand the sequence to topography relationship using isolated hydrophobic helices.

Individual hydrophobic α-helices (hydrophobic peptides) have been shown to be a versatile and easily manipulated model system to study the sequence-structure relationship in TM proteins (82). The reason is that TM helices are, to a large degree, independent folding units. These peptides are usually studied after incorporation into model membrane vesicles. Use of model membrane vesicles has a number of advantages. These include the abilities to control environmental factors like lipid composition and bilayer width (which cannot be controlled in cells or detergent-micelle based studies) and pH (which cannot be controlled in cells).

In this work, a set of fluorescence methods developed in our lab were used to efficiently define various topographical states of model membrane-inserted hydrophobic α-helices and to understand the equilibria describing topographic stability. This model membrane system was used to identify the minimum length required to form a stable TM helix and its dependence upon sequence and environment. In addition, the ability of hydrophilic residues to shift transverse position of TM helices within lipid bilayers was studied and the shift propensities for a complete series of hydrophilic residues were

measured. In conjunction with shifts in the TM domain, the structural consequences of a hydrophilic mutations in the TM domain of ErbB2 receptor was investigated. Finally, in collaboration with Dr. Eckard Wimmer in Department of Molecular Genetics and Microbiology, the membrane topography of Poliovirus 3A and 3AB proteins was characterized.

CHAPTER 2

EXPERIMENTAL PROCEDURES

Materials. A series of 1,2-diacyl-*sn*-glycero-3-phosphocholines (phosphatidylcholines, PC): diC14:1Δ9cPC (dimyristoleoyl-PC, DMoPC); diC16:1Δ9cPC (dipalmitoleoyl-PC, DPoPC); diC18:1Δ9cPC (dioleoyl-PC, DOPC); diC20:1Δ11cPC (dieicosenoyl-PC, DEiPC); diC22:1Δ13cPC (dierucoyl-PC, DEuPC) and diC24:1Δ15cPC (dinervonoyl-PC, DNPC) were purchased from Avanti Polar Lipids (Alabaster, AL). Concentrations of lipids purchased as liquid solutions in chloroform were confirmed by dry weight. The lipids were stored in chloroform at -20ºC. 10-doxylnonadecane (10-DN) was custom synthesized by Molecular Probes (Eugene, OR). It was stored as a 5 mM stock solution in ethanol at -20 ºC.

Model Membrane Vesicle Preparation. Model membrane (unilamellar) vesicles were prepared using the ethanol dilution method as previously described (16, 24). Peptides dissolved in 1:1 (v/v) 2-propanol/water and lipids dissolved in chloroform were mixed and dried under a stream of N_2 gas. Samples were then dried under high vacuum for 1h. The dried peptide/lipid samples were then dissolved in a minimum volume (typically 10 μl) of ethanol and diluted to the desired final volume (typically 800 μl) using PBS (10 mM sodium phosphate and 150 mM NaCl, pH 7.0), with constant vortexing. Low and high pH samples were prepared using PBS (10 mM sodium phosphate and 150 mM NaCl) adjusted to the required pH using glacial acetic acid (pH 4.0) or NaOH (pH 9.0), respectively.

This method was slightly modified for the Polio 3A anchor peptides. Due to the insolubility of the anchor peptides in ethanol, the procedure was modified to use dimethylsulfoxide (DMSO). In the modified procedure, peptide dissolved in DMSO was mixed with the lipids dissolved in chloroform and then dried under N_2 gas and high vacuum. The dried lipid/peptide mixtures were dissolved in 10 μl DMSO and then diluted with PBS, pH 7.0 as described above. Control experiments with previously studied hydrophobic peptides that form transmembrane α-helices (29, 30) showed that substitution of DMSO for ethanol did not alter transmembrane topography upon incorporation into lipid vesicles (data not shown). With exception of the shifts peptides in Chapter 4, the final concentrations for the model membrane samples were 2 μM peptide and 500 μM lipid. For shift peptides, final concentration of 2 μM peptide and 200 μM

lipid was used.

Preparation of Model Membrane Vesicles Containing Protein. For experiments in which $3A^m$ or $3AB^m$ proteins were reconstituted into model membrane vesicles to form proteoliposomes, lipid vesicles were prepared using the ethanol-dilution method (Ref). Lipids dissolved in chloroform were dried under a stream of N_2 gas, followed by drying under high vacuum for 1h. The dried lipid samples were dissolved in a minimum volume (10 μl) of ethanol, and then diluted to the final volume (typically 800 μl), using PBS (10 mM sodium phosphate and 150 mM NaCl, adjusted to pH 7.0) with constant vortexing. The samples were then allowed to equilibrate for 30-60 min at room temperature. Then aliquots of protein [20 μl from 0.5 mg/ml protein stocks containing octylglucoside (OG)] were added to the pre-formed vesicles, and incubated for an additional 1 h before fluorescence was measured. Samples contained final concentrations of 12.5 μg/ml protein and 500 μM lipids. Since octylglucoside was rapidly diluted to far below its cmc in this protocol, it should not have affected vesicle integrity. Confirming this, a protocol in which the protein was diluted into buffer before addition of vesicles gave similar fluorescence and fluorescence quenching results to those with the protocol described above (data not shown).

Fluorescence Measurements. Fluorescence data was obtained on SPEX τ2 Fluorolog spectrofluorometer operating in steady-state fluorescence mode at room temperature. Excitation slits of 2.5 mm (4.5 nm band-pass) and emission slits of 5 mm (9 nm band-pass) were used for all measurements. The fluorescence emission spectra were measured over the range 300-375 nm. Fluorescence from background samples containing lipid and buffer with no peptide were subtracted to calculate reported fluorescence values. All measurements were made at room temperature.

Acrylamide Quenching Measurements. To measure acrylamide quenching, fluorescence intensity and emission spectra were first measured in samples containing peptides incorporated into model membranes or background samples, prepared as described above. Then a 50 μl aliquot of acrylamide from a 4 M stock solution dissolved in water

was added. After a brief incubation (5 min), the fluorescence was remeasured. In these experiments, fluorescence intensity was measured using an excitation wavelength of 295 nm and emission wavelength of 340 nm. This excitation wavelength was chosen to reduce acrylamide absorbance (and the resulting inner-filter effect). Fluorescence intensity was corrected both for dilution from addition of acrylamide and due to the inner-filter effect (83). To determine emission λmax, Trp emission spectra in the presence of acrylamide were measured with an excitation wavelength of 280 nm, which gave stronger fluorescence intensity than with excitation at 295 nm despite the increased inner-filter effect due to acrylamide absorbance at 280 nm. Previous controls show that in these experiments the emission spectra λmax is not affected by this choice of excitation wavelength (83).

10-Doxylnonadecane Quenching Measurements. To measure quenching by 10-DN, the fluorescence of samples containing model membrane-incorporated peptide was compared to that in samples containing 10-DN. To prepare the later, samples were prepared as described above except that either 10% mol (for DOPC) or 12% mol (for DEuPC) of the lipid was replaced with an equivalent mol % of 10-DN. Fluorescence intensity was measured using an excitation wavelength of 280 nm and emission wavelength of 330 nm. The emission spectra were measured with excitation wavelength of 280 nm.

Calculation of Acrylamide/10-DN Quenching Ratio. The acrylamide/10-DN quenching ratio (Q-ratio) was used to estimate Trp depth in the bilayer. The ratio was calculated from the formula Q-ratio = $[(F_o/F_{acrylamide})-1]/ [(F_o/F_{10\text{-}DN})-1]$, where F_o is the fluorescence of a sample with no quencher present and $F_{acrylamide}$ and $F_{10\text{-}DN}$ are the fluorescence intensities in presence of acrylamide or 10-DN respectively. The Q-ratio varies inversely with depth of the Trp in the membrane (83).

Circular Dichroism Measurements. Circular Dichroism (CD) spectra were recorded at room temperature using a JASCO J-715 CD spectrometer using 1 mm path length quartz cuvettes. Typically, final spectra were the average of 50 scans taken at a rate of 50 nm/min. Estimation of α-helical content was done using DICHROWEB, an online server

for secondary structure analyses from CD data (84). Intensities in background samples (lipid without peptides) were subtracted before analysis of secondary structure. The final concentrations using for CD measurements were 2 μM peptide and 500 μM lipid, unless otherwise noted.

Calculation of Effective TM Length ($L_{TM\ eff}$). Bilayer width at which λmax was a minimum was identified from a polynomial fit of the λmax vs. bilayer width curves using the SlideWrite program (Advanced Graphics Solution, Encinitas, CA). Correlation coefficients (r^2) were greater than 0.99 for all fits. $L_{TM\ eff}$ (in units of numbers of residues) was calculated using the formula: $L_{TM\ eff}$ = bilayer core width at λmax minimum/ 1.5 Å per residue; where bilayer width = 1.8 Å × number of acyl chain carbon atoms – 4.5 Å (16)

CHAPTER 3

EFFECT OF SEQUENCE HYDROPHOBICITY AND BILAYER WIDTH UPON THE MINIMUM LENGTH REQUIRED FOR THE FORMATION OF TRANSMEMBRANE HELICES IN MEMBRANES

Transmembrane segments of membrane proteins are predominantly composed of hydrophobic α-helical segments. Understanding the dependence of hydrophobic helix behavior upon amino acid sequence would vastly improve our ability to predict membrane protein structure, folding and function.

The formation and behavior of short TM helices are poorly characterized. Short TM helices may be more common than generally thought because the length of the TM segment may be smaller than that based on naïve hydrophobicity calculations. In recent work on polio virus 3A/3AB proteins we found the 22-residue hydrophobic anchor of the 3A protein can adopt a TM structure, but the actual length of the TM segment is only about 16 residues (85).

Because short hydrophobic sequences often form TM states with borderline stability (16, 56, 85) it is also important to define how sequence controls their equilibration between TM and non-TM states. This equilibrium can often impact membrane-protein function (17, 85-92) and genomic analysis suggests that the number of sequences that can undergo TM/non-TM interconversion may be considerable (28).

The behavior of short TM helices is also of interest because of the role of TM helix length in trafficking between membranes. It has been observed that the apparent TM sequences of Golgi proteins are generally shorter (15 residues) than those (18 residues) of plasma membrane proteins (93-95), and a preferential interaction of short TM α-helices with the thinner bilayers of Golgi apparatus is believed to be one mechanism of retention in the Golgi (93-95). The predicted role of helix length in this type of sorting is supported by studies showing the cellular location of simple TM sequences is a strong function of length (94, 96-98).

Artificial hydrophobic α-helices with simple amino acid compositions are useful for further studies of the relationship between helix length and behavior in membranes. Artificial helices have already been widely used to study the sequence-structure relationship in model membranes, and this system has a number of advantages, including the abilities to control environmental factors such as lipid composition and bilayer width and pH (which cannot be controlled in cells and/or detergent-micelle based studies), and the ability to analyze helix behavior with a variety of techniques, including diffraction, NMR, IR and fluorescence spectroscopy (16, 24, 71, 82, 99-102).

We have developed a set of methods using fluorescence properties to define the topographical states of membrane-inserted hydrophobic α-helices containing a single Trp residue in their hydrophobic core as a function of sequence and bilayer width (16, 24, 29, 30, 78, 83, 85). In a previous study using helix-forming Lys-flanked hydrophobic sequences, we found that in DOPC bilayers 15 residue-long polyLeu type sequences result in stable TM insertion, but that the TM configuration is not very stable when the polyLeu sequence is 11 residues long (16). We also found that polyLeu sequences containing internal charged residues may form truncated TM segments with as little as 11 consecutive hydrophobic residues (29, 49).

However, these studies did not define the minimum length capable of forming a stable TM helix for sequences with more biologically relevant hydrophobicities, or how TM stability would be affected by the identity and charge of hydrophilic residues surrounding the hydrophobic sequence. Defining the importance of these parameters was the aim of the present study. Sequences containing polyLeu or polyLeuAla hydrophobic cores of varying lengths, and sequences with various hydrophilic residues flanking the hydrophobic core, were used to precisely define the minimum length required to form a stable TM helix and its dependence upon sequence and environment. We found that even moderately hydrophobic sequences can form autonomous short TM segments under conditions of considerable negative mismatch, and that the extent to which a TM configuration is formed can be controlled by physiologically relevant changes in bilayer width and pH. This information should aid the prediction of short TM helices from sequence data, and their behavior in different membranes.

RESULTS

Using Fluorescence Emission λmax, Fluorescence Quenching, and Bilayer Width Variation to Define the Topography of the Membrane-Inserted Hydrophobic Helices.

The fluorescence properties of a Trp residue located at the center of the hydrophobic sequence was used to define the topography of membrane-inserted peptides (16, 24). When such a peptide adopts a TM orientation this Trp locates at or near the bilayer center, which results in blue-shifted Trp emission λmax (315-320 nm). However, if the peptide adopts a membrane-bound non-TM topography in which the peptide resides close to the bilayer surface, then the Trp locates close to the surface, and the λmax red shifts, generally to 335-345 nm (16, 24). The exact λmax value in the non-TM state value depends upon how deeply the peptide is buried in the non-TM state, and upon whether in the non-TM state the Trp faces aqueous solution or the bilayer interior (16, 24). Values of λmax in between those for the TM and non-TM state are characteristic of mixtures of TM and non-TM topographies (16, 24) or of a shifted TM state wherein only a part of the hydrophobic sequence forms the membrane-spanning segment, and so the Trp is shifted to an intermediate depth (29, 49). These alternatives can also be distinguished from each other (see below).

The effect of changing bilayer width (and thus changing the degree of hydrophobic mismatch between bilayer width and hydrophobic helix length) upon Trp depth aids the characterization of topography, and can help define the length of a TM helix (Figure 4) (16, 24, 29, 49). [Lipids with monounsaturated acyl chains are used in these studies so that the bilayers remain in the fluid state at room temperature.] Several studies have shown that for a Trp at the center of a hydrophobic sequence fluorescence is generally most blue-shifted when a hydrophobic peptide is incorporated into the widest bilayer in which the TM configuration is stable (16, 24, 29, 49). As a result, the bilayer width at which fluorescence is most blue-shifted distinguishes short; medium and long TM helices (see Figure 4). As bilayer width is further increased, so that *negative* mismatch between helix length and bilayer width develops, Trp λmax red shifts due to the peptide forming an increasing amount of the non-TM state (16, 24). When the TM

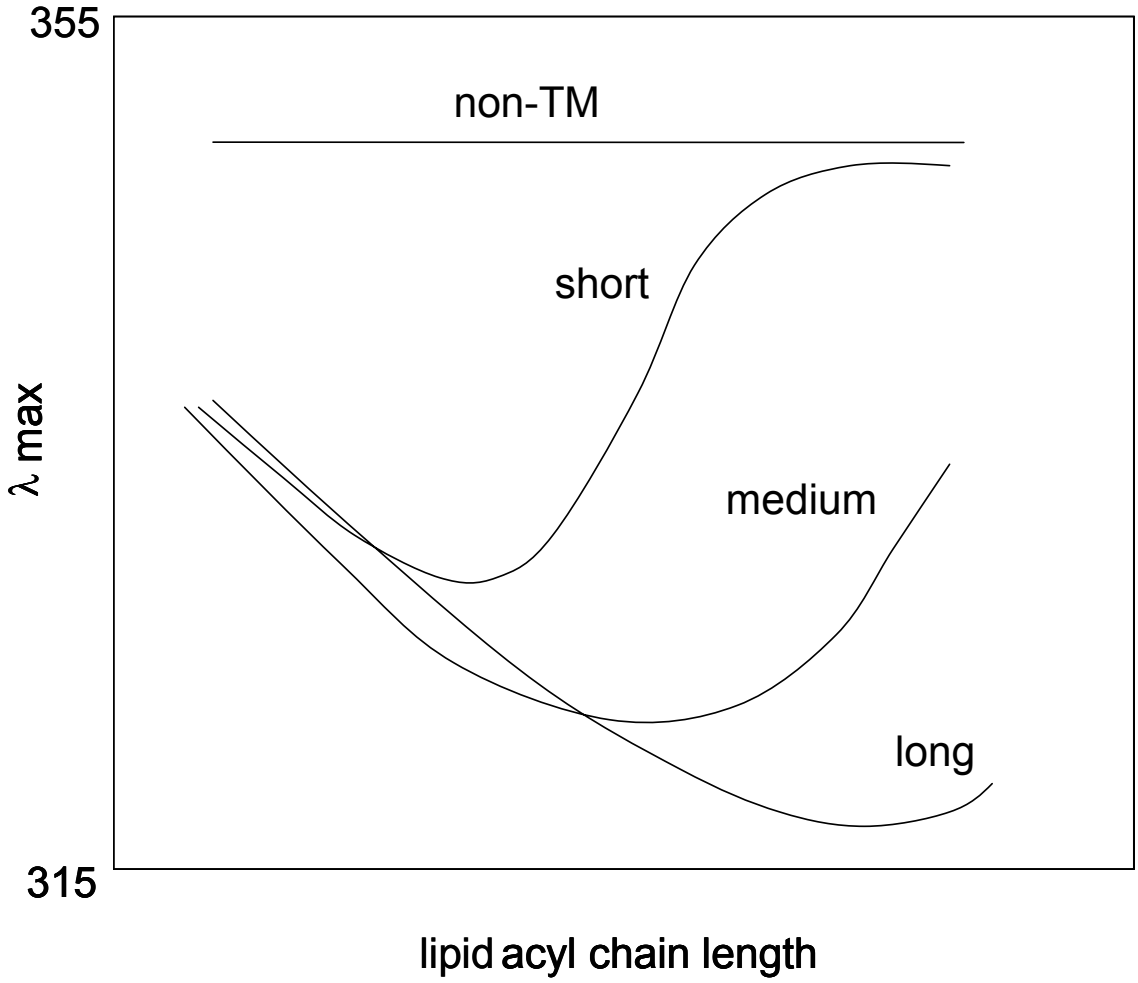

Figure 4. Schematic representation of the dependence of Trp λmax upon lipid acyl chain length for hydrophobic peptides with different lengths and tendencies to form a TM topography (16, 24, 29). Short, medium, and long refer to the length of hydrophobic sequences sufficiently hydrophobic to form TM sequences in the absence of negative mismatch. Non-TM shows the behavior of a sequence insufficiently hydrophobic to form a TM state at any bilayer width.

state is fully lost, the red shift reaches a limiting value. This point can usually only be detected for short and medium length TM helices (Figure 4).

When bilayer width is decreased from the maximum width at which the TM configuration is stable (i.e., in conditions of *positive* mismatch between helix length and bilayer width) there is also a red shift, although generally smaller than that under conditions of negative mismatch (16, 24). This positive mismatch-induced red shift arises from the fact that a Trp at the bilayer center automatically is located closer to the surface as bilayer width decreases, combined with effects due to promotion of (weak) oligomerization by conditions of positive mismatch (16, 24, 30). [It appears that the fluorescence of a Trp at the center of the bilayer is more red-shifted when buried in an oligomer than when exposed to lipid (30, 78)] When a membrane-bound helix does not form a TM state, but instead sits near or at the surface of the bilayer in non-TM form, a Trp at the center of the sequence shows highly red-shifted fluorescence that is not sensitive to bilayer width (upper line in Figure 4).

Interpretation of λmax results is aided by combining them with more direct measurements of Trp depth. To do this, a dual fluorescence quenching method can be used. This method utilizes two quenchers of Trp fluorescence, acrylamide and 10-DN. Acrylamide (although membrane permeable (83)) resides primarily in the aqueous solution and preferentially quenches the fluorescence of Trp residues near the membrane surface, while 10-DN, a membrane-inserted quencher, preferentially quenches the fluorescence of Trp buried in the membrane bilayer (83). The ratio of acrylamide quenching to 10-DN quenching (Q-ratio) responds nearly linearly to Trp depth in the bilayer, with a low quenching ratio (< 0.2) indicating a deeply located Trp near the center of the bilayer, while a high Q-ratio (1.0-3.0) is usually indicative of a Trp near the bilayer surface (83).

Intermediate Q-ratios can arise either from peptides adopting a mixture of conformations with shallow and deep Trp depths, or from peptides that adopt a "single" shifted TM conformation with an intermediate Trp depth. These two alternatives can be resolved by measurement of quencher-induced shifts in Trp λmax (29, 49, 83). If a membrane inserted peptide forms co-existing deep and shallow conformations, then its

Trp emission will be composite of red-shifted and blue-shifted emission spectra. In such samples, acrylamide will preferentially quench the shallow Trp, inducing a blue shift in λmax. Conversely, 10-DN will preferentially quench the deep Trp, and induce red shifts. The difference in λmax in the presence of acrylamide and 10-DN, which depends on the amount of each population present, can be up to 15 nm (49, 83). If only a single Trp depth population is present, the difference in λmax in the presence of acrylamide and 10-DN is very small (0-2 nm) (49, 83).

Effect of Helix Length and Sequence upon Topography of Membrane-Inserted Short Hydrophobic Helices: 17 Hydrophobic Residues.

Using these methods, peptides with short hydrophobic sequences (13-17 residues) were studied in order to determine the minimum length hydrophobic sequence forming stable TM helices (Table 1). PolyLeu (pL)-type sequences were compared to two different types of polyLeuAla (pLA)-type sequences. The first type had alternating Leu and Ala residues, and the second had a block of Leu residues followed by a block of Ala residues. All sequences had a Trp in the center of the hydrophobic sequence to probe helix position within the bilayer. The also had two flanking ionizable residues, Lys unless otherwise noted, at both the N and C-termini of the hydrophobic core sequence.

Figure 5 shows the effect of bilayer width on Trp emission λmax for pL and pLA peptides at pH 7.0. For sequences with [including the Trp] 17 hydrophobic residues (pL_{16}, $p(LA)_8$ and pL_8A_8), the pattern of λmax as a function of bilayer width (Figure 5A) showed a minimum with very blue-shifted emission in DOPC vesicles (DOPC has 18 carbon acyl chains) and/or DEiPC vesicles (DEiPC has 20 carbon acyl chains) and a significant red shift in wider bilayers. This pattern indicated that in DOPC vesicles the Trp is near the bilayer center, and thus the 17 hydrophobic residue sequences were forming relatively stable TM helices in DOPC vesicles, but in much wider bilayers the Trp located more shallowly, consistent with some degree of formation of a non-TM state.

These conclusions are confirmed by fluorescence quenching data (Figure 6). All three peptides with 17 hydrophobic residues exhibited low Q-ratios in DOPC vesicles

Table 1: List of Peptides Used in this Study.

Peptide	Sequence
$pL_{12} = (^{KK}pL_{12})$	Ac-(= acetyl)-$K_2GL_6WL_6K_2A$-NH_2
pL_{14}	Ac-$K_2GL_7WL_7K_2A$-NH_2
pL_{16}	Ac-$K_2GL_8WL_8K_2A$-NH_2
$p(LA)_6$	Ac-$K_2G(LA)_3W(LA)_3K_2A$-NH_2
$p(LA)_7$	Ac-$K_2G(LA)_3LWA(LA)_3K_2A$-NH_2
$p(LA)_8$	Ac-$K_2G(LA)_4W(LA)_4K_2A$-NH_2
pL_6A_6	Ac-$K_2GL_6WA_6K_2A$-NH_2
pL_7A_7	Ac-$K_2GL_7WA_7K_2A$-NH_2
pL_8A_8	Ac-$K_2GL_8WA_8K_2A$-NH_2
$^{KH}pL_{12}$	Ac-$KHGL_6WL_6HKA$-NH_2
$^{HH}pL_{12}$	Ac-$H_2L_6WL_6H_2$-NH_2
$^{HD}pL_{12}$	Ac-$HDGL_6WL_6DHA$-NH_2

These peptides were purchased from Anaspec Inc. (San Jose, CA). Peptides were purified via reverse-phase-HPLC using a C18 column with 2-proponal/water/0.5% v/v trifluoroacetic acid as mobile phase as described previously (103). Peptide purity was confirmed using MALDI-TOF mass spectrometry (Proteomics Center, Stony Brook University). We estimated that final purity was on the order of 90% or better. After drying the HPLC fractions the peptides were stored in 1:1 (v/v) 2-proponal/water at 4 ºC. Peptide concentrations were measured by absorbance spectroscopy on a Beckman DU-650 spectrophotometer using extinction coefficient for Trp of 5560 $M^{-1}cm^{-1}$ at 280 nm.

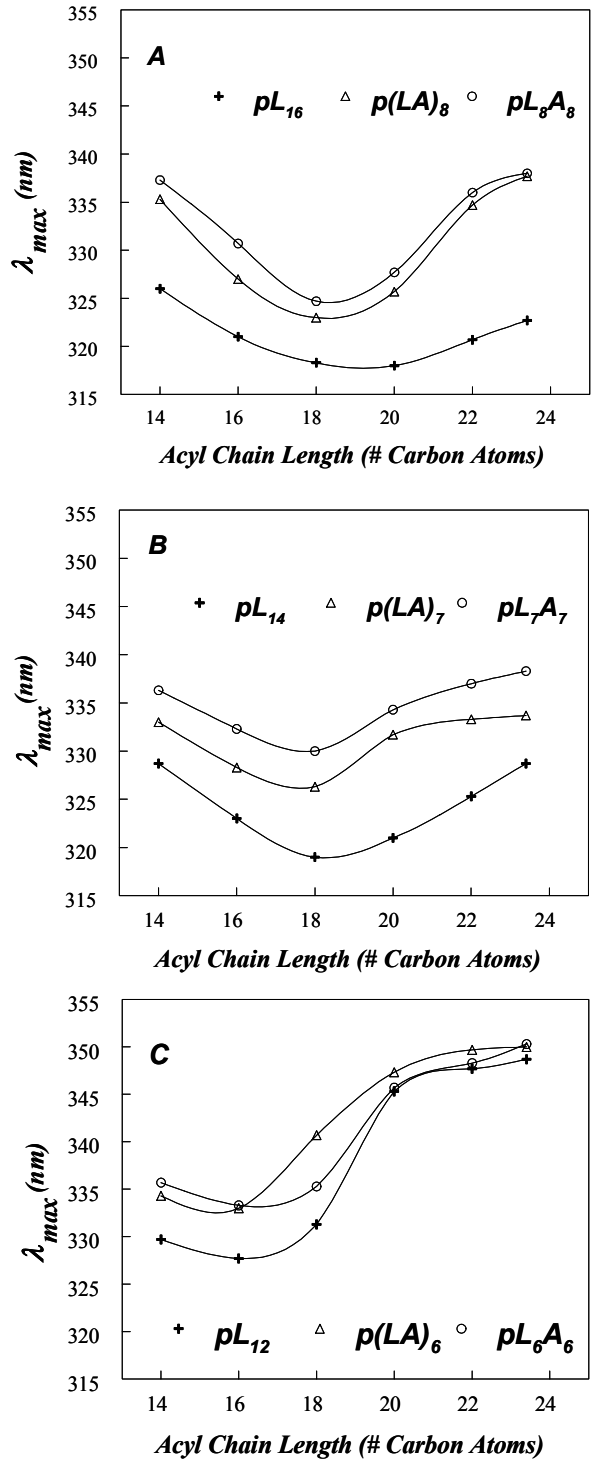

Figure 5. Effect of lipid acyl chain length on Trp emission λmax of pLeu and pLeuAla peptides of varying lengths incorporated into phosphatidylcholine vesicles at pH 7.0. (A) pLeu and pLeuAla peptides with 17-residue hydrophobic core. (B) pLeu and pLeuAla peptides with 15-residue hydrophobic core. (C) pLeu and pLeuAla peptides with 13-residue hydrophobic core. Samples contained 2 μM peptide incorporated into 500 μM lipid dispersed in PBS at pH 7.0. The average values of triplicate samples are shown.

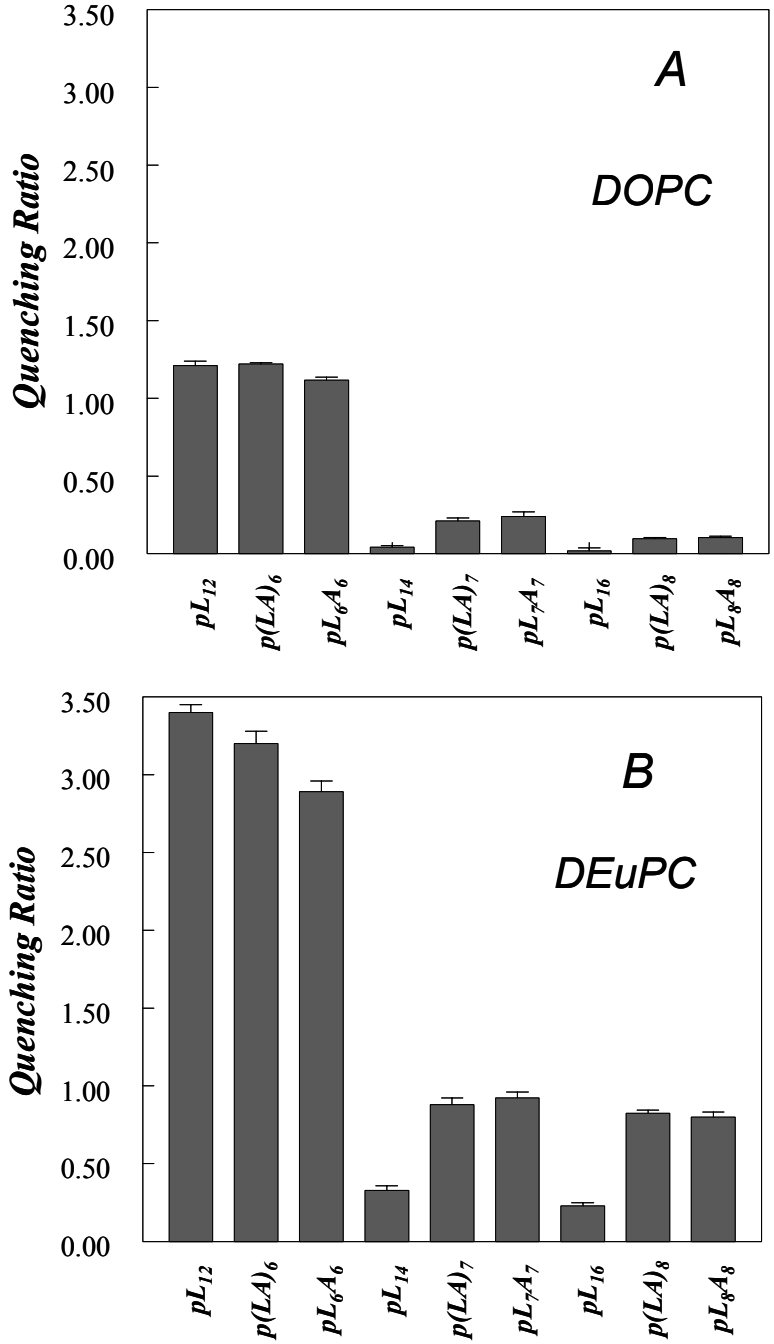

Figure 6: Quenching ratios for pLeu and pLeuAla peptides of varying lengths incorporated into DOPC or DEuPC vesicles at pH 7.0. (A) Quenching ratio of peptides in DOPC vesicles at pH 7.0. (B) Quenching ratio of peptides in DEuPC vesicles at pH 7.0. Samples contained 2 μM peptide incorporated into 500 μM lipid dispersed in PBS at pH 7.0. Average and standard deviation from a minimum of 3 samples are shown

.

(Figure 6A) corresponding to either fully or almost fully TM configurations with the Trp near the bilayer center, and higher Q-ratios (Figure 6B) in DEuPC vesicles (DEuPC has 22 carbon acyl chains) indicating a shallower Trp depth that corresponds to some degree of formation of shallow, non-TM state with the Trp closer to the bilayer surface. The λmax values in Figure 5A also show that the $p(LA)_8$ and pL_8A_8 give significantly more red-shifted fluorescence than pL_{16} at all bilayer widths, strongly suggesting that the Trp in the former peptides located more shallowly than in the latter peptide. This is confirmed by the observation that $p(LA)_8$ and pL_8A_8 exhibited higher Q-ratios than pL_{16} in both DOPC and DEuPC vesicles (Figure 6).

Furthermore, for $p(LA)_8$ and pL_8A_8 the red shift in λmax appears to approach a limiting value as bilayer width is increased (Figure 5A), indicating nearly complete formation of the non-TM state in very wide bilayers, while for the pL_{16} peptide in wide bilayers the Trp remains relatively blue-shifted, indicating that the TM state still predominates. This conclusion is supported by the quenching data in DEuPC vesicles (Figure 6B), which shows high Q-ratios characteristic of a shallow Trp for the former peptides, but a low Q-ratio for pL_{16} indicating that a predominant amount pL_{16} remained in the TM state, in which Trp locates very deeply.

The differences between λmax and Trp depths for pL_{16} and the $p(LA)_8$ and pL_8A_8 peptides incorporated into moderate-width (DOPC) and even thinner bilayers may result from the TM configuration being less stable for the latter two peptides. However, it is also possible that part of the difference between can be explained by the $p(LA)_8$ and pL_8A_8 peptides forming a TM state with a wider distribution of Trp depths than that of pL_{16} (see Discussion). Consistent with this hypothesis, Table 2 shows that acrylamide and 10-DN do not induce large shifts in λmax for pLA peptides in DOPC vesicles, indicating that the pLA peptides in DOPC vesicles do *not* form two populations with very different Trp depths (i.e. co-existing TM and non-TM states), despite locating more shallowly than the pL peptide.

Table 2: Quencher-Induced Shifts in Trp Emission λmax for Membrane-Inserted pL and pLA Peptides in DOPC and DEuPC Bilayers. The

Peptide	Lipid	λmax (nm) [a]	λmax (nm) (acrylamide)	λmax (nm) (10-DN)	|Δλmax| (nm) [b]
pL_{16}	DOPC	318	319	318	1
	DEuPC	321	321	320	1
$p(LA)_8$	DOPC	323	322	324	2
	DEuPC	334	333	336	3
pL_8A_8	DOPC	324	324	325	1
	DEuPC	335	335	339	4
pL_{14}	DOPC	319	320	320	0
	DEuPC	325	325	328	3
$p(LA)_7$	DOPC	326	323	329	6
	DEuPC	333	333	337	4
pL_7A_7	DOPC	330	326	333	7
	DEuPC	337	338	342	4
pL_{12}	DOPC	331	329	339	10
	DEuPC	347	347	349	2
$p(LA)_6$	DOPC	340	337	348	11
	DEuPC	349	347	349	2
pL_6A_6	DOPC	335	330	344	13
	DEuPC	348	347	349	2

[a] Reported λmax values are averages from three to six samples. The values were generally reproducible within ± 1nm. The λmax values have been rounded to whole numbers. [b] Δλmax is the absolute value of difference between λmax in the presence of acrylamide and λmax in the presence 10-DN.

Effect of Helix Length and Sequence upon Topography of Membrane-Inserted Short Hydrophobic Helices: 15 Hydrophobic Residues.

Qualitatively, the pattern of both λmax (Figure 5B) and Q-ratios (Figure 6) for sequences with 15 hydrophobic residues (pL_{14}, $p(LA)_7$ and pL_7A_7) was similar to that for sequences with 17 hydrophobic residues. However, sequences with 15 hydrophobic residues exhibited more red-shifted Trp fluorescence (Figure 5B) than sequences with 17 hydrophobic residues (Figure 5A), consistent with the former having less stable TM insertion due to having shorter hydrophobic segments. This conclusion was supported by the observation that the bilayer width at which λmax is a minimum was thinner for pL_{14} (18 acyl chain carbons), than for pL_{16} (20 acyl chain carbon atoms), and the observation that both $p(LA)_7$ and pL_7A_7 showed near-limiting red shifts in bilayers with 20 acyl chain carbon atoms while $p(LA)_8$ and pL_8A_8 only showed near-limiting red shifts in wider bilayers with 22 acyl chain carbon atoms. Quenching ratios confirmed this difference between 15- and 17- hydrophobic residue sequences. In DOPC vesicles (Figure 6A), the Q-ratios are slightly higher, and thus Trp depth was slightly shallower, for the peptides with 15 hydrophobic residues than it was for the corresponding peptides with 17 hydrophobic residues. The less stable TM insertion of the 15 hydrophobic residue peptides was also confirmed by quencher-induced λmax shifts in DOPC vesicles (Table 2). In contrast to the behavior of $p(LA)_8$ and pL_8A_8, quenching-induced λmax shifts in DOPC vesicles were significant for $p(LA)_7$ and pL_7A_7, indicating that the latter peptides formed significant amounts of both TM and non-TM states in DOPC vesicles, while the former peptides did not (they formed much less non-TM state).

As in the case of the analogous sequences with 17 hydrophobic residues, the pL_{14} peptide showed more blue-shifted fluorescence than the $p(LA)_7$ or pL_7A_7 peptides at all bilayer widths (Figure 5B), indicative of a shallower Trp location for the latter peptides. In agreement with this data, Q-ratios (Figure 6) confirmed that pL_{14} forms structures with a deeper Trp depth than $p(LA)_7$ and pL_7A_7. In addition, in DOPC vesicles the pL_{14} peptide did not show the significant quencher-induced λmax shifts seen with $p(LA)_7$ or pL_7A_7 (Table 2), also consistent with its maintaining a more stable TM configuration (similar to the pL_{16} peptide).

The difference between Q-ratios (and λmax) for $p(LA)_7$ and pL_7A_7 and those for

$p(LA)_8$ and pL_8A_8 were not as large in DEuPC vesicles as they were in DOPC vesicles (Figure 5A, 5B, and Figure 6B), probably because in DEuPC vesicles the non-TM state is already predominant in all of these cases. In contrast, Q-ratios and λmax both indicate that in DEuPC vesicles pL_{14} has a shallower Trp depth than pL_{16}. Nevertheless, the TM state appears to predominate for pL_{14} in DEuPC vesicles as judged by the observation that λmax and Q-ratio values for this peptide in DEuPC vesicles (325 and 0.32, respectively) were closer to the values it exhibited in DOPC vesicles (319 and 0.04, respectively), in which the TM state is formed, than they were to that for pLA_7 and pL_7A_7 peptides in DEuPC vesicles (333-337 nm and 0.88-0.92, respectively), cases in which the peptides appear to be almost fully in the non-TM state.

Effect of Helix Length and Sequence upon Topography of Membrane-Inserted Short Hydrophobic Helices: 13 Hydrophobic Residues.

The λmax values for peptides with 13 hydrophobic residues (pL_{12}, $p(LA)_6$ and pL_6A_6) also follow patterns somewhat analogous to that observed for sequences with 15 or 17 hydrophobic residues. However, the peptides with 13 hydrophobic residues exhibited much more red-shifted Trp fluorescence (Figure 5C), than observed for peptides with 15 or 17 hydrophobic residues, and this, plus λmax vs. bilayer width profiles, were indicative of even less stable TM insertion and shorter TM segments than for the peptides with 15 or 17 hydrophobic residues. The latter conclusion is supported by the observation that for all of the peptides with 13 hydrophobic residues the bilayer width at which λmax is a minimum is that of DPoPC vesicles (DPoPC has 16 carbon acyl chains), thinner than that giving a minimum λmax for the 15 and 17 hydrophobic residue peptides.

Quenching ratios and quencher-induced λmax shifts again support the conclusions derived from λmax data. In DOPC vesicles, pL_{12}, $p(LA)_6$, and pL_6A_6 show high Q-ratios and large quencher induced λmax shifts, indicating a large amount of the non-TM state is present, (Figure 5C). The lesser stability of the TM state for pL_{12} relative to pL_{14} and pL_{16}, demonstrated by its exhibiting a high Q-ratio (Figure 6A) and large quencher-induced λmax shifts in DOPC vesicles (Table 2), is particularly striking. This

difference is confirmed by behavior in DEuPC vesicles, in which pL_{12} differs from pL_{14} and pL_{16} in that it fully forms the non-TM state as judged a very high Q-ratio (Figure 6B).

For all of the peptides with a 13-residue hydrophobic sequence the limiting λmax in wide bilayers was significantly more red-shifted (close to 350 nm) than for 15- and 17-residue long hydrophobic sequences (generally 335-340 nm), indicative of a shallower Trp location in the case of the 13-residue hydrophobic sequences. Consistent with this conclusion, the Q-ratio for the peptides with 13-residue hydrophobic sequences in the non-TM state (~3) was larger than that of the peptides with the 15- and 17-residue hydrophobic sequences in the non-TM state (~1) (Figure 6). This difference could reflect either a shallower peptide location for the 13 residue hydrophobic peptides in the non-TM state or a difference in Trp orientation in the non-TM state (see Discussion). Another possible explanation was that the peptides with 13 hydrophobic residues were not fully membrane-bound. However, control experiments in which vesicles containing pL_6A_6 were chromatographed on Sepharose 4B confirmed that membrane binding was complete (data not shown).

It is noteworthy that although a Q-ratio value of about 1 can represent a fully non-TM configuration, because of the high Q value in the non-TM state for the sequences with 13 hydrophobic residues, the value of about 1 observed for pL_{12}, $p(LA)_6$, and pL_6A_6 in DOPC vesicles is indicative of a mixture of deep and shallow configurations. This is confirmed by the very large quencher-dependent λmax shifts observed for pL_{12}, $p(LA)_6$, and pL_6A_6 in DOPC vesicles (Table 2).

As with the longer peptides, the pL_{12} peptide shows more blue-shifted fluorescence than the $p(LA)_6$ and pL_6A_6 peptides in DOPC vesicles. However, the difference is small, and no difference is detected by Q-ratio, suggesting that the stability of the TM state for the pL_{12} peptide is not much greater than that for $p(LA)_6$ or pL_6A_6.

Secondary Structure of Peptides: Effect of Helix Length and Mismatch.

Previous studies have shown the types of peptides studied here form α-helices when membrane-associated (16, 104). To confirm this was true for the specific combinations of sequence and hydrophobic residue lengths studied in this report, the peptides were incorporated into vesicles composed of DOPC or DEuPC and then helix

content was estimated from circular dichorism (CD) spectra. Estimated helix contents were found to be in the range of 80-90% (Data not shown). The results show that the peptides were highly helical in both the TM and non-TM state.

Minimum Length Required for Stable TM Helix Formation.

The data from the experiments above was further analyzed to define the sequence/bilayer width dependence of the minimum length required for TM helix formation. To do this, the dependence of Trp λmax upon negative mismatch (the degree to which bilayer width exceeds the length of the hydrophobic sequence) was calculated (Figure 7). The value of λmax was used as a crude measure of the fraction of peptide molecules in the TM configuration, based on the observation that λmax in the TM state falls in the 315-320 nm range, and that for the non-TM state usually falls in the 340-350 nm range. The amount of negative mismatch (in angstroms) was calculated for each peptide/lipid vesicle combination as described in the legend to Figure 7.

Figure 7A shows the behavior of the pL type peptides as a function of negative mismatch, combining the results in this study (triangles) with those of our previous study on pL_{10} and pL_{18} peptides (circles) (16). The dependence of λmax upon negative mismatch indicates that the TM state for pL sequences is tolerant of up to ~11-12 Å negative mismatch before the non-TM state predominates (Figure 7A). This degree of mismatch would be roughly equivalent to that for an 11-12 residue long hydrophobic sequence in a DOPC bilayer.

It should be noted that there was good agreement between λmax behavior as a function of bilayer width for the pL peptides studied here and those studied previously, with the behavior the pL_{12}, pL_{14} and pL_{16} falling between that previously determined for pL_{10} and pL_{18} [see Figure 1B in Ren et al. (16)]. [Note the change in nomenclature in this report: in Ren et al (16) the subscript used was larger by one residue because it designated the total number of hydrophobic core residues including the Trp.]

Figure 7B shows that the pattern of λmax vs. negative mismatch for the pLA-type peptides was in general similar to that for the pL-type peptides, with very little difference

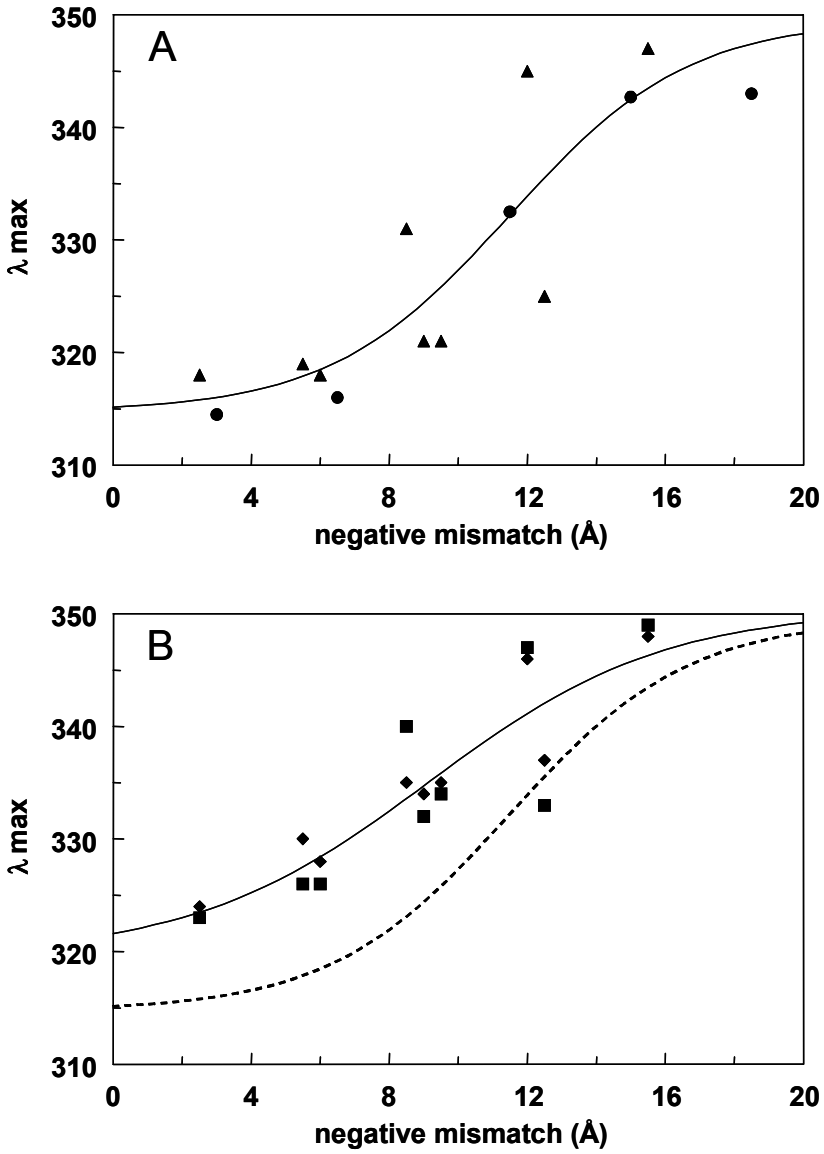

Figure 7. Dependence of Trp λmax upon the degree of negative mismatch between hydrophobic segment length and bilayer width. (A) pL peptides. Data from Figure 5 (▲) and for pL_{10} and pL_{18} peptides from Ren et al., 1999 (16) (●) in DOPC, DEiPC and DEuPC vesicles. Solid line shows sigmoidal fit to the data, with a limiting λmax of 350 nm at infinite negative mismatch using SlideWrite program. (B) pLA peptides. Data derived from Figure 5 is shown for p(LA)n (■) and pLnAn (♦) in DOPC, DEiPC and DEuPC vesicles. Dashed line shows the sigmoidal fit from panel A. for comparison. Negative mismatch was calculated from the formula: bilayer width (16) - hydrophobic sequence length = 1.5 Å × number of hydrophobic residues.

for the p(LA)n (squares) and pLnAn (diamonds) series. However, the TM configuration

or the pLA peptides was more sensitive to mismatch than that for the pL peptides (compare solid and dashed line in Figure 7B). For the pLA peptides the maximum degree of mismatch at which the TM state predominates (i.e. the midpoint of the sigmoidal curve) is about 9Å, which is equivalent to a 13h residue long hydrophobic sequence in a DOPC bilayer. In addition, there seems to be a slightly more gradual dependence of TM stability upon the degree of negative mismatch for the pLA peptides.
It should be noted that vesicle curvature is unlikely to have affected these conclusions. Control experiments using peptides inserted into MLV gave λmax vs. bilayer width results very similar to those obtained with SUV (Data not shown). Furthermore, it should be noted that the observed behavior of the peptides represents their equilibrium behavior. Control experiments using membrane-bound decane to reversibly increase bilayer width and alter the TM/non-TM equilibrium (83) demonstrated that (as judged by red-shifted λmax and increased acrylamide quenching) the membrane-inserted state formed by a short hydrophobic peptide (pL_{12}) rapidly and reversibly converted from the TM state to the non-TM configuration when bilayer width was altered *in situ* by decane addition or removal (data not shown).

Effect of Flanking Hydrophilic Residues on the Minimum Length Hydrophobic Sequence Forming a Stable TM Helix.

Because the identity of the hydrophilic residues flanking a hydrophobic sequence could influence the effective hydrophobic sequence length, the effect of different ionizable residues flanking the hydrophobic core upon stability of the TM configuration was studied. The behavior of pL_{12} sequences flanked on both on N- and C-termini either by 2 Lys, 1 Lys + 1 His, 2 His, or 1 His + 1 Asp was examined.

Figure 8 shows the dependence of Trp λmax upon bilayer width for these peptides at different pHs. At pH 4.0, where His and Lys both carry positive charges while Asp is largely uncharged [(49)and see below], peptides flanked with two Lys-residues ($^{KK}pL_{12}$), 1 Lys + 1His ($^{KH}pL_{12}$) or 2 His ($^{HH}pL_{12}$) showed similar patterns of λmax vs. bilayer width, with fluorescence most blue-shifted for peptide inserted into (16 carbon acyl chain) DPoPC vesicles (Figure 8A). [In this section the designation $^{KK}pL_{12}$ is used for the

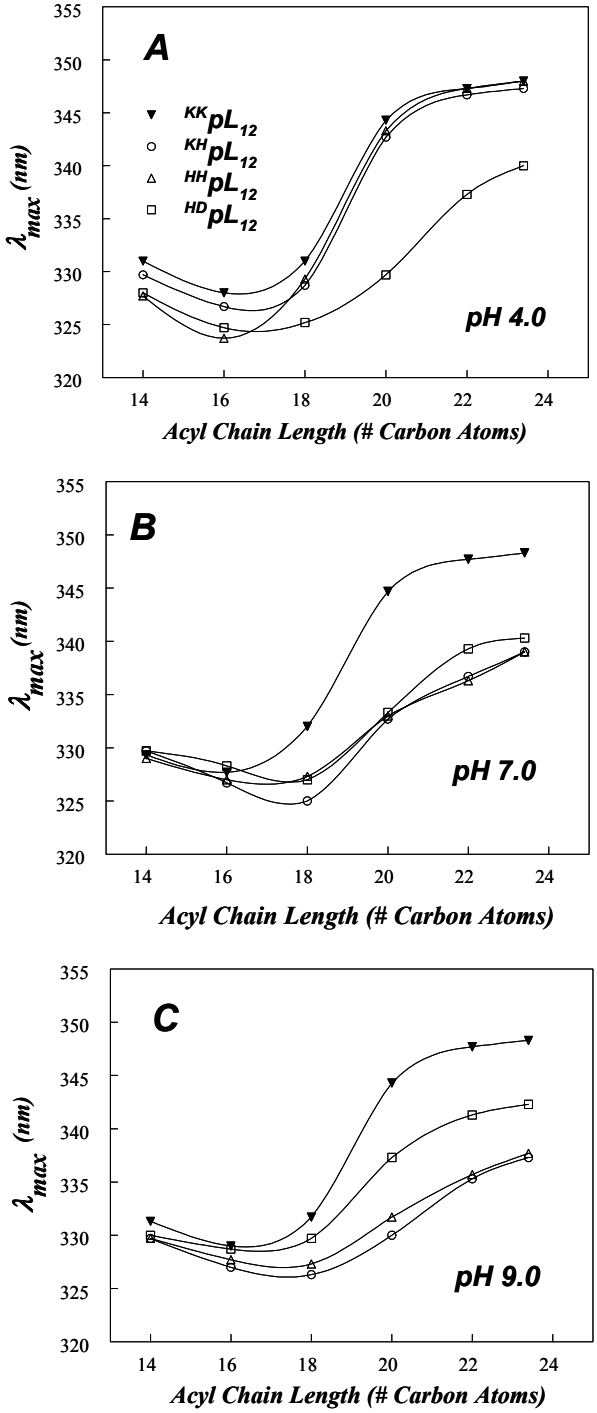

Figure 8: Effect of lipid acyl chain length on Trp emission λmax for pLeu peptides with varying flanking residues incorporated into phosphatidylcholine vesicles at: (A) pH 4.0; (B) pH 7.0 (C); pH 9.0. Symbols: (▲) $^{KK}pL_{12}$, (○) $^{KH}pL_{12}$, (Δ) $^{HH}pL_{12}$, and (□) $^{HD}pL_{12}$. The samples contained 2μM peptide incorporated into 500 μM lipid dispersed in pH-adjusted PBS. Average values from 3 samples are shown.

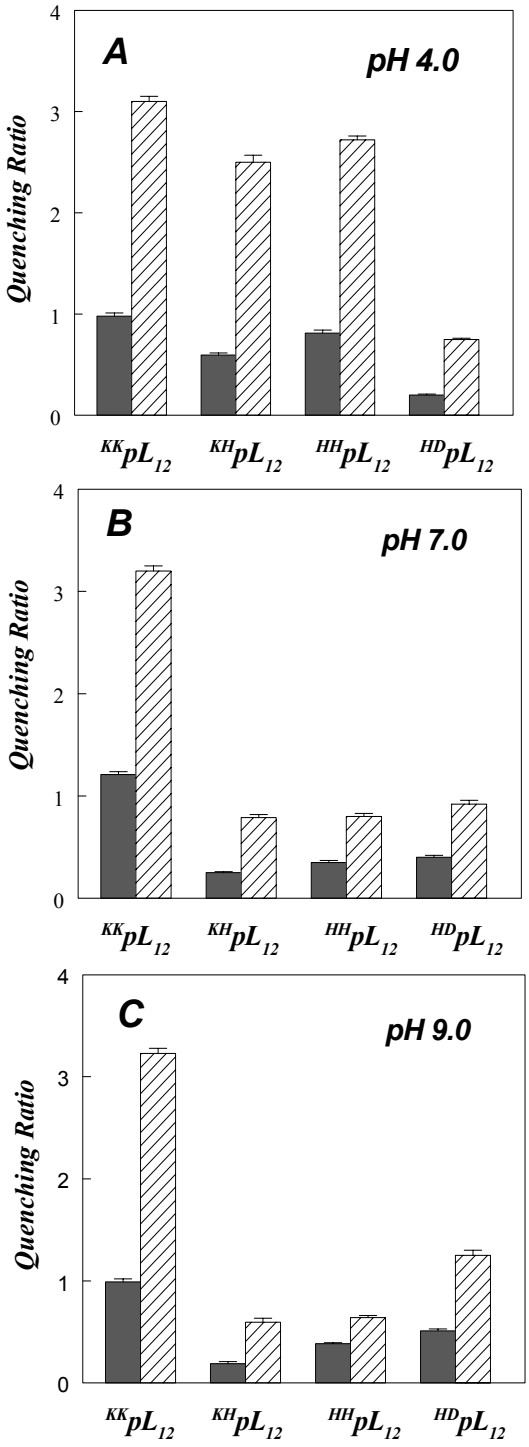

Figure 9: Quenching ratios for pL_{12} peptides with varying flanking residues incorporated into DOPC (filled bars) or DEuPC (striped bars) vesicles. (A) Q-ratios at pH 4.0, (B) Q-ratios at pH 7.0, (C) Q-ratios at pH 9.0. Samples contained 2 μM peptide incorporated into 500 μM lipid dispersed in PBS of different pH. Average and standard deviation for triplicates are shown

pL_{12} peptide for clarity.] In addition, in both DOPC and DEuPC bilayers Trp quenching data showed similar Q-ratios for these peptides (Figure 9A). As noted above in the case of $^{KK}pL_{12}$, these λmax and Q-ratio values are indicative of the formation of a mixture of TM and non-TM state in DOPC bilayers, and formation of the non-TM state in wider bilayers. The presence of a mixture of TM and non-TM conformations in DOPC vesicles for these three peptides is confirmed by the observation of large quencher-induced shifts (Table 3). Combined, this data confirms these three peptides have very similar TM stabilities at low pH. At most, $^{KH}pL_{12}$ and $^{HH}pL_{12,}$ gave λmax values in DOPC bilayers that are very slightly more blue-shifted, and Q-ratios slightly lower, than that for $^{KK}pL_{12}$, suggesting slightly more stable TM insertion than for $^{KK}pL_{12}$. These results indicate that the effect of flanking Lys^+ and His^+ residues upon the stability of the TM configuration do not differ greatly. This result is interesting because Lys snorkeling, which is the positioning of the Lys side chain so that its amino charge should be close to the bilayer surface (75), should help stabilize a TM configuration relative to a like-charged residue that cannot snorkel as well (i.e. His)(see Discussion).

Relative to the Lys- and His-flanked peptides at pH 4, the HD-flanked peptide ($^{HD}pL_{12}$) adopted a somewhat more stable TM topography when inserted into DOPC vesicles at pH 4, as judged by its more blue-shifted λmax and lower Q-ratios relative to the other peptides (Figures 8A and 9A, respectively). In fact, for $^{HD}pL_{12}$ in the TM state appears to predominate in DOPC as judged by the lack of strong quencher-induced shifts in λmax (Table 3). The effective length of the TM sequence also appears to be slightly longer than that of the other peptides, as judged by an increase in the acyl chain length at which λmax is at a minimum (Figure 8A). These results reflect the fact that it is easier to place an uncharged Asp near or within the polar/hydrophobic boundary of the bilayer than it is to place a charged residue near this boundary (105).

These experiments were repeated at pH 7 (Figures 8B and 9B) and pH 9 (Figures 5C and 6C). At pH 9 Lys will remain cationic (30), while the other flanking residues should deprotonate, so that His is uncharged and Asp is anionic. Consistent with this, $^{KK}pL_{12}$ did not exhibit any pH-dependence in λmax or Q-ratio, while all the other peptides exhibited a significant pH-dependence in these parameters (compare Figures 8A,

Table 3: Quencher-Induced Shifts in Trp Emission λmax for Membrane-Inserted Peptides in DOPC and DEuPC Bilayers: Peptides with Different Hydrophilic Flanking Residues.

Peptide	pH	Lipid	λmax (nm)[a]	λmax (nm) (acrylamide)	λmax (nm) (10-DN)	|Δλmax| [b] (nm)
$^{KK}pL_{12}$	4	DOPC	330	328	339	11
		DEuPC	347	347	349	2
$^{KH}pL_{12}$	4	DOPC	329	328	335	7
		DEuPC	347	346	348	2
$^{HH}pL_{12}$	4	DOPC	329	326	341	15
		DEuPC	347	346	348	2
$^{HD}pL_{12}$	4	DOPC	325	324	325	1
		DEuPC	337	336	339	3
$^{KK}pL_{12}$	7	DOPC	331	329	339	10
		DEuPC	347	347	348	1
$^{KH}pL_{12}$	7	DOPC	325	325	326	1
		DEuPC	337	335	340	5
$^{HH}pL_{12}$	7	DOPC	327	327	329	2
		DEuPC	337	333	337	4
$^{HD}pL_{12}$	7	DOPC	327	327	327	0
		DEuPC	339	339	342	3
$^{KK}pL_{12}$	9	DOPC	331	328	340	12
		DEuPC	347	347	349	2
$^{KH}pL_{12}$	9	DOPC	325	325	326	1
		DEuPC	335	333	338	5
$^{HH}pL_{12}$	9	DOPC	327	327	329	2
		DEuPC	336	332	337	5
$^{HD}pL_{12}$	9	DOPC	330	329	333	4
		DEuPC	341	339	341	2

[a] Reported λmax values are averages from three samples. The values were generally reproducible within ± 1nm. The λmax values have been rounded to whole numbers. [b] Δλmax is the absolute value of difference between λmax in the presence of acrylamide and λmax in the presence 10-DN

8B, and 8C and Figures 9A, 9B, and 9C). To confirm that there was a change in protonation, the pKa of the flanking residues was determined from the effect of pH upon the fluorescence of the membrane-inserted peptides (Figure 10). The lack of charge on His at pH 9 was confirmed by pH dependence of the fluorescence of $^{KH}pL_{12}$ and $^{HH}pL_{12}$ peptides, which indicated an apparent (His) pKa close to pH 7. A pH-dependent change in fluorescence was also observed for the $^{HD}pL_{12}$ peptide, and it appeared that the first (Asp) pKa occurred near pH 5-5.5 and the second (His) pKa near 8. This Asp pKa value is in agreement with previous studies on closely related sequences, which indicate that the pKa for an Asp residue near the end of a hydrophobic sequence occurs in the range 5-7 (49). In the case of $^{HD}pL_{12}$ His pKa may be increased (relative to the $^{KH}pL_{12}$ and $^{HH}pL_{12}$ peptides) by a favorable interaction between the His and the charged Asp residue.

When λmax (Figure 8C) and Q-ratio (Figure 9C) were measured for membrane-inserted $^{KH}pL_{12}$ and $^{HH}pL_{12}$ at pH 9 (i.e. when the His was uncharged) the values obtained indicated that the peptides had an increased tendency to form the TM state relative to that at pH 4, while for the $^{HD}pL_{12}$ peptide at pH 9 (i.e. when Asp was charged) a decreased tendency to form the TM state was detected relative to that at pH 4.

The stabilization of the TM state at pH 9 in the case of the $^{KH}pL_{12}$ and $^{HH}pL_{12}$ peptides is consistent with the loss at pH 9 of the quencher-induced shifts observed at low pH (Table 3). This indicates that these peptides no longer form a mixture of TM and non-TM states at pH 9. Similarly, the destabilization of the TM state for the $^{HD}pL_{12}$ peptide at pH 9 is consistent with the observation of increased quencher-induced shifts in Trp fluorescence in DOPC vesicles at this pH, indicating formation of co-existing TM and non-TM states (Table 3). These shifts are not seen at pH 4, where the TM state predominates. Thus, comparison of behavior at high and low pH shows that when flanking ionizable residues are charged, they destabilize the TM state to a much greater degree than when they are uncharged, at least for short hydrophobic helices (see Discussion).

At pH 7, λmax (Figure 8B), quenching (Figure 9) and quencher-dependent λmax shift data (Table 3) tended to be intermediate between that at pH 4 and pH 9, with the $^{KH}pL_{12}$ and $^{HH}pL_{12}$ sequences behaving more like they do at pH 9 than at pH 4. The

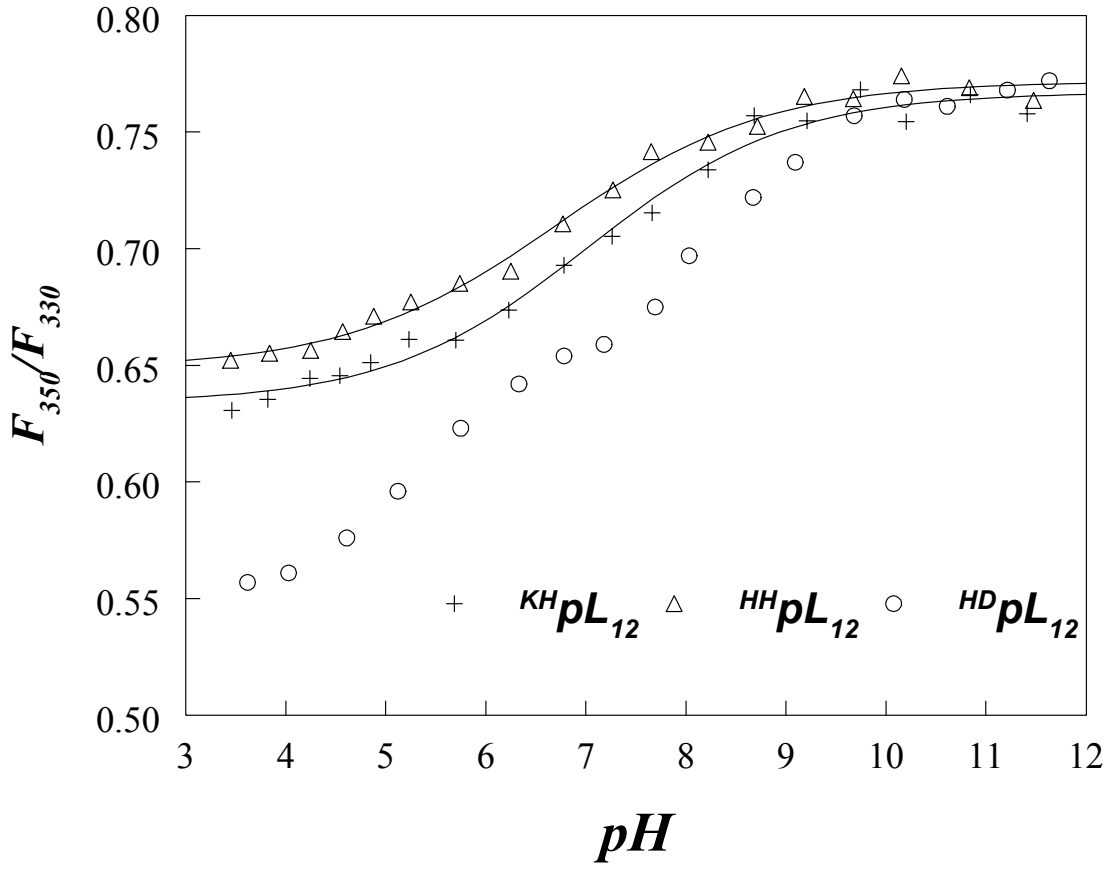

Figure 10. Effect of pH on the fluorescence emission of $^{HH}pL_{12}$, $^{KH}pL_{12}$, and $^{HD}pL_{12}$ peptides. Ethanol dilution vesicles were prepared as for other samples, except increasing all volumes 2.5-fold (final volume 2 ml) samples. After the fluorescence emission intensity was measured at 330 and 350 nm, pH was increased by adding 1-10 μl aliquots of either 0.5 or 2 M NaOH while mixing. After addition of each aliquot of NaOH, samples were allowed to equilibrate for approximately 2 min before fluorescence was remeasured. Previous experiments have shown that this to be a sufficient time for equilibration of pH across the bilayer (49). Intensities were corrected for background fluorescence and dilution by NaOH. The pH dependence of F_{350}/F_{330}, the ratio of fluorescence intensity at 350 nm and 330 nm (which is sensitive to changes in Trp λmax (49)) was measured. pKa values were estimated by fitting this ratio to a sigmoidal function using the SlideWrite program.

intermediate behavior pattern is consistent with the His, and perhaps Asp, being partially charged at pH 7

.

DISCUSSION

The Minimum Length Threshold for Transmembrane Helices: Dependence Upon Bilayer Width and Sequence Hydrophobicity.

This study investigated how negative hydrophobic mismatch and sequence combine to affect the relative stability of TM and non-TM configurations of short membrane-inserted hydrophobic helices. The results show that for highly hydrophobic sequences, 11-12 consecutive hydrophobic residues is about the minimum to form a TM configuration sufficiently stable to be the predominant configuration (i.e. 11-12 is the minimum TM length) in a bilayer with a biologically relevant width (i.e. DOPC). Less hydrophobic sequences have to be longer to form a stable TM state. However, the effect of hydrophobicity was relatively modest. For an alternating Leu and Ala sequence, 13 consecutive residues is the minimum necessary to form a predominantly TM state in DOPC vesicles. This sequence is of more biological relevance, because the hydrophobicity of an alternating Leu/Ala sequence is more typical of TM sequences in membrane proteins (28). By assuming a near-linear relationship between minimum TM length and hydrophobicity, we can derive a formula for estimating minimum TM length for a hydrophobic sequence surrounded by charged residues. Using our TM tendency scale (28) as a measure of hydrophobicity gives the formula: Minimum TM length = 15.6 – (2.1 × Average TM Tendency Value of Core Sequence) …….*Equation 1*

As an alternative, using the biological hydrophobicity scale of Hessa *et al*. (10)gives the formula: Minimum TM length = 14.3 + (4.5 × Average Biological Hydrophobicity value of Core Sequence)……*Equation 2*

(These equations have been corrected for Trp and Gly residues in our peptides, see below.) Since biological hydrophobicity was derived for residues near the bilayer center, it should be most accurate equation for synthetic sequences with deep Trp or Tyr residues, such as those used in this study, while TM tendency is more appropriate for natural sequences in which Trp and Tyr are generally located close to the edge of the

bilayer.

We do not yet know over how wide a range of sequences these equations are useful. At most, they should only be valid for moderately-to-highly hydrophobic sequences, and they can *not* be applied to weakly hydrophobic sequences, as illustrated by the relationship of the energetics of TM insertion vs. hydrophobic sequence length, shown schematically in Figure 11. The free energy of burial of hydrophobic residues will basically be proportional to the number of hydrophobic residues multiplied by the average per residue free energy of burial. However, the energetic behavior of the hydrophilic flanking residues is more complex. In the region of negative mismatch, the unfavorable free energy associated with burial of hydrophilic flanking residues (or equivalently, that of any compensating bilayer distortions, see below) should become progressively worse as hydrophobic sequence length decreases. In the region of positive mismatch, there should still be a residual unfavorable free energy associated with locating hydrophilic flanking residues in the polar headgroup region close to the bilayer surface, because the polar headgroup forms a more non-polar environment than aqueous solution, but this free energy should be only weakly dependent on the length of the hydrophobic sequence. The reasons for this are that the polar headgroup region is not highly hydrophobic and any helix tilting to maintain burial of hydrophobic residues under conditions of positive mismatch (see below), will tend to result in a nearly constant headgroup position relative to the bilayer surface (as shown schematically in Figure 8). Because of this, weakly hydrophobic sequences should tend to exhibit a high minimum TM length value that is strongly dependent upon the exact value of sequence hydrophobicity (Figure 11). This sensitivity to hydrophobicity would be somewhat ameliorated if helix tilt is disfavored due to disturbed lipid packing by tilted helices, and/or if there is a strong tendency of weakly hydrophobic residues to protrude into aqueous solution (66).

The weak dependence of minimum TM length upon hydrophobicity for moderately-to- highly hydrophobic sequences means that correcting for the destabilizing effect of the Trp that was placed in the center of the hydrophobic sequences (10) did not

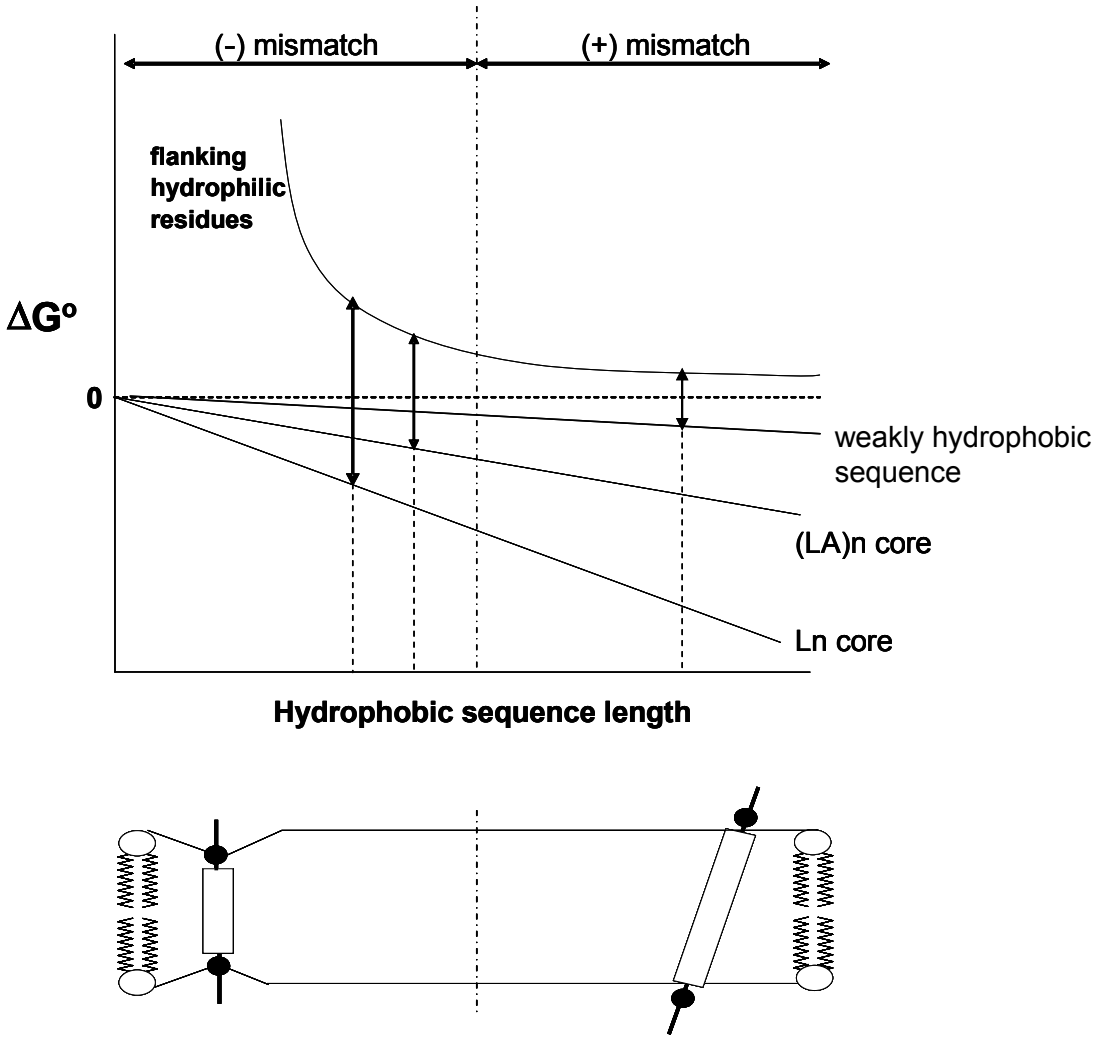

Figure 11. Schematic illustration of the energetics of TM helix stability as a function of hydrophobic sequence length. ΔG^o is the free energy of the TM configuration relative to that of the non-TM configuration. The energetic contributions of the hydrophobic core and flanking hydrophilic sequences are shown as separate components. The vertical dashed-and-dotted line represents the boundary between negative and positive mismatch. The TM configuration of the helix is shown below the graph under conditions of negative (left) and positive (right) mismatch. The double arrows are shown at the minimum TM length (given by the intercept of the dashed lines and x-axis), which is the point at which ΔG^o for membrane burial of the hydrophobic core (down arrow) = ΔG^o for membrane burial of the flanking hydrophilic residues (up arrow). Notice that for a weakly hydrophobic sequence the minimum TM length would fall in the region of positive mismatch and would be very sensitive to the hydrophobicity of the peptide core.

significantly modify the value of minimum TM length. Based on the hydrophobicity of Trp (10), the decrease in hydrophobicity due to a Trp should only have increased the effective minimum TM length for our peptides by about 0.2 residues (calculation not shown).

Furthermore, this effect is more than cancelled out by the Gly residue that was contiguous to the hydrophobic sequences [Gly was present so that the results could be compared to previous studies (10, 16, 24) - the Gly was originally a purity marker for chemical synthesis (106)]. Based on the conclusion that a polar residue flanking a hydrophobic sequence increases the effective length of a hydrophobic sequence by about half as much as a non-polar residue (see below), the Gly should have decreased the apparent minimum TM length of the hydrophobic core by ~ ½ a residue. Thus, overall the core sequences used in this study should only behave slightly differently than sequences with pure Leu or pure LeuAla hydrophobic cores.

Difference in Energetic Effects of Leu and Ala Upon TM vs. Non-TM Membrane Insertion.

Ala is significantly less hydrophobic than Leu, and peptides with hydrophobic cores composed entirely, or almost entirely, of Ala are not stable in the TM state (10, 50, 51, 107). This raises the question: what was the loss of TM stability due to Ala in the pLA peptides? Estimating the fraction of peptide molecules in the TM and non-TM configurations state under conditions of 10Å of negative mismatch (the fraction in the non-TM configuration being roughly given by the red shift of λmax at 10Å mismatch relative to λmax at no mismatch divided by the limiting red shift at infinite mismatch relative to that no mismatch, see Figure 4) allows calculation of both an approximate ΔG^o for the TM/non-TM equilibrium and a $\Delta\Delta G^o$ for the difference in TM stability between a pL and pLA sequence. [It should be noted that we did not correct average λmax values for the difference in intensity in the TM and non-TM states because we found that the intensity in the non-TM state was only 5-20% less than in the TM state (data not shown).]

This calculation yields an estimate a $\Delta\Delta G^o$ of ~0.50 kcal/mole more stable TM insertion for a pL sequence relative to a pLA sequence. For $p(LA)_7$, this would correspond to 0.07 kcal/mole per Leu-to-Ala substitution. However, upon conversion of

the TM to non-TM state, Ala at the end of a hydrophobic sequence will not change their membrane depth/exposure to aqueous solution significantly, and of the remaining Ala on the average about half will point towards the center of the bilayer in the non-TM state, and so would not be likely to contribute much to the difference in energy between TM and non-TM states. In the case of $p(LA)_7$ these considerations result in an estimate of 0.2 kcal/mole less stable TM insertion per Leu-to-Ala substitution for residues moving form a deep to shallow location upon conversion of the TM state to the non-TM state.

Even this value is smaller than the $\Delta\Delta G^o$ predicted by the biological hydrophobicity scale for a Leu to Ala substitution (0.66 kcal/mole) (10). In the case of biological hydrophobicity the non-TM state is likely to be the solution state, and it has been found that ΔG^o for partition between aqueous environments and the bilayer surface is about half of the ΔG^o for partition between aqueous to hydrophobic environments (105). Thus, $\Delta\Delta G^o$ predicted by biological hydrophobicity might be as low as 0.33 kcal/mole. The remaining difference between this value and that we observe (0.2 kcal/mol) may involve the location of our peptides in the non-TM state. Our sequences were much more hydrophobic than those used to estimate energy for peptides at the membrane-solution interface (105), and so our peptides are likely to be located more deeply in the non-TM state, decreasing the difference between free energy in the TM state and surface-bound non-TM state.

The value of $\Delta\Delta G^o$ we obtained should not be over-generalized. First, the number of Leu to Ala substitutions affected by the change from a TM to non-TM state depends on helix length. Second, the accuracy of these calculations is limited by the fact that λmax is not an exact measure of the fraction of peptide in a TM configuration due to factors such as sequence-dependent differences in the λmax of a pure TM form and pure non-TM form. This latter factor certainly is responsible for the scatter in the λmax data in Figure 4 at very high mismatch values. On the other hand, the weighting of average λmax in mixtures of TM and non-TM forms due to conformation-dependent differences in Trp intensity (quantum yield), is not of much concern because the peptides used exhibited only small intensity changes in different configurations (data not shown). In any case, the analysis of λmax shifts provides a useful first estimate of free energy

differences.

The Minimum Length Threshold for Transmembrane Helices: Effect of the Hydrophilic Residues Flanking the Hydrophobic Sequence.

As noted above, the membrane burial of hydrophilic residues flanking the hydrophobic sequence is likely to be a major factor destabilizing TM insertion of short TM helices. Consistent with this, the experiments in this report demonstrated that when ionizable residues flanking the hydrophobic sequence are charged, they destabilize the TM state to a much greater degree than when they are uncharged. The strongly destabilizing effect of charged flanking residues is not surprising because in the TM state their local environment should be more hydrophobic than in aqueous solution, even if not nearly as hydrophobic as that in the core of the bilayer. However, it was surprising that under conditions in which the flanking residues were charged the His-flanked peptides had a similar TM stability as Lys-flanked peptides. It might be predicted that Lys would be less destabilizing because it has a long side chain and so can position its charged amino group at a much shallower location than the depth of the Lys backbone (i.e. snorkel) (60). A possible explanation is that although His cannot snorkel to as great a degree as Lys, its positive charge should be somewhat delocalized, which would reduce destabilization of the TM state.

It was also found that for both $^{KH}pL_{12}$ at high pH and $^{HD}pL_{12}$ at low pH, conditions in which the pLeu sequence is immediately bounded by *uncharged* ionizable residues, the TM state was considerably more stable than at pH values at which these residues were charged. In both these cases, λmax vs. bilayer width profiles and Q-ratio values fell between those of pL_{12} and pL_{14} sequences (compare Figures 5 and 8). Thus, the effective minimum sequence length to form a predominantly TM state was about one residue longer when the two residues flanking the sequence were charged than when they were uncharged. This fits a rule in which the effective minimum TM configuration-forming length equals the number of hydrophobic residues plus about ½ of the number of uncharged hydrophilic residues flanking the hydrophobic core. Studies of sequences in which the identity of the flanking uncharged hydrophilic residues are varied will be required to confirm and refine this conclusion.

Insights into the Details of TM and Non-TM Topographies From Trp Depth.

It should be noted that the depth of Trp in membranes is affected by factors in addition to whether sequences are TM or non-TM. Peptide orientation in the shallow, non-TM state is one such factor, as we found previously for longer helices (49). In the non-TM state, membrane-bound helices orient to place their more polar face towards the aqueous solution. Helical wheel representations of the sequences used in this study (not shown), indicate that for the 13 hydrophobic residue sequences, Lys and Trp are aligned on one helix face to a greater degree than for the other length sequences studied. If the Lys-containing face points toward the aqueous solution, the Trp would also do so, and this would explain why the non-TM state for the 13 hydrophobic residue sequences gave a more red-shifted λmax and higher Q-ratio than the other sequences.

A factor that may affect Trp depth in the TM state is how firmly a TM state is anchored in a specific position. A peptide forming a TM state with ends that are not tightly anchored at the bilayer surface might be able to undergo considerable movement perpendicular to the plane of the membrane, allowing formation of a distribution of TM structures in which the Trp is not always located exactly at the center of the bilayer even though the Trp is in the center of the hydrophobic sequence (Figure 12). Since such movements should be less energetically costly for peptides with core sequences that are not highly hydrophobic, they should be larger for LeuAla sequences than for all Leu sequences. This might contribute to the red shift observed for the pL_8A_8 and $p(LA)_8$ sequences relative to the pL_{16} sequence in DOPC, even if all three peptides form fully TM states.

Bilayer Response to Negative Mismatch: Effect Upon the Conformational Stability of Short TM Helices and Biological Implications.

Natural membranes have nonpolar cores of about 30Å in width, and about 20 hydrophobic residues are believed to be required to span the bilayer. However, the latter

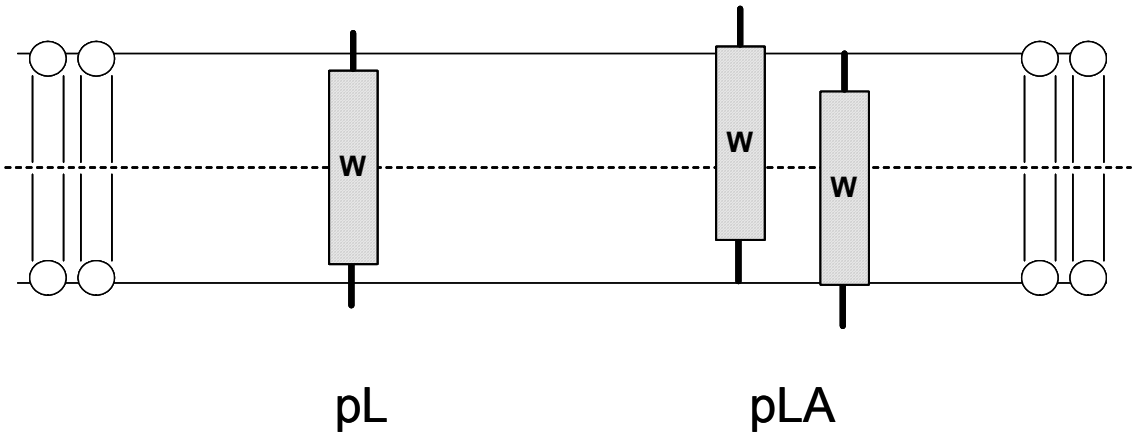

Figure 12. Schematic illustration of possible difference in anchoring of the TM state for pL (left) and pLA (right) peptides. Trp is shown as a W. Note that the average Trp distance from the bilayer center is greater for the pLA peptides even though average Trp location is at the bilayer center in both cases. Distortion in bilayer structure induced by peptides is not shown

number overlooks the ability of lipid bilayers to respond to mismatch. The observation in this report that short hydrophobic sequences have the ability to maintain a TM configuration in the presence of considerable negative mismatch can be most easily explained by mismatch-induced changes in bilayer structure. This explanation is consistent with studies showing that membrane proteins can maintain native structure and function to significant degree in the presence of mismatch (70, 108-111). Such studies suggest that forced hydrophobic matching occurs because TM proteins deform the surrounding lipid bilayer, which has flexible acyl chains, to adjust its hydrocarbon thickness to try to match the length of the hydrophobic surface of the protein (60, 70-72, 112). Indeed, studies in model membranes have established that hydrophobic helix length can affect local bilayer structure in this fashion when there is mismatch between the length of the hydrophobic sequence and the width of the hydrophobic segment of the bilayer (59, 60).

On the other hand, some of the ability to tolerate mismatch is likely to involve adjustments in protein structure (60). For example, when helices are especially long (i.e. under conditions of *positive* mismatch), changes in helix tilt might compensate for mismatch (60). For single TM helices significant changes in tilt as a function of bilayer width have inferred indirectly (16), and directly observed for some sequences (24, 61-65), although in other cases tilt changes have been reported to be rather small (66).

If the maximum amount of negative mismatch that can be tolerated is affected by the limits of lipid deformation, then mechanical bilayer properties, which have already been proposed to affect function via changes in TM helix dynamics (113), could be a major factor in controlling the amount of mismatch that can be tolerated by short TM helices. Since membranes rich in cholesterol and sphingolipids are likely to be less easily deformed than those rich in unsaturated phospholipids, this could be of biological significance. Differential sorting of short and long TM helices to different membranes in eukaryotic cells (see Introduction), is thought to be due to the fact that the plasma membrane bilayer is significantly wider than that of the Golgi or endoplasmic reticulum(72, 93). This width difference might be due to a combination of differential

content of cholesterol, differential lipid acyl chain saturation, or TM protein effects (72). In any case, because these membranes also have different amounts of sphingolipids and cholesterol, they may differ in their ability to distort in response to mismatch, and this could also impact the dependence of sorting upon TM helix length.

Other Factors that May Alter Minimum TM Length In Vitro and In Vivo.

In addition to average core hydrophobicity and flanking residue hydrophilicity, minimum TM length might be affected by several variables *in vivo*. One such variable examined in this report was the effect of a hydrophobicity gradient along the peptide sequence. We found very little difference between LeuAla sequences with uniform hydrophobicity and LeuAla sequences with a hydrophobicity gradient. This implies that it is not necessary to sacrifice TM stability in order to design a sequence with a hydrophobicity gradient. In contrast, a recent study has shown that the amphiphilicity of a sequence should have a very significant effect on TM stability (114). Helix-helix interactions are another obvious variable that would affect the stability of the TM configurations. If there are favorable interactions in the TM state relative to the surface state, the TM state should be stabilized. [In this study, we used flanking sequences that minimize helix-helix interaction via electrostatic repulsions (78)]. A third important variable, noted above, is the structure of the membrane lipids. In preliminary studies we have found that lipid headgroup structure can stabilize or destabilize TM insertion and thus alter minimum TM length (K. Shahidullah and E. London, unpublished observations). Finally, it should be noted that kinetic trapping during biosynthesis might alter minimum TM length *in vivo*. If, during biosynthesis, a short TM sequence is more stable within the translocon than in the lipid bilayer, it might be permanently trapped in the TM state after release from the translocon if surrounded by hydrophilic sequences that are too large to cross a lipid bilayer. For all these reasons, formation of stable or metastable TM helices with hydrophobic cores shorter than 11 residues long cannot be ruled out (56).

CHAPTER 4

THE CONTROL OF TRANSMEMBRANE HELIX TRANSVERSE POSITION IN MEMBRANES BY HYDROPHILIC RESIDUES

Transmembrane α-helices are the primary membrane-inserted segments of membrane proteins. Because isolated TM helices are independently folding units, the dependence of their behavior upon sequence can yield fundamental insights into the membrane protein structure/function relationship. Indeed, studies of individual TM helices have led to important advances in understanding membrane protein folding, topography, interactions with lipids, and interactions with other helices (16, 24, 50, 65, 82, 100, 102, 104, 115-117)

TM helices are predominantly composed of hydrophobic residues that are buried in the membrane. Polar and ionizable (charged) residues are less abundant in TM segments because the energetic cost involved in burying a hydrophilic residue in the nonpolar environment of the bilayer. Nevertheless hydrophilic residues within a TM sequence are very important in determining helix behavior. In many cases, hydrophilic residues have been shown to promote TM helix association (30, 32, 37, 39, 78, 118). The ability of the hydrophilic residues to form hydrogen bonds (31, 119) or salt bridges (45) with other membrane inserted hydrophilic residue drive these TM helix-helix interactions. Hydrophilic residues can also alter the topography of a membrane-inserted hydrophobic sequence. The introduction of hydrophilic residues in a hydrophobic sequence destabilizes the TM state. This can result in change from a TM topography to a membrane-bound non-TM state, i.e. one in which the helix moves close to the bilayer surface(10, 16, 24). In some cases, helices with intermediate hydrophobicity can equilibrate between TM and non-TM states (16, 24, 29, 120, 121).

However, even when the TM state is maintained in presence of highly hydrophilic residues, hydrophilic residues can still affect the position of a helix within the bilayer such that there is a transverse shift (i.e. a change in the distance of amino acid residues from the center of the bilayer) so that the hydrophilic residues locate at (or close to) the bilayer surface (44, 45, 47-49, 85). This shift can shorten the effective length of the hydrophobic segment that spans the lipid bilayer (47-49). Transverse shifts are important because membrane proteins, unlike soluble proteins, are positionally-constrained in a fixed plane relative to the plane of the membrane. Two separate sequences (e.g. on two different helices or two different membrane proteins) may only interact properly if they are located in the same plane. Thus, TM helix position can control membrane protein

function via a mechanism that has no analog for soluble proteins.

The possibility that changes in the TM position of proteins might be functionally important was pointed out long ago (122), and there already have been several examples in which transverse shifts in TM helix position appear to have an important role in function**.** In the case of bacterial chemoreceptors it has been well-documented that shifts in TM helix position control signal transduction by modulating kinase activity inside the cell (123-125). Similarly, in integrins, the activation of the receptor by ligand binding results in movement of the part of a TM helix out of the lipid bilayer, effectively shortening the TM helix by 4-5 residues (126). Based on the difference in the transverse position of TM hydrophobic helices containing charged and uncharged Asp we have suggested that Asp ionization state could alter TM helix transverse positions as a protein cycles between acidic vacuoles and the plasma membrane in a functionally important manner (49).

In pioneering studies, differences in the ability of several types of hydrophilic residues to shift TM helix position in the translocon was measured by von Heijne and colleagues using glycosylation mapping (9, 45-48). In the present report, transverse shifts in TM hydrophobic helices were measured for the complete series of hydrophilic residues within lipid bilayers. To do this a series of membrane-inserted peptides suitable for detecting shifts in bilayers with physiologically-relevant bilayer widths was designed. The fluorescence of a Trp residue located at the center of the hydrophobic sequence was used to monitor the behavior of the peptides. We found that the extent of shift depends on the identity of the hydrophilic residue, and that even a weakly polar residue, such as Gly or Ser, can induce significant shifts in helix position. These results imply that the identity of the TM insertion boundaries of a TM sequences can be a much more ambiguous and even dynamic parameter than generally realized. In many cases, membrane protein TM helices are likely to be able to undergo facile switching between TM states that differ in their transverse position and function.

RESULTS

Using Fluorescence Emission λmax and Fluorescence Quenching to Define the Topography of the Membrane-Inserted Hydrophobic Helices.

The fluorescence properties of a Trp residue located at the center of a hydrophobic sequence was used to define the topography of membrane-inserted helical peptides (16, 24, 29, 49). There are several topographies that helical peptides can form in membranes. A full TM orientation in which the Trp locates at or near the bilayer center (Figure 13, center), results in blue-shifted Trp emission λmax (320-325 nm for the peptides in this study) (16, 24). If the peptide adopts a non-TM membrane-bound topography, in which it resides close to the bilayer surface, then the Trp locates close to the surface (Figure 13, left) and the λmax red shifts strongly (to as high as 345-350 nm) (16, 24). The exact λmax value in the non-TM state value depends upon how deeply the peptide is buried, and upon whether the Trp faces aqueous solution or the bilayer interior when the peptide is in the non-TM state (29, 49). Values of λmax between those for the TM and non-TM states are observed for mixtures of TM and non-TM topographies (16, 24), and for a shifted TM state wherein only a part of the hydrophobic sequence forms the membrane-spanning segment (e.g. to allow a polar residue to locate close to the bilayer surface), and so the Trp is shifted to an intermediate depth (29, 49)(Figure 13, right). These two alternatives can be distinguished (see below).

Interpretation of λmax results is aided by combining them with more direct measurements of Trp depth. To do this, a dual fluorescence quenching method was used (83). This method utilizes two quenchers of Trp fluorescence, acrylamide and 10-DN. Acrylamide, although membrane permeable (83), resides primarily in aqueous solution and preferentially quenches the fluorescence of Trp residues near the membrane surface, while 10-DN, a membrane-inserted quencher, preferentially quenches the fluorescence of Trp buried in the membrane bilayer (83). The ratio of acrylamide quenching to 10-DN quenching (quenching ratio or Q-ratio) responds nearly linearly to Trp depth in the bilayer, with a low Q-ratio (as low as 0.05-0.1) indicating a deeply located Trp near the center of the bilayer, while a high Q-ratio (1.0-3.0) usually indicates a Trp near the bilayer surface (83).

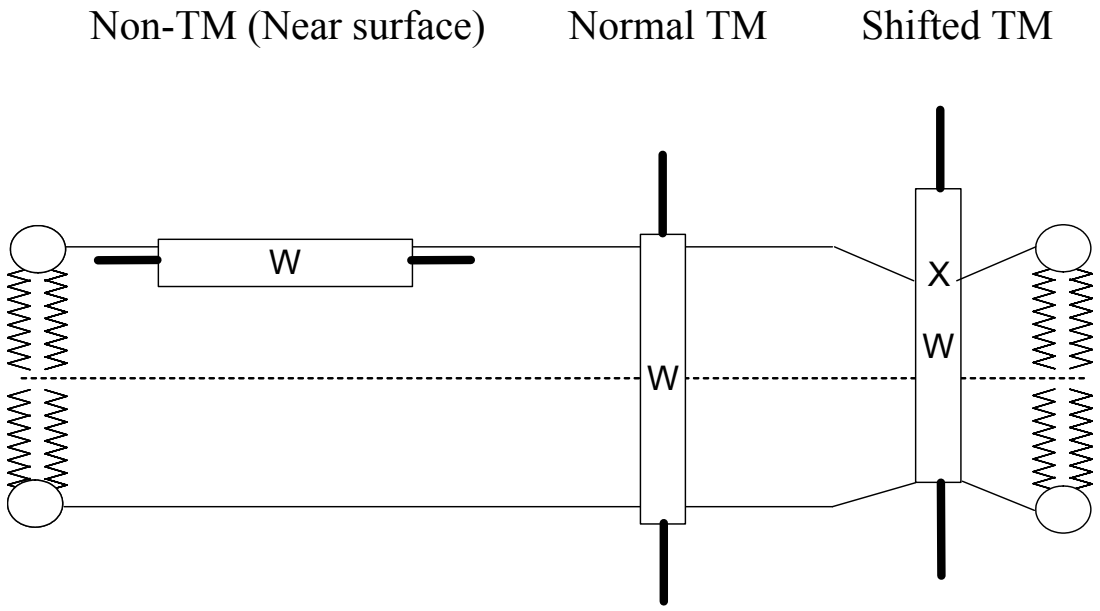

Figure 13. Schematic comparison of three distinct topographies of hydrophobic helices (rectangles) in lipid bilayers. The position of a Trp (W) residue located in the center of the hydrophobic sequence is shown. The dashed line represents the plane of the center of the bilayer. Left: Non-TM state in which the helix and W residue lie close to the bilayer surface. Center: Normal TM state in which there is near-match between helix length and bilayer width and W residue is at the bilayer center. Right: Shifted-TM state in which there is a near match between the total hydrophobic helix length and bilayer width, but in which part of the helix has moved out of the core of the bilayer in order for a hydrophilic residue (X) to locate nearer the bilayer surface. There is negative mismatch when the X residue shifts to the bilayer surface, and a resulting symmetric distortion of the bilayer (48). Notice that in this case the W residue is at an intermediate depth.

As in the case of λmax, intermediate Q-ratios can arise either from peptides adopting a mixture of conformations with shallow and deep Trp depths, or from peptides adopting a shifted TM conformation with an intermediate Trp depth.

Cases in which a Trp is at an intermediate depth can be distinguished from cases in which mixtures of shallow and deep Trp are present by measurement of quencher-induced shifts in Trp λmax (29, 49, 83). If a membrane-inserted peptide forms co-existing deep and shallow conformations, then its Trp emission spectrum will be a composite of blue- and red-shifted emission spectra arising from the deep and shallow conformations, respectively. In such samples, acrylamide preferentially quenches the shallow Trp, inducing a blue shift in λmax. Conversely, 10-DN preferentially quenches the deep Trp, inducing a red shift. In such cases, the difference in λmax in the presence of acrylamide and 10-DN can be up to 15 nm (29, 49, 83). On the other hand, for a homogenous population with a single intermediate Trp depth, the difference in λmax in the presence of acrylamide and 10-DN is very small (0-2 nm) (29, 49, 83). It should be noted that due to incomplete quenching, the λmax values in the presence of a quencher often are not the exact values of the pure shallow state or pure deep state.

Topography of Membrane-Inserted p(LeuAla) Peptides With a Hydrophilic Substitution: Effect Upon Trp Depth in DOPC Vesicles.

The peptides studied were of the pLA-type (16, 24, 29, 30, 49, 78), consisting of 25-residues with a helix-forming 21-residue hydrophobic core composed of alternating L and A residues, a Trp at the center of the hydrophobic sequence, a single variable (X) residue located five residues from the N-terminal end of the hydrophobic sequence, and flanking di-Lys sequences at both its N and C-termini [general sequence: acetyl-KKLALA**X**ALALAWLALALALALAKK-amide)] (Table 4). This sequence was chosen because it is long enough form a stable TM structure even if the TM segment begins after residue X (i.e. if the TM sequence is formed by residues 8-23 (16). In addition, a shift between the topography in which the entire hydrophobic sequence (residues 3-23) forms the TM segment and one in which residues 8-23 form the TM segment results in an easily-detected change in Trp depth. Sequences with X = L (parental peptide), or a "hydrophilic" residue: S, T, G, Y, P, Q, N, H, R, K, E or D, were compared.

Table 4. List of Hydrophobic Peptides Used in this Study.

Peptide	***Primary Sequence***
$p(LA)_{10}$	Acetyl-$K_2(LA)_5W(LA)_5K_2$-NH_2
$pLAG_7$	Acetyl-$K_2(LA)_2GA(LA)_2W(LA)_5K_2$-$NH_2$
$pLAY_7$	Acetyl-$K_2(LA)_2YA(LA)_2W(LA)_5K_2$-$NH_2$
$pLAS_7$	Acetyl-$K_2(LA)_2SA(LA)_2W(LA)_5K_2$-$NH_2$
$pLAT_7$	Acetyl-$K_2(LA)_2TA(LA)_2W(LA)_5K_2$-$NH_2$
$pLAH_7$	Acetyl-$K_2(LA)_2HA(LA)_2W(LA)_5K_2$-$NH_2$
$pLAP_7$	Acetyl-$K_2(LA)_2PA(LA)_2W(LA)_5K_2$-$NH_2$
$pLAK_7$	Acetyl-$K_2(LA)_2KA(LA)_2W(LA)_5K_2$-$NH_2$
$pLAR_7$	Acetyl-$K_2(LA)_2RA(LA)_2W(LA)_5K_2$-$NH_2$
$pLAQ_7$	Acetyl-$K_2(LA)_2QA(LA)_2W(LA)_5K_2$-$NH_2$
$pLAN_7$	Acetyl-$K_2(LA)_2NA(LA)_2W(LA)_5K_2$-$NH_2$
$pLAE_7$	Acetyl-$K_2(LA)_2EA(LA)_2W(LA)_5K_2$-$NH_2$
$pLAD_7$	Acetyl-$K_2(LA)_2DA(LA)_2W(LA)_5K_2$-$NH_2$
$pLAS_8$	Acetyl-$K_2(LA)_2LS(LA)_2W(LA)_5K_2$-$NH_2$
$pLAN_8$	Acetyl-$K_2(LA)_2LN(LA)_2W(LA)_5K_2$-$NH_2$
$pLAE_8$	Acetyl-$K_2(LA)_2LE(LA)_2W(LA)_5K_2$-$NH_2$
pA^4E_7	Acetyl-$K_2A_4EA(LA)_2W(LA)_5K_2$-NH_2
pG^4E_7	Acetyl-$K_2G_4EA(LA)_2W(LA)_5K_2$-NH_2

These peptides were purchased from Anaspec Inc. (San Jose, CA). Peptides were purified via reverse-phase-HPLC using a C18 column with 2-proponal/water/0.5% v/v trifluoroacetic acid as the mobile phase as described previously (103). Peptide purity was confirmed using MALDI-TOF mass spectrometry (Proteomics Center, Stony Brook University). We estimated that final purity was on the order of 90% or better. After drying the HPLC fractions the peptides were stored in 1:1 (v/v) 2-proponal/water at 4 ºC. Peptide concentrations were measured by absorbance spectroscopy on a Beckman DU-650 spectrophotometer, using ε for Trp of 5560 $M^{-1}cm^{-1}$ at 280 nm.

Helix position was estimated from Trp depth, using both the Trp λmax and fluorescence quenching assays described above. Figure 14 shows λmax and Q-ratio data for the peptides incorporated into vesicles composed of DOPC (which has C18:1 acyl chains) at pH 7. For almost all X residues, λmax (325-330nm) and Q-ratio (0.05-0.25) values (Figures 14A and 14B, respectively) indicate a relatively deep Trp location consistent with a primarily TM topography. The λmax and Q-ratio values are very closely correlated with each other, confirming that both parameters measure Trp depth (Figure 15). Averaging the results from λmax and Q-ratio indicates that Trp depth becomes progressively less deep in the order X= L<G~Y<T<R~H<S<P<K<Q~E<N<D. In almost all cases there are no significant quencher-induced shifts in λmax (Δλmax) (Table 5), indicating that the decrease in Trp depth when X is hydrophilic is associated with a shift in the TM position of the helix to locate the X residue closer to the surface of the bilayer, rather than formation of a population in a non-TM state. An exception to this is X = D, which forms a significant amount of the non-TM state in DOPC vesicles as judged by quencher-induced λmax shifts. This suggests that the D residue induces such a large shift in the TM position that the residual TM hydrophobic segment is too short to be *fully* stable in the TM state in DOPC bilayers. This interpretation is supported by measurements of the effective TM length for this peptide (see below). There are also some peptides (X = S, K, and perhaps R) in which there are modest quencher-induced shifts in DOPC vesicles. These cases involve two blue-shifted states as judged by λmax values in the presence of quencher, suggesting that they are cases in which un-shifted and shifted TM states co-exist.

The absolute change in Trp depth in the presence of a hydrophilic X residue in Å can be roughly estimated by using standard curves derived in previous studies for the dependence of Trp depth on λmax (a 2 nm red shift equals slightly less than a ~1Å decrease in Trp depth) and Q-ratio (an increase of 0.1 in Q-ratio is equivalent to slightly more than a ~1Å decrease in Trp depth) (24, 83). This reveals that the near-maximal change in depth (i.e. for X = N relative to X = L) corresponds to a movement of Trp of ~3-4 Å closer to the bilayer surface. This movement is close to the 3.4 Å predicted when a hydrophilic residue moves to the membrane interface and so the effective length of the TM segment decreases from 21 to 16 residues (see Discussion).

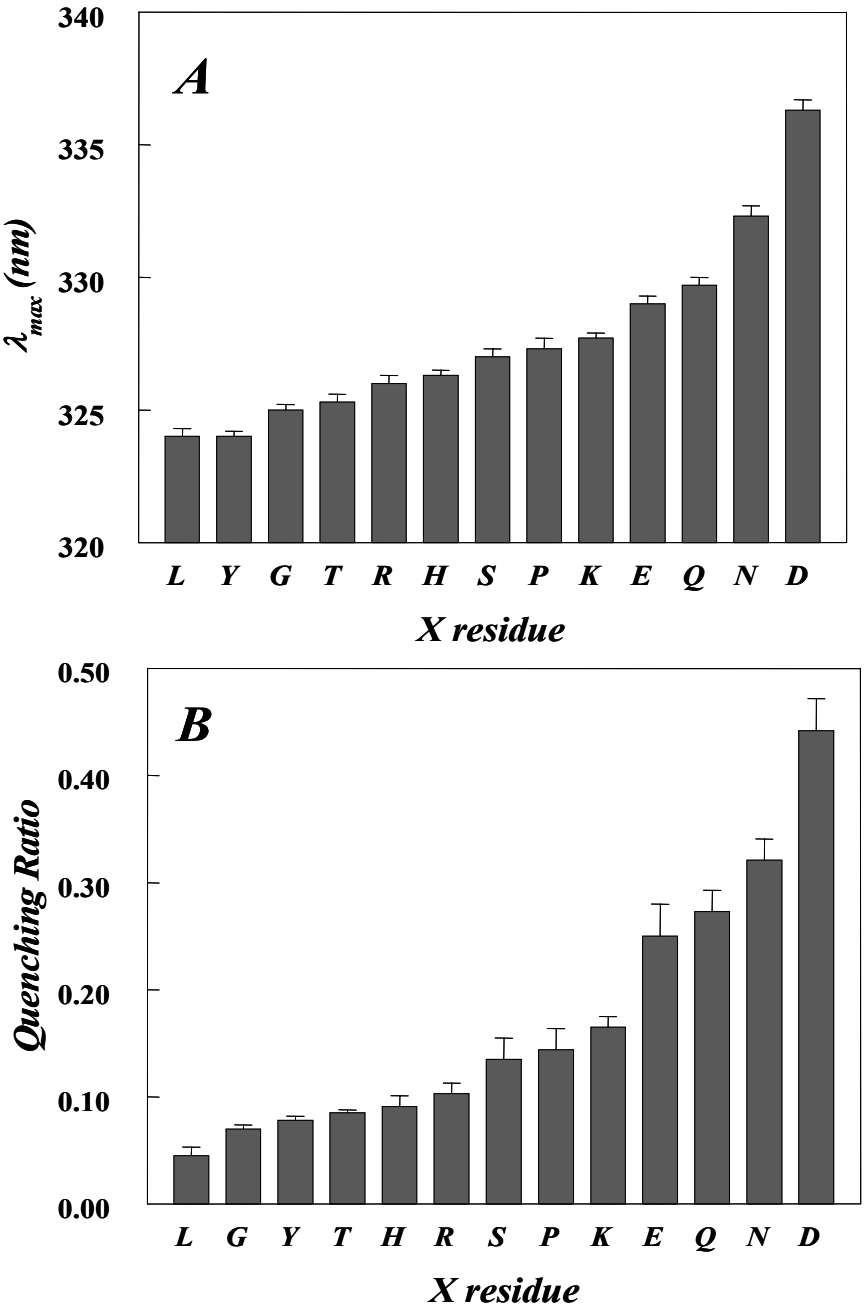

Figure 14. Trp λmax and quenching ratio for pLA peptides with single substitutions at position 7 when incorporated into DOPC vesicles at pH 7.0. (A) Trp emission λmax. (B) Quenching ratio. Samples contained 2 μM peptide incorporated into 200 μM lipid dispersed in PBS. Average values from three to six samples and standard deviations are shown.

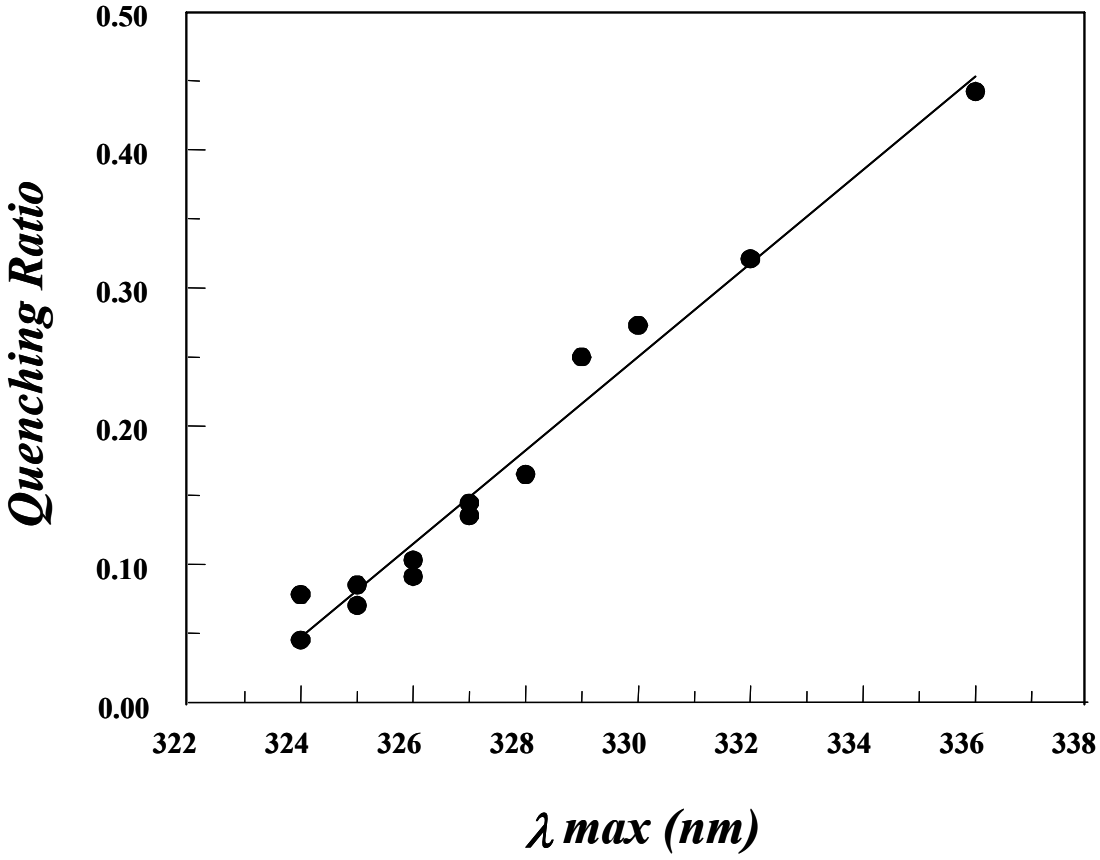

Figure 15. Correlation between λmax and quenching ratio for peptides incorporated into DOPC vesicles at pH 7.0. Data is from Figure 14.

Table 5. Quencher-induced shifts in Trp emission λmax and $L_{TM\ eff}$ values for pLA peptides with single substitutions at position 7 when incorporated into vesicles at pH 7.0.

X Residue	Acyl Chain Length[a]	λ_{max} (nm) [b]	λ_{max} (nm) Acrylamide	λ_{max} (nm) 10-DN	$\Delta\lambda$max [c](nm)	$L_{TM\ eff}$ [d] (number of residues)
Leu	18	324	325	325	0	20.9
	20	323	322	323	1	
	22	327	327	331	4	
Gly	18	325	324	325	1	19.8
	20	326	325	329	4	
	22	332	325	339	14	
Tyr	18	324	322	324	2	18.4
	20	328	324	330	6	
	22	339	335	344	9	
Thr	18	325	324	326	2	18.5
	20	330	325	330	5	
	22	338	326	342	16	
His	18	326	326	327	1	18.0
	20	340	335	343	8	
	22	345	343	346	3	
Arg	18	326	325	328	3	17.7
	20	340	331	347	16	
	22	347	347	348	1	
Ser	18	327	326	330	4	18.9
	20	331	326	331	5	
	22	340	337	342	5	
Pro	18	327	327	328	1	17.8
	20	337	337	346	9	
	22	344	343	345	2	
Lys	18	328	326	330	4	17.6
	20	338	335	345	10	
	22	347	347	347	0	

Continued…

Glu	18	329	329	331	2	17.3
	20	340	336	344	9	
	22	345	342	347	5	
Gln	18	330	329	330	1	17.1
	20	341	336	347	12	
	22	347	346	348	2	
Asn	18	332	332	333	1	17.2
	20	341	337	343	6	
	22	347	347	347	0	
Asp	18	336	333	340	7	16.6
	20	344	345	348	3	
	22	348	346	348	2	

[a]18 = DOPC vesicles, 20 = DEiPC vesicles and 22 = DEuPC vesicles. [b]λmax values are average from 3-6 samples and the λmax values were reproducible to within ± 1nm. [c]Δλmax is the difference between λmax in the presence of 10-DN and that in the presence of acrylamide. [d]Note that the $L_{TM\ eff}$ does not apply to a specific acyl chain length given on the left.

It is important to note that the dependence of λmax and Q-ratio upon X residue identity do not exactly parallel X residue hydrophilicity. Other variables, such as the ionization state of a side chain and side chain 'snorkeling' [i.e. formation of a conformation in which long side chains orient such that the polar group at the end of the side chain locates as close as possible to the bilayer surface (75)] affect the extent of shift (see below).

Topography of Membrane-Inserted p(LeuAla) Peptides With a Hydrophilic Substitution: Effect Upon Trp Depth in DEuPC and DEiPC Vesicles.

The pattern of the change in λmax and Q-ratio as a function of X residue identity was different when the peptides were incorporated into vesicles composed of DEuPC (which has C22:1 acyl chains), a lipid forming much wider bilayers than DOPC (16) (Figure 16 and Table 5). In DEuPC vesicles, there is negative hydrophobic mismatch, because the width of the hydrophobic core of the bilayer (~ 35Å) exceeds the length of the full hydrophobic sequence (21 residues, ~ 31.5Å). Several studies have shown that negative mismatch destabilizes TM states relative to non-TM states (16, 24, 29, 30, 49). Consistent with this, the peptides exhibit much more red-shifted λmax and much higher Q-ratios than observed in DOPC vesicles. The red shift and Q-ratio are again affected by the identity of the X residue, and increase in the order X = L < G < T< Y < S < P < H < R ≤ K ≤ Q ≤ E ≤ N < D. This order is somewhat different than that in DOPC vesicles (the reasons for this are discussed below). The differences between peptides with X= H, R, K, Q, E, N and D are very small, with the values of λmax (345-348 nm) and Q-ratio (3-3.5) being indicative of a Trp location very close to the bilayer surface. This indicates that these seven sequences are fully forming the non-TM topography in DEuPC vesicles. However, these peptides remain bound to the DEuPC vesicles, as their fluorescence is still accessible to 10-DN quenching and their Trp emission λmax (346-348 nm) is not consistent with being dissolved in aqueous solution (on our instrument the λmax for Trp in water is about 355 nm). Nor does there seem to be a sub-population of these peptides in solution, as there are no significant quencher induced-λmax shifts when λmax = 345-348 nm (Table 5).

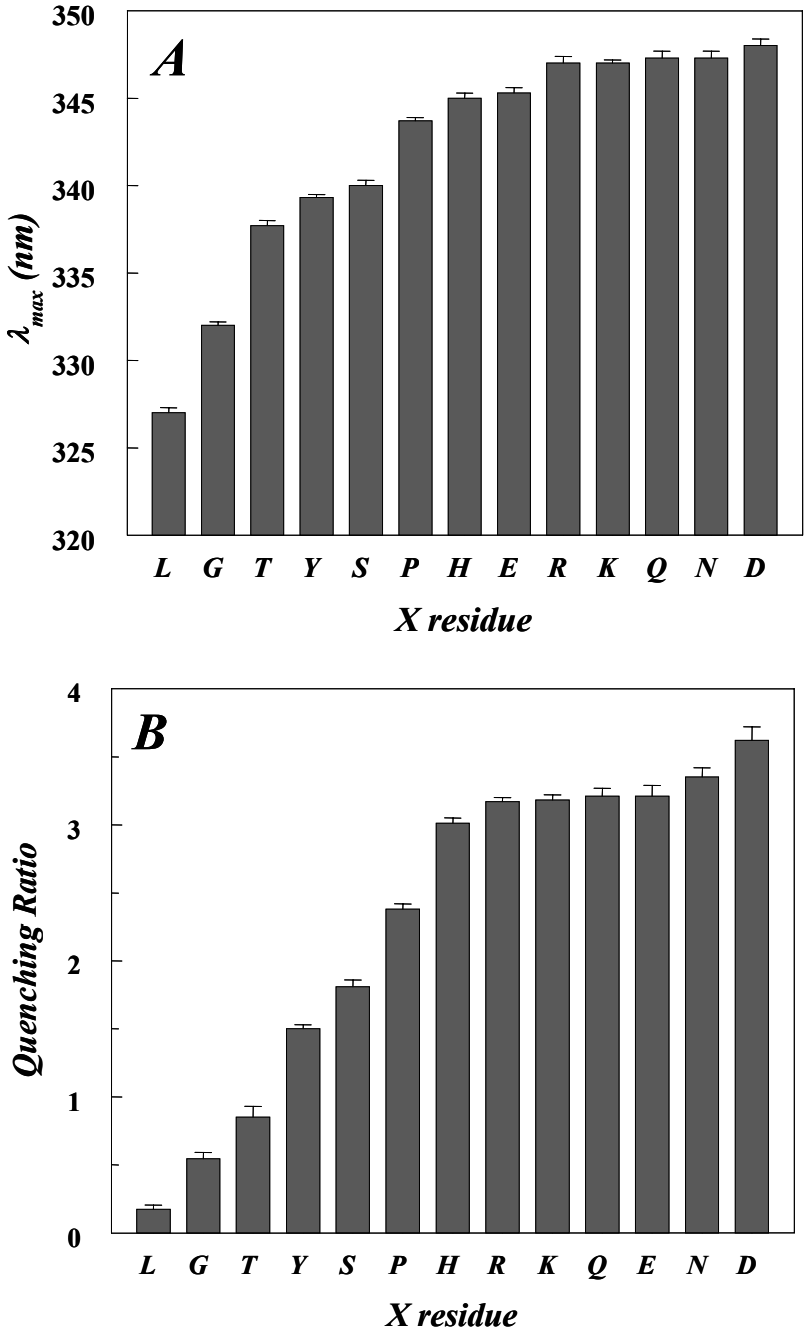

Figure 16. Trp λmax and quenching ratio for pLA peptides with single substitutions at position 7 when incorporated into DEuPC vesicles at pH 7.0. (A) Trp emission λmax. (B) Quenching ratio. Samples contained 2 μM peptide incorporated into 200 μM lipid dispersed in PBS. Average value from three to six samples and standard deviations are shown.

The peptides that exhibit intermediate λmax values in DEuPC vesicles (with X= G, Y, T or S) form mixtures of the non-TM and TM states as judged by large quencher-induced λmax shifts (Δλmax) (Table 5). As noted above, such shifts are characteristic of co-existing shallow and deep Trp depth populations. This conclusion is confirmed by the behavior of the peptides in vesicles composed of DEiPC (which has C20:1 acyl chains), a lipid forming bilayers with a width intermediate between that of DOPC and DEuPC (16). It would be expected that the TM state would have an intermediate stability in DEiPC vesicles, and consistent with this Table 5 shows that almost all of the peptides incorporated into DEiPC vesicles tended to give λmax and Q-ratio values intermediate between those in DOPC vesicles and DEuPC vesicles, and very large quencher-induced large shifts in λmax, indicative of TM/non-TM mixtures.

Analysis of Δλmax as a function of the λmax in the absence of quencher illustrates the correlation of quencher-induced λmax shifts with the relative amounts of TM and non-TM topographies present (Figure 17). The largest quencher-induced λmax shifts should occur when the populations of TM and non-TM states are nearly equal, which corresponds to λmax ~ 335 nm (in absence of quencher), half-way between λmax in the TM state and non-TM state (345-348 nm). This pattern is observed in Figure 17 for peptides incorporated into DEiPC and DEuPC vesicles. In contrast, when the peptides are incorporated into DOPC vesicles, peptides with intermediate λmax values tend to exhibit small Δλmax values (Table 5), consistent with the presence of a single shifted TM population.

Using the Effect of Bilayer Width Upon Helix Behavior to Investigate the Topography of Membrane-Inserted Helices.

Shifts in helix position were also detected by the decrease in the number of residues spanning the lipid bilayer when the X residue moves closer to the bilayer surface (Figure 13**,** right). This decrease in length can be detected via the decrease in the stability of the TM state under conditions of negative mismatch. The degree of negative mismatch is controlled by the length of the membrane spanning sequence and the width of the bilayer. The TM state of a short hydrophobic helix is destabilized in much thinner

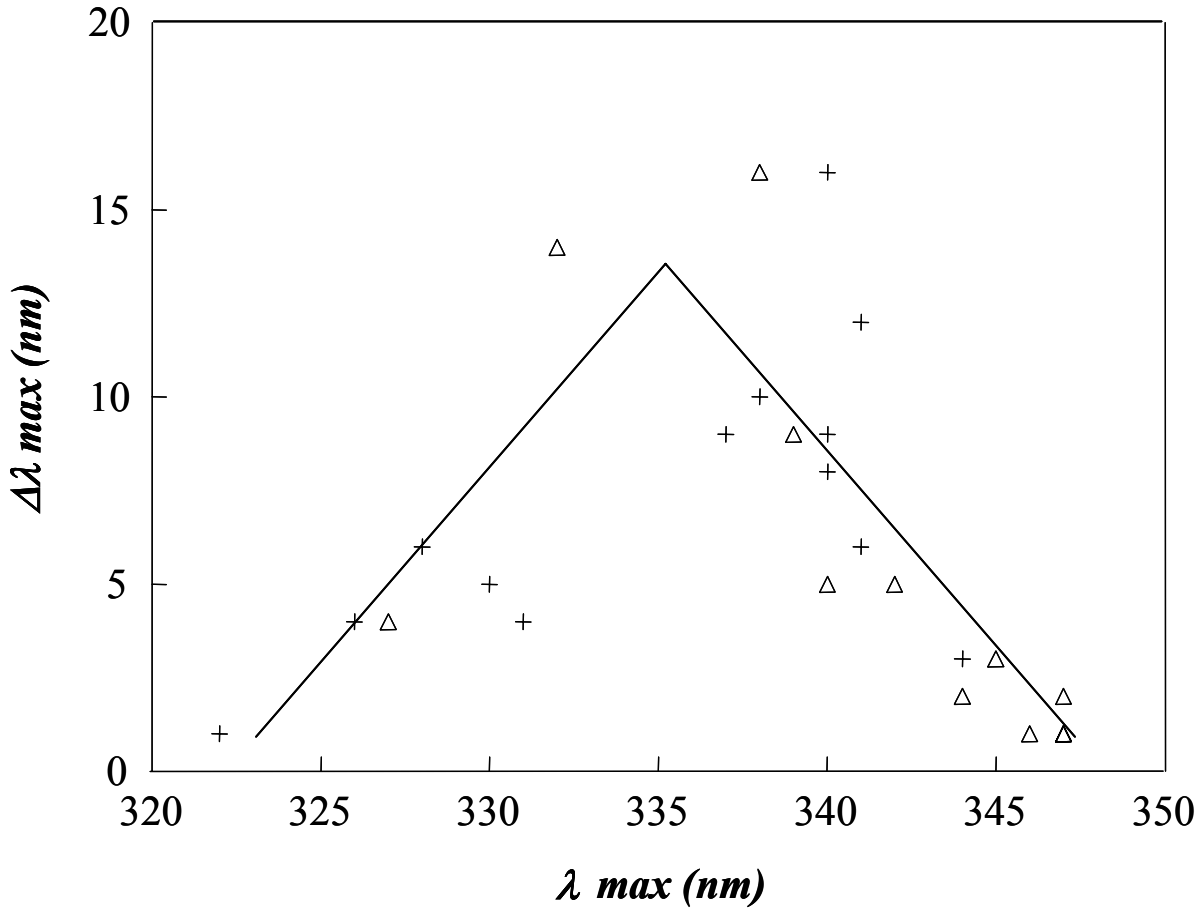

Figure 17. Dependence of the shift induced by quenchers upon λmax in the absence of quencher for peptides incorporated into DEuPC (Δ) or DEiPC (+) vesicles. Data from Table 5.

bilayers than is the TM state of a long hydrophobic helix (16, 24, 29, 49). Previous studies have shown that Trp fluorescence is most blue-shifted at about the maximum bilayer width at which the TM state is not significantly destabilized by negative mismatch (see Figure 4) (16, 24). Trp fluorescence becomes red-shifted in wider bilayers due to formation of the non-TM state, in which Trp locates shallowly. Fluorescence also generally red shifts, although to a lesser degree, in thinner bilayers (i.e., in conditions of *positive* mismatch between helix length and bilayer width) (16, 24). This is due to the fact that the distance of a Trp at the center of a bilayer to the membrane surface automatically decreases as bilayer width decreases. In addition, there can be a modest red shift due to (weak) oligomerization under conditions of positive mismatch in thin bilayers (16, 24, 30).

The bilayer width at which Trp fluorescence was most blue shifted was defined as the "effective TM length" ($L_{TM\ eff}$). This is the bilayer width (in units of acyl chain length) at which there is a near-match between the width of the hydrophobic core of the bilayer and the length of the hydrophobic sequence. $L_{TM\ eff}$ can also be expressed in Å or as the number of residues that span this bilayer width (see Chapter 2).

It should be noted that the decrease in the length of a TM segment in the presence of a hydrophilic X reside can exceed both the decrease in X residue depth and the change in Trp depth, by simple geometrical factors described in the Discussion. In addition, $L_{TM\ eff}$ sometimes differs from the actual length of the membrane spanning sequence (L_{TM}), especially in the presence of snorkeling X residues. This difference can contain valuable information (see Discussion.)

Effective TM Length of Membrane-Inserted p(LeuAla) Peptides With a Hydrophilic Substitution.

Figure 18 shows the effect of bilayer width on the Trp emission λmax for the various pLA peptides at pH 7.0. The parental peptide (X = L) has a profile with a λmax minimum in DEiPC bilayers, indicative of an $L_{TM\ eff}$ ~31.5Å (16). This is corresponds to the predicted $L_{TM\ eff}$ for the 21-residue (residues 3-23) hydrophobic core sequence of this peptide (21 residues × 1.5 Å rise per residue = 31.5Å). The presence of hydrophilic X substitutions resulted in the λmax minimum occurring in thinner bilayer widths.

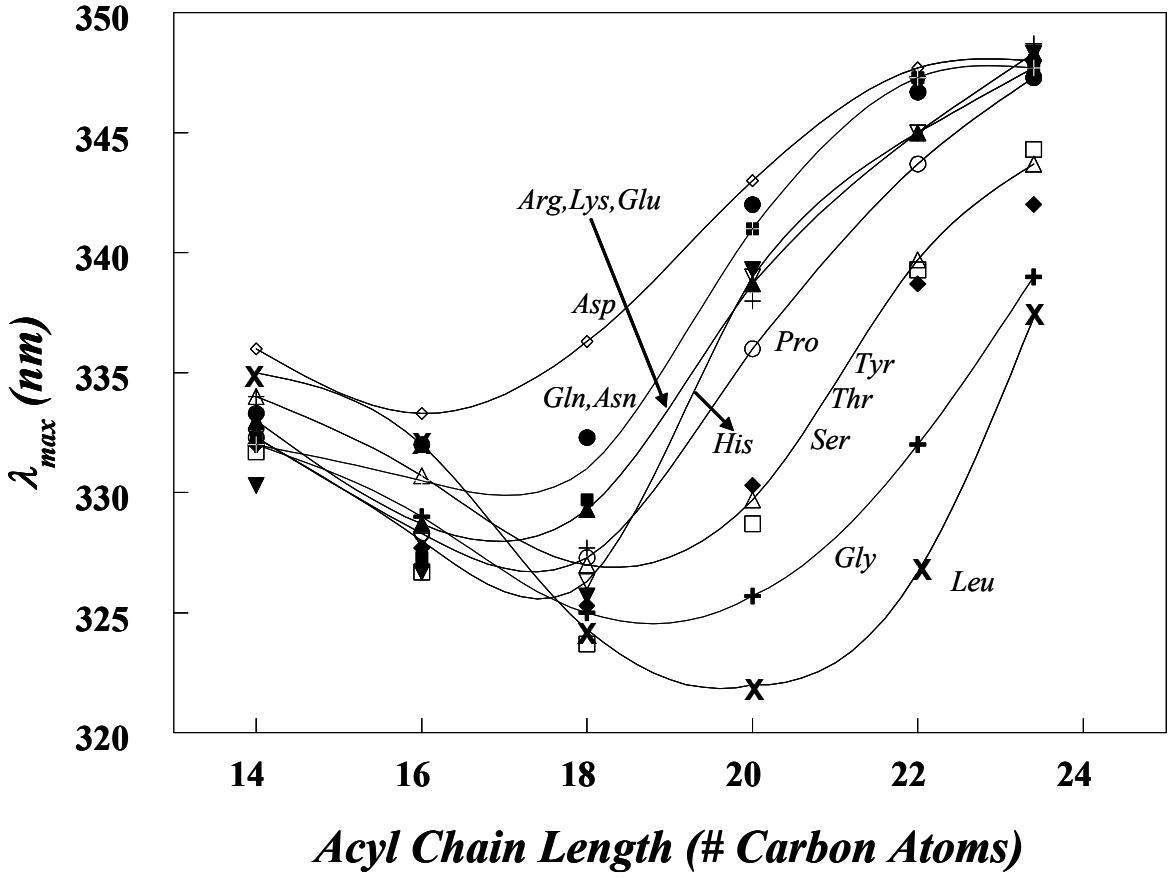

Figure 18. Effect of lipid acyl chain length upon Trp emission λmax for pLA peptides with single substitutions at position 7 at pH 7. The substitutions are Leu (X); Gly (+); Tyr (□); Ser (Δ); Thr (♦); Pro (○); His (▽); Lys (+); Arg (▼); Glu (▲); Asn (●); Gln (■) and Asp (◊). The lipids used were a series of di n:1 phosphatidylcholines, in which n is the number of carbon atoms per acyl chain and the number 1 indicates that the acyl chains were monounsaturated. Samples contained 2 μM peptide incorporated into 200 μM lipid dispersed in PBS. The λmax values shown are averages from three to six samples. λmax values were reproducible to within ±1nm.

This shows that the hydrophilic substitutions decrease the effective length of the TM segment. $L_{TM\ eff}$ values for pLA peptides with various X residues are given in Table 5. In the most extreme case, when X = D, $L_{TM\ eff}$ decreases to 16.6 residues (25Å), close to the value (16 residues, 24Å) expected when the X residue shifts to the bilayer surface and the TM segment extends from residue 8 to 23. Intermediate $L_{TM\ eff}$ values, indicative of an intermediate extent of helix shift, are observed for the other X residues. The overall order in which $L_{TM\ eff}$ decreases is: X = L > G > T > Y ~ S > P > K ~ E ~ H ~ R ~ Q ~ N > D. This is very similar, but not identical, to the order of the dependence of Trp depth in DOPC vesicles upon X residue type. In particular, residues having long side chains (e.g. K and R) tend to have a relatively larger effect on $L_{TM\ eff}$ than on Trp depth. This behavior is likely to be related to snorkeling, and this subject is explored in detail in the Discussion section.

How pH Affects the Topography of the p(LA) Peptides with Ionizable Residues.

In order to investigate the effect of charge on an ionizable X residue upon TM helix behavior, the first step was to measure their pK_as. To do this, samples containing peptides inserted into vesicles prepared at low pH were titrated with base as described previously (30, 49). Changes in ionization were detected by pH-induced changes on Trp emission (49) (Figure 19). The pK_a values in DOPC vesicles were 5.5, 6.7 and 7.0 for X= Asp, Glu and His residues, respectively, and are no more than 0.1 units higher in DEuPC vesicles (data not shown). The pK_a values for X = Lys and Arg residues could not be determined, presumably because they occur at too high a pH and/or are masked by deprotonation of Lys residues flanking the hydrophobic sequence.

Next, λmax and Q-ratio were measured for samples containing X = D, E, and H peptides when into DOPC vesicles under conditions in which the X residues would be fully protonated (pH 4.0), or fully deprotonated (pH 9.0) based on their pK_a values (Figure 20). Trp depth was shallowest when the X residues were charged (pH 4 for the X = H peptide and at pH 9 for the X = D and X = E peptides), and thus most hydrophilic. This indicates that in the charged state H, D, and E residues resist burial within the lipid bilayer and thus induce large shifts in TM helix position. For X = H^+ the change in Trp depth relative to X = L was ~2.5-3 Å. It is difficult to specify Trp depth for the TM

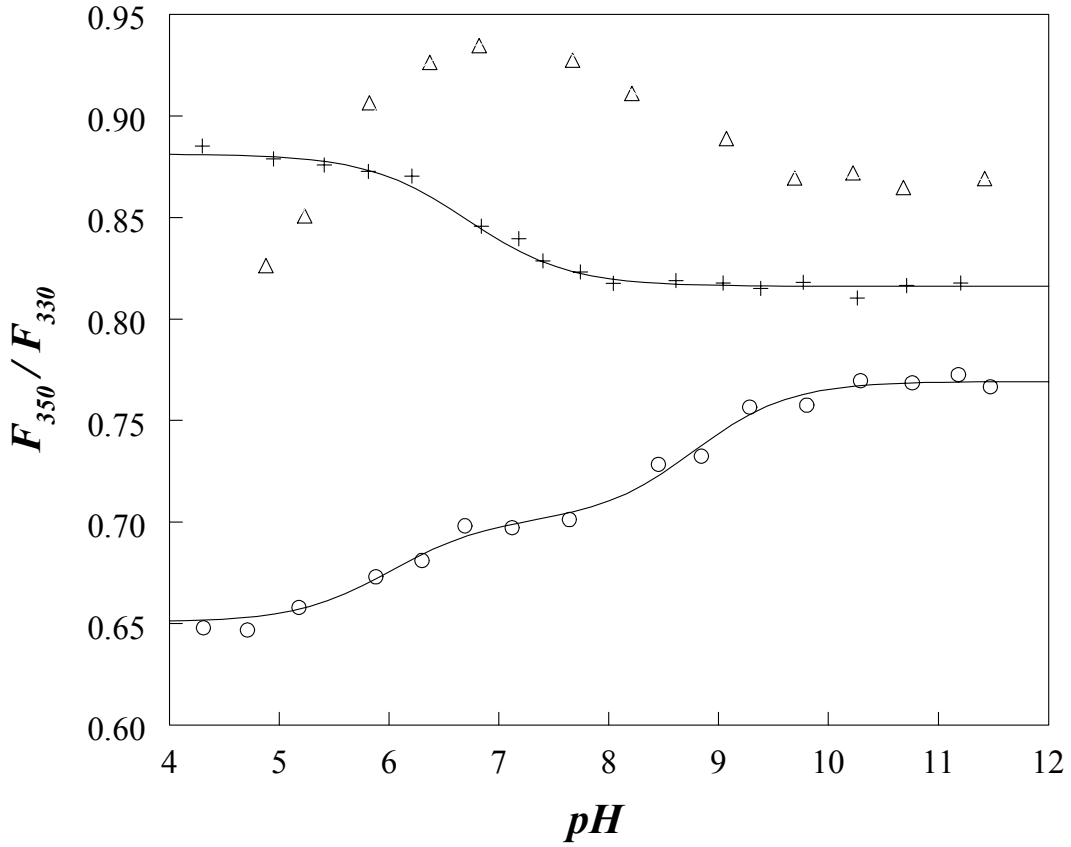

Figure 19. Effect of pH on the fluorescence emission of pLA peptides with Glu, Asp or His in position 7 when incorporated into DOPC vesicles. Vesicles were prepared at low pH as for other samples, except increasing all volumes 2.5-fold (final volume 2 ml). After fluorescence emission intensity was measured at 330 and 350 nm, pH was increased by adding 1-10 μl aliquots of either 0.5 or 2 M NaOH while mixing. After addition of each aliquot, samples were allowed to equilibrate for approximately 2 min before fluorescence was remeasured. Intensities were corrected for background fluorescence and dilution by NaOH. The pH dependence of F_{350}/F_{330}, the ratio of fluorescence intensity at 350 nm and 330 nm [which is sensitive to changes in Trp λmax (49)], was calculated. pKa values were estimated by fitting this ratio to a single or double sigmoidal function using the SlideWrite program. The pKa values estimated were 5.5 and 8.6 for X= Asp peptide (Δ); 6.7 and 8.8 for X= Glu peptide (○) and 7.0 for X = His peptide (+)**.** The second pKa, when observed, is likely due to deprotonation of one or more of the Lys residues flanking the hydrophobic sequence (49).

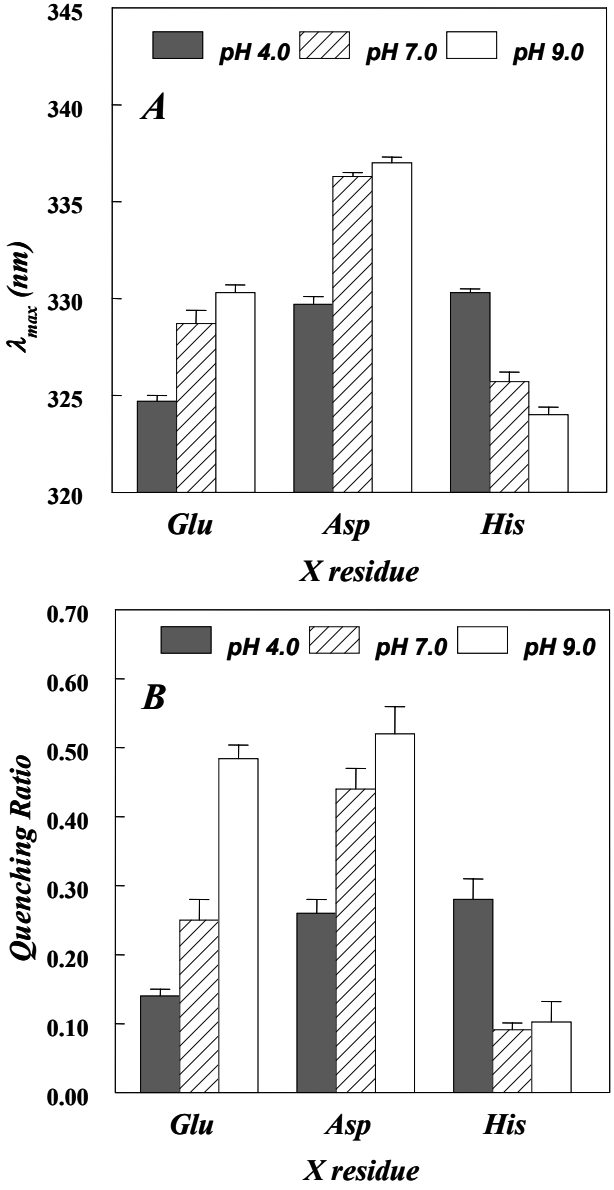

Figure 20. Effect of pH on the Trp emission λmax and quenching ratio for pLA peptides containing Asp, His or Glu residue at position 7 when incorporated into DOPC vesicles at different pH. (A) Trp emission λmax of Asp, His and Glu peptides in DOPC vesicles at pH 4.0 (filled bars), pH 7.0 (striped bars) and pH 9.0 (white bars). (B) Quenching ratio for peptides incorporated into DOPC vesicles at pH 4.0 (filled bars), pH 7.0 (striped bars) and pH 9.0 (white bars). The samples contained 2 μM peptide incorporated into 200 μM lipid dispersed in pH-adjusted PBS. Average values from three samples and for Q-ratios standard deviations are shown. λmax values were reproducible to within ±1nm

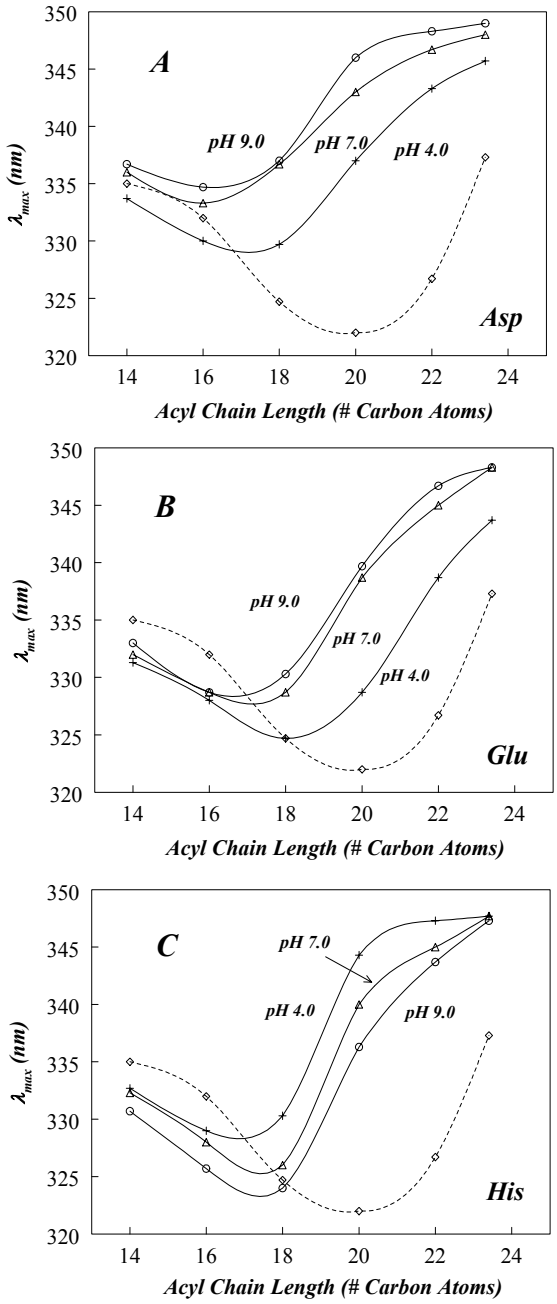

Figure 21. Effect of lipid acyl chain length on Trp emission λmax of pLA peptides with Asp, His or Glu at position 7 at different pH. (A) Peptide with Asp substitution. (B) Peptide with Glu substitution. (C) Peptide with His substitution. Symbols: pH 4 (○), pH 7 (Δ), pH 9 (+). The curve for the parental pLA peptide with Leu at position 7 (◊, dashed line) is shown for comparison. Experimental conditions are as in Figure 18. Average values from three samples are shown. λmax values were reproducible to within ±1nm

Table 6. Quencher induced shifts in Trp emission λmax and $L_{TM\ eff}$ values for pLA peptides with Asp, His or Glu substitutions at position 7 when incorporated into DOPC vesicles at different pH. Samples contained 2 μM peptide and 200 μM lipid dispersed in pH-adjusted PBS.

X Residue	pH	λmax (nm) [a]	λmax (nm) Acrylamide	λmax (nm) 10-DN	Δλmax [b] (nm)	$L_{TM\ eff}$ (number of residues)
Glu	4.0	325	324	325	1	18.7
	7.0	329	329	331	2	17.3
	9.0	330	329	333	4	17.1
Asp	4.0	330	329	331	2	17.5
	7.0	336	333	340	7	16.6
	9.0	337	334	340	6	16.8
His	4.0	330	329	331	2	17.3
	7.0	326	326	327	1	18.0
	9.0	324	324	325	1	18.0

[a]Reported λmax values are average from three samples. The λmax values were reproducible to within ± 1nm. [b]Δλmax is the absolute value of difference in Trp λmax in presence of 10-DN and Trp λmax in presence of acrylamide.

population formed by the X= D^- and E^- peptides because they form a mixture of populations in which it is likely that some of the non-TM form is present as judged by quencher-induced shifts in λmax (Table 6). However, an estimate of the extent of TM helix shifts when Asp and Glu are charged can be obtained from $L_{TM\ eff}$ values derived from λmax vs. bilayer width curves (Figure 21). For X = H^+, E^-, and D^- $L_{TM\ eff}$ values (Table 6) are 3.6, 3.8, and 4.1 residues, respectively, shorter than that for the X = L peptide (Table 5). It should be noted that the value of $L_{TM\ eff}$ is in reasonable agreement with Trp depth for the H^+ residue ($L_{TM\ eff}$ predicting a shift of Trp depth by 2.4 Å relative to the X = L peptide, see Discussion). Although locating more shallowly than the X = L peptide, peptides with uncharged ionizable X residues (at pH 9 for X = H and at pH 4 for X = D and X = E) affect Trp depth in DOPC vesicles to a much lesser degree than when charged (Figure 20). The effects of H^o and E^o residues on Trp depth are modest, giving a 0.5-1 Å shallower Trp location than when X = L, while that of D^o is substantial, with a 2-3 Å shallower Trp than when X = L. $L_{TM\ eff}$ for peptides with uncharged ionizable residues are also shorter than for the X = L peptide, confirming the shift in TM helix position. The decreases in $L_{TM\ eff}$ values for X = E^o, H^o and D^o are ~2.2, 2.9 and 3.4 residues, respectively, relative to that for the X = L peptide (Table 6). The value of $L_{TM\ eff}$ are in reasonable agreement with Trp depth for the D^o residue ($L_{TM\ eff}$ predicting a shift of Trp depth by 2.3 Å relative to the X=L peptide) but larger than expected for E^o, and more strikingly so for H^o ($L_{TM\ eff}$ predicting a shift of Trp depth of 1.5 and 2Å further from the bilayer center, respectively, see Discussion). The likely origin of this difference is described in the Discussion.

Effect of a Change in the Position of the Hydrophilic Residue In the Hydrophobic Sequence Upon Hydrophilic Residue-Induced Transverse Shifts.

We also examined whether a change in the position of a hydrophilic residue within the hydrophobic sequence would affect the extent to which it would shift TM helix position. To do this, pLA peptides with the hydrophilic (X) residue moved from position 7 to position 8 were used [general sequence: Acetyl-KKLALALX**L**ALAWLALALALAL AKK-amide] (Table 4). Figure 22 shows a comparison of Trp emission λmax (Figure 22A) and Q-ratio (Figure 22B) for pLA peptides with hydrophilic substitutions at

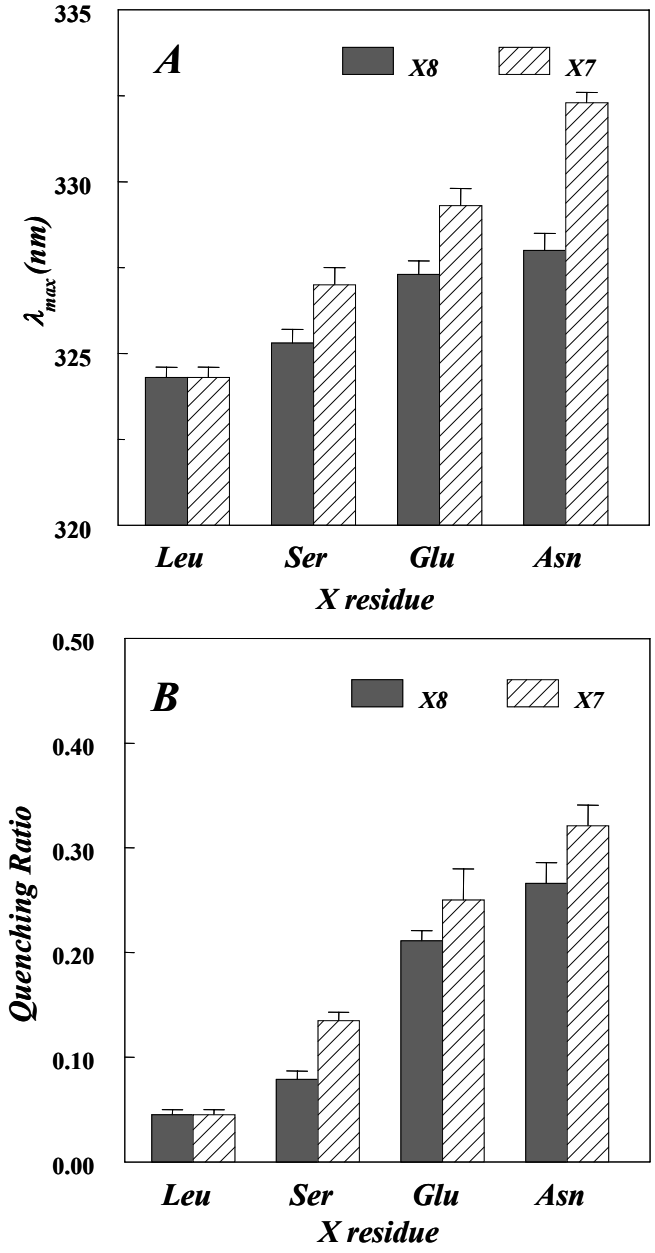

Figure 22: Effect of the position of the hydrophilic residue within the hydrophobic core of pLA peptide on the Trp emission λmax and quenching ratio when incorporated into DOPC vesicles at pH 7.0. (A) Trp λmax for peptides with single substitution at position 8 (filled bars) or position 7 (striped bars). (B) Quenching ratio for peptides with single substitutions at position 8 (filled bars) and position 7 (striped bars). The samples contained 2 μM peptide incorporated into 200 μM lipid dispersed in PBS. Average values from three samples and for Q-ratios standard deviation are shown. λmax values were reproducible to within ±1nm

position 8 (= X8 peptides) to that for peptides having hydrophilic substitutions at position 7 (=X7 peptides), when incorporated into DOPC vesicles. The order of the dependence of Trp depth upon the identity of the X residue (X = L < S < E < N) is the same for X8 and X7 peptides. This shows that the relative effects of different hydrophilic residues are not altered by the small change in X residue position in the sequence. However, the Trp residue is deeper for the X8 peptides (filled bars) than for X7 peptides (striped bars). This indicates that the TM segment shifts less in the X8 sequences than in the X7 sequences. This is confirmed by measurements of $L_{TM\ eff}$, derived from the effect of bilayer width upon λmax (Figure 23), which show that the X8 peptides exhibit a larger $L_{TM\ eff}$ than the corresponding X7 peptides (Table 7).

This pattern is the opposite of that predicted if the X residues were moving to the same location at the bilayer surface for the X7 and X8 peptides. In that case, the Trp depth would have been shallower and the shift greater in the case of the X8 peptides, in which the Trp is closer to the X residue. Two factors are likely to contribute to the tendency of hydrophilic X8 residues to shift TM helix position less hydrophilic X7 residues. First, the length of the hydrophobic sequence shifted out the bilayer core if the X residue moves to the bilayer surface is longer for the X8 peptides (5 residues) than for the X7 peptides (4 residues). The movement of these residues out of the bilayer core is energetically unfavorable, and thus they should resist shift to a greater extent for the X8 peptides. Second, for the X8 peptides the length of the truncated TM sequence formed if the X residue moves to the bilayer surface (15 residues) is shorter than that formed by the X7 series (16 residues). Thus, the negative mismatch forming upon helix shifting should result in a greater degree of energetically unfavorable strain on the bilayer for the X8 peptides if the X residue shifted to the same location for the X7 and X8 peptides.

Effect of the Hydrophobicity of the Non-Polar Residues Shifted Out of the Hydrophobic Core of the Bilayer Upon Transverse Shifts.

The experiments above suggested that the hydrophobicity of a sequence pushed out of the bilayer upon a transverse shift could affect the extent of the shift induced by hydrophilic X residues. To test this hypothesis, we measured the transverse positions of peptides varying the sequence (residues 3-6) that would be shifted out of the core of the

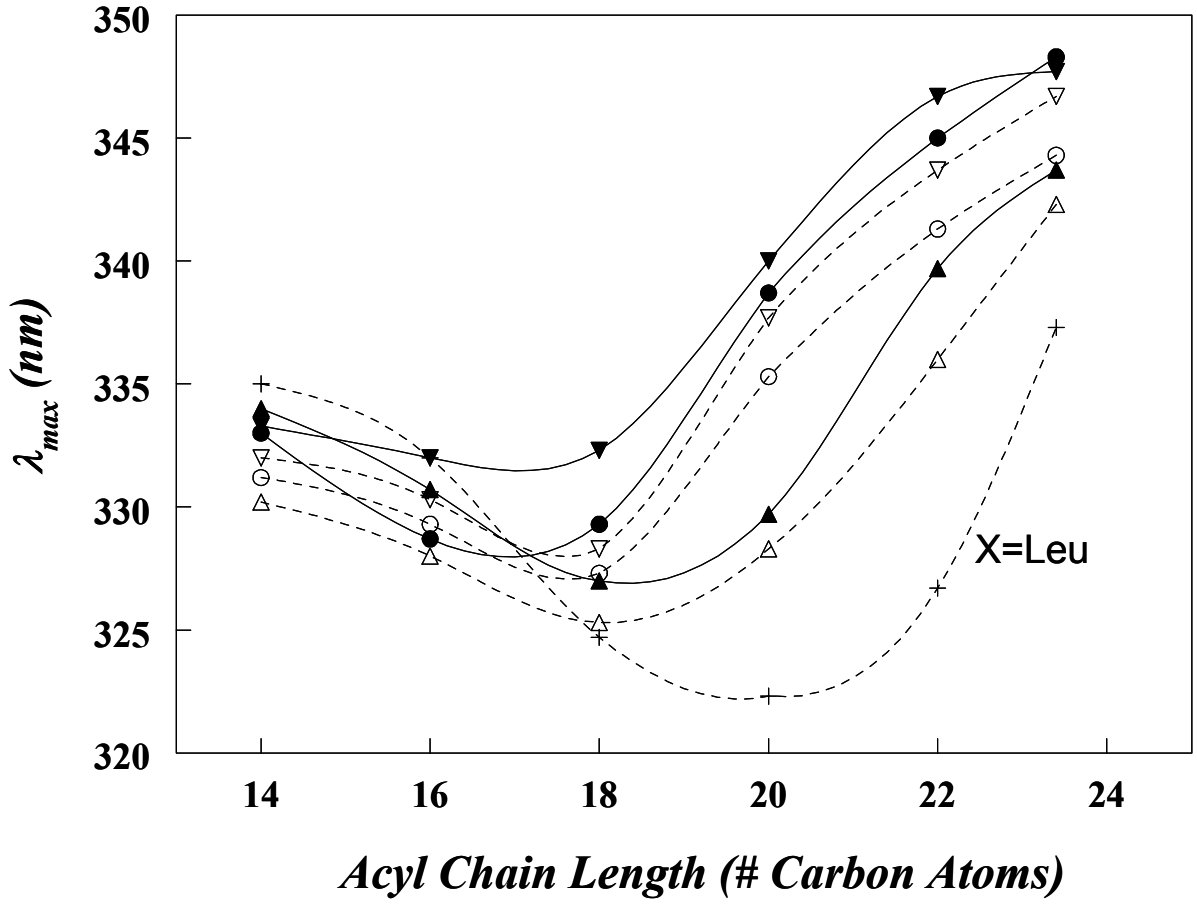

Figure 23: Effect of lipid acyl chain length on Trp emission λmax of pLA peptides with single hydrophilic residues at position 7 or 8 when incorporated into vesicles at pH 7.0. Substitutions: Ser (Δ); Glu (○), and Asn (∇). Substitutions at position 8 are shown as open symbols and dashed lines, and substitutions at position 7 are shown as filled symbols and solid lines. The curve for the parental (X = L) peptide (+, dashed line) is also shown for comparison. Experimental conditions are as in Figure 18. Average from three samples is shown. λmax values were reproducible to within ±1nm.

Table 7. Quencher induced shifts in Trp emission λmax and $L_{TM\ eff}$ values for pLA peptides with Asn, Glu or Ser substitutions at position 8 when incorporated into DOPC vesicles at pH 7. Samples contained 2 μM peptide and 200 μM lipid dispersed in PBS.

X Residue	**λmax (nm)** [a]	**λmax (nm) Acrylamide**	**λmax (nm) 10-DN**	**Δλmax** [b] **(nm)**	**$L_{TM\ eff}$ (number of residues)**
Asn	328	327	328	1	17.6
Glu	327	326	328	2	17.5
Ser	325	325	326	1	18.6

[a]Reported λmax values are average from three samples. The λmax values were reproducible to within ± 1nm. [b]Δλmax is the absolute value of difference in Trp λmax in presence of 10-DN and Trp λmax in presence of acrylamide.

lipid bilayer by the movement of an X residue at position 7 to the bilayer surface [general sequence: Acetyl-K_2Z_4EALALAWLALALALALAKK-amide] (Table 4) In the sequences compared the X residue was E and the Z residues (residues 3-6) were $(LA)_2$, A_4 or G_4. The pK_a of Glu for the Z = $(LA)_2$, A_4 and G_4 peptides, determined as described above, is 6.7, 7.1 and 7.3, respectively (data not shown). Thus, to compare sequences with both protonated and ionized Glu, experiments were carried out at pH 4.0 and pH 9.0, respectively.

When these peptides are incorporated in DOPC vesicles at pH 4.0 (Glu protonated) Trp depth decreases in the order Z = $(LA)_2 < A_4 < G_4$ as judged by both by λmax (filled bars in Figure 24A) and Q-ratio (filled bars in Figure 24B) suggesting that the E residue shifts increasingly towards the bilayer surface in that order. In the case of the peptide with the Z = G_4, sequence, there appears to be some non-TM state formed in DOPC vesicles at pH 4 as judged by the observation that it (unlike the peptides with Z = $(LA)_2$ or Z=A_4 sequences) exhibits significant quencher-induced shifts of λmax (Table 8). The conclusion that the shift increases in the order Z = $(LA)_2 < A_4 < G_4$ is supported by $L_{TM\ eff}$ values derived from the effect of lipid acyl chain length on Trp λmax (Figure 25A). At pH 4.0, $L_{TM\ eff}$ for the Z = $(LA)_2$, A_4 and G_4 peptides decrease relative to the parental [Z = $(LA)_2$, X = L] peptide by 2.2, 3.3, and 3.8 residues, respectively (Table 8).

When these peptides are incorporated in DOPC vesicles at pH 9.0 (Glu ionized) Trp depth decreases in the same order as at pH 4, Z = $(LA)_2 < A_4 < G_4$, as judged by both by λmax (striped bars in Figure 24A) and Q-ratio (striped bars in Figure 24B). This indicates that the dependence of helix shift on Z sequence follows the same order when Glu is protonated or ionized. However, Trp depth at pH 9.0 is shallower than at pH 4.0 for all three peptides. In addition, quencher-induced λmax shifts suggest that when incorporated into DOPC vesicles at pH 9 there is a mixture of a shifted TM and non-TM topography formed by all three peptides (Table 8). The conclusion that at pH 9.0 the degree of shift increased in the order Z = $(LA)_2 < A_4 < G_4$ and that the shift is greater than at pH 4 is supported by $L_{TM\ eff}$ values (Figure 25B). At pH 9.0, $L_{TM\ eff}$ decreased relative to the parental [Z = $(LA)_2$, X=L] peptide by about 3.9, 4.8 and 4.9 residues for the Z = $(LA)_2$, A_4 and G_4 peptides, respectively (Table 8).

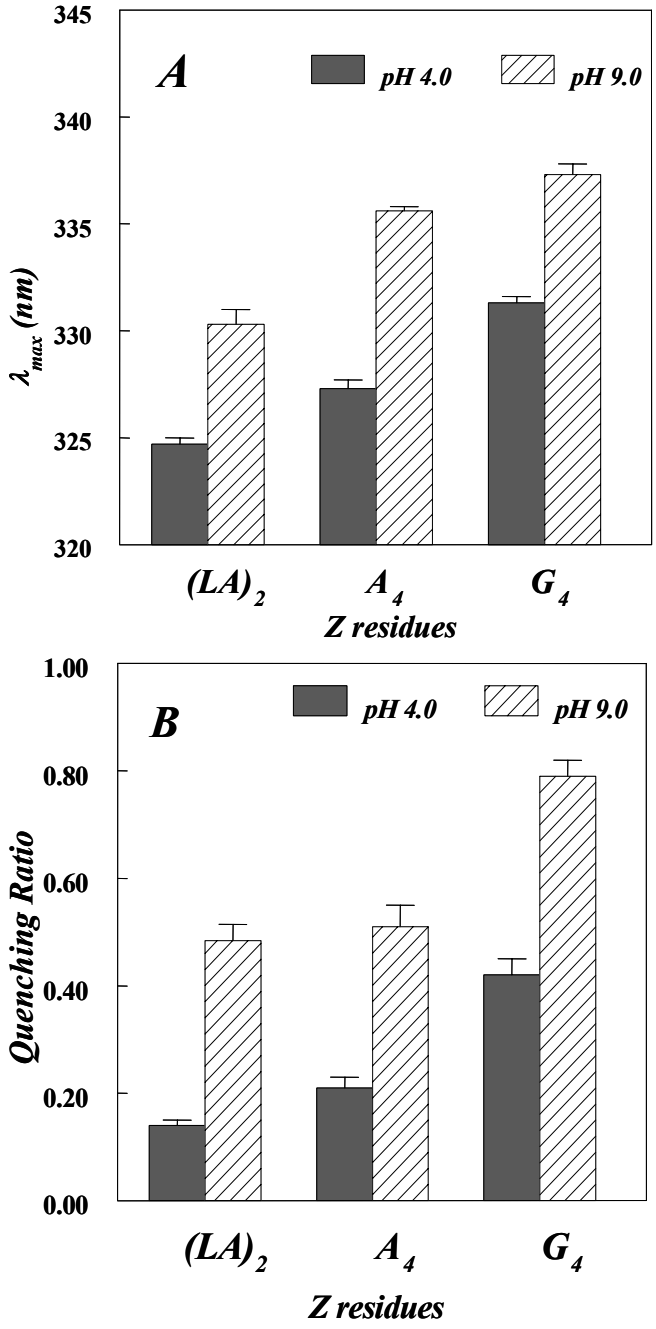

Figure 24: Trp λmax and quenching ratio of Glu-containing pLA peptides with varying 'Z' residues (residues 3-6) when incorporated into DOPC vesicles. (A) Trp emission λmax in DOPC vesicles at pH 4.0 (filled bars), and pH 9.0 (striped bars). (B) Quenching ratio for peptides incorporated into DOPC vesicles at: pH 4.0 (filled bars) and pH 9.0 (striped bars). The samples contained 2 μM peptide incorporated into 200 μM lipid dispersed in pH-adjusted PBS. Average obtained from three samples and for Q-ratios standard deviations are shown. λmax values were reproducible to within ±1nm.

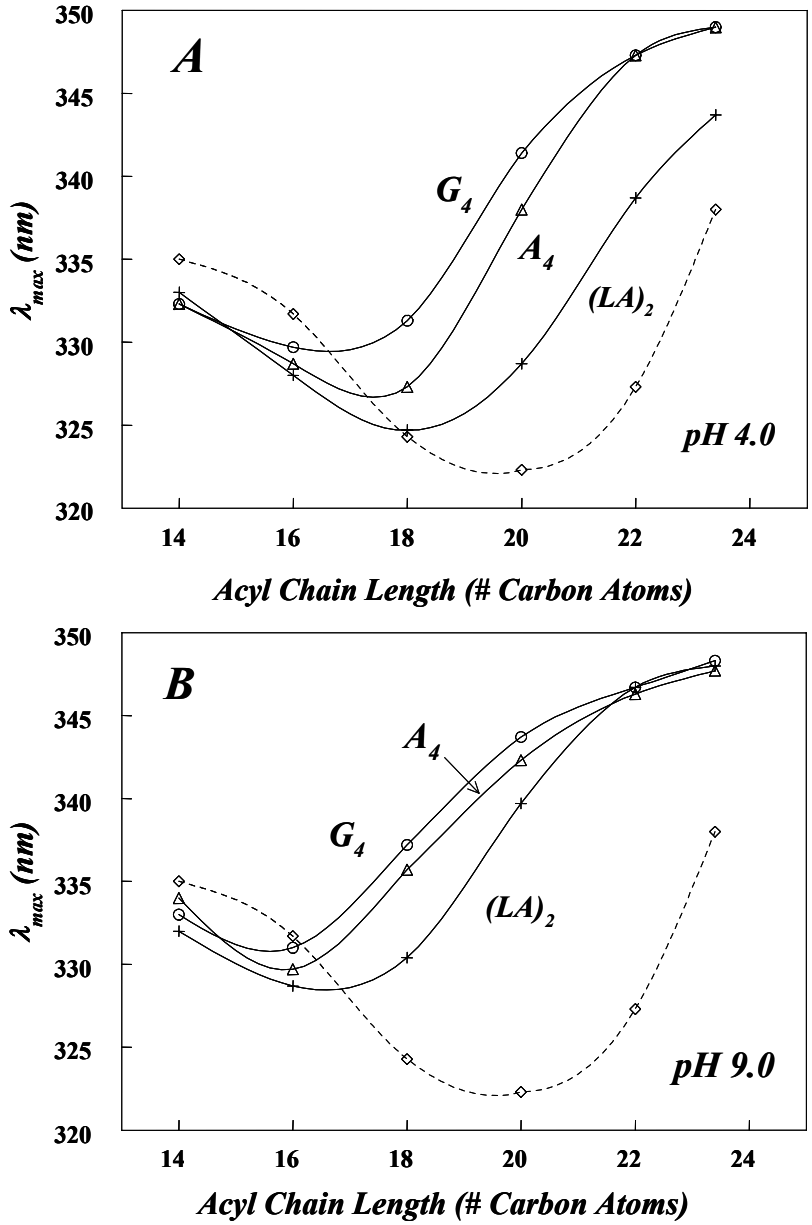

Figure 25. Effect of lipid acyl chain length on Trp emission λmax of X=Glu pLA peptides with varying Z residues (residues 3-6) incorporated into vesicles. (A) pH 4.0 (B) pH 9.0. Z residues: $(LA)_2$ (+), A_4 (Δ) and G_4 (○). The curve for the parental pLA peptide with X = L and Z = $(LA)_2$ (dashed line) is shown for comparison. Experimental conditions are as in Figure 18. Average value of three samples is shown. λmax values were reproducible to within ±1nm.

Table 8. Quencher induced shift in Trp emission λmax and $L_{TM\ eff}$ values for pLA peptides with Glu at position 7 and different Z residues (at positions 3-6) when incorporated into DOPC vesicles at pH 4.0 or pH 9.0.

Z residues	**pH**	**λmax (nm)** [a]	**λmax (nm) Acrylamide**	**λmax (nm) 10-DN**	**Δλmax** [b] **(nm)**	**$L_{TM\ eff}$ (number of residues)**
$(LA)_2$	4.0	325	324	325	1	18.7
	9.0	330	329	333	4	17.1
A_4	4.0	327	327	328	1	17.7
	9.0	336	335	338	3	16.1
G_4	4.0	331	329	335	6	17.1
	9.0	337	335	340	5	15.9

[a]Reported λmax values are average from three samples. The λmax values were reproducible to within ± 1nm. [b]Δλmax is the absolute value of difference in Trp λmax in presence of 10-DN and Trp λmax in presence of acrylamide.

Secondary Structure of the pLA peptides: Circular Dichroism (CD) Measurements

In order to evaluate the secondary structure of the various pLA peptides used in this study, CD measurements were carried out (data not shown). For almost all peptides and conditions studied, the α-helix content is estimated to be 80-85 %, which corresponds to helix formation by the entire hydrophobic sequence. This is true both for peptides incorporated into DOPC vesicles and incorporated into DEuPC vesicles, with only about 1% loss in helix content in DEuPC vesicles. Many of the peptides form the non-TM state in DEuPC vesicles, so these results indicate that, at least for those peptides, the non-TM state is as helical as the TM state. There is a very small sequence dependence of helix content: more polar the X residue or Z residues, the lower the helix content (maximum 5-10 % decrease). This can be explained if residues extruded from the bilayer have a lower tendency to form a helix. Since the more highly polar residues induce a larger shift, they would extrude more residues and thus induce the largest changes in secondary structure. The lowest helix values are observed with X = Pro, consistent with its helix-breaking properties.

DISCUSSION

Defining the TM Helix-Shifting Propensities of Hydrophilic Residues Using Fluorescence.

This study used TM helices incorporated into model membrane vesicles to examine how features of hydrophobic helix sequence influence TM helix position within membranes. In seminal studies using a glycosylation-mapping technique, von Heijne and colleagues defined the effects of several polar and ionizable residues upon the transverse position of TM helices at the time that they are likely to be associated with the translocon (9, 45-48) . Their technique probes the boundary of a TM segment via the fact that an exofacial Asn residue in an extra-membranous segment of a membrane protein has to be 12 residues away from the membrane surface to be accessible to glycosylation by oligosaccharyl transferase. Our experiments have extended studies of transverse shift to lipid bilayers and to all types of hydrophilic residues, measuring the position and length of the TM helix itself. Several previous studies show that in the model membrane system

TM helices form their equilibrium structures (24, 29, 30) and this equilibrium behavior within a lipid bilayer is particularly relevant to post-translational shifts in TM helix position. In addition, in our system we could vary pH to look at the behavior of ionizable residues in both the charged and uncharged states. Thus, this report yields a more detailed picture of the sequence-dependence of TM helix topography.

It is important to understand the mathematical relationship between the distance that a hydrophilic X residue shifts towards the bilayer surface (the surface defined here as the boundary of the hydrophobic core of the bilayer), the resulting changes in the length of the TM helix spanning the bilayer, and Trp depth. Under conditions in which there is initially no hydrophobic mismatch (Figure 26A) the movement of the X residue to the surface (by n Å) should equal the length by which TM-spanning sequence decreases, and a Trp at the center of the hydrophobic sequence should shift ½n Å away from the bilayer center, assuming that the negative mismatch induced by the shortening of the TM sequence is accommodated by a symmetric positioning within the lipid bilayer, as inferred previously by Monné and von Heijne (48). At the other extreme is the case in which there is initially positive mismatch and a tilted TM helix (Figure 26B). If positive mismatch is lost after the shift of the X residue to the surface (by n Å), the decrease in the length of the TM spanning sequence will be $n/\cos\theta$ Å, where θ is the tilt angle prior to helix shift. The Trp residue will again shift ~ ½n Å away from the bilayer center.

In our experiments, peptide lengths were such that they should switch from slight positive mismatch to moderate negative mismatch upon movement of the X residue to the surface (Figure 26C). Based on the considerations described above this movement would decrease the length of the TM sequence (L_{TM}) from 21 to 16 residues (7.5Å), move the X residue 6.8 Å closer to the bilayer surface (assuming that 19 hydrophobic residues span a DOPC bilayer under conditions of hydrophobic match (16, 24), and shift the Trp residue ~3.4 Å away from the bilayer center. When X was a highly hydrophilic residue with a short side chain or when the hydrophobicity of the Z residues was low, observed shifts approached these values (see Results).

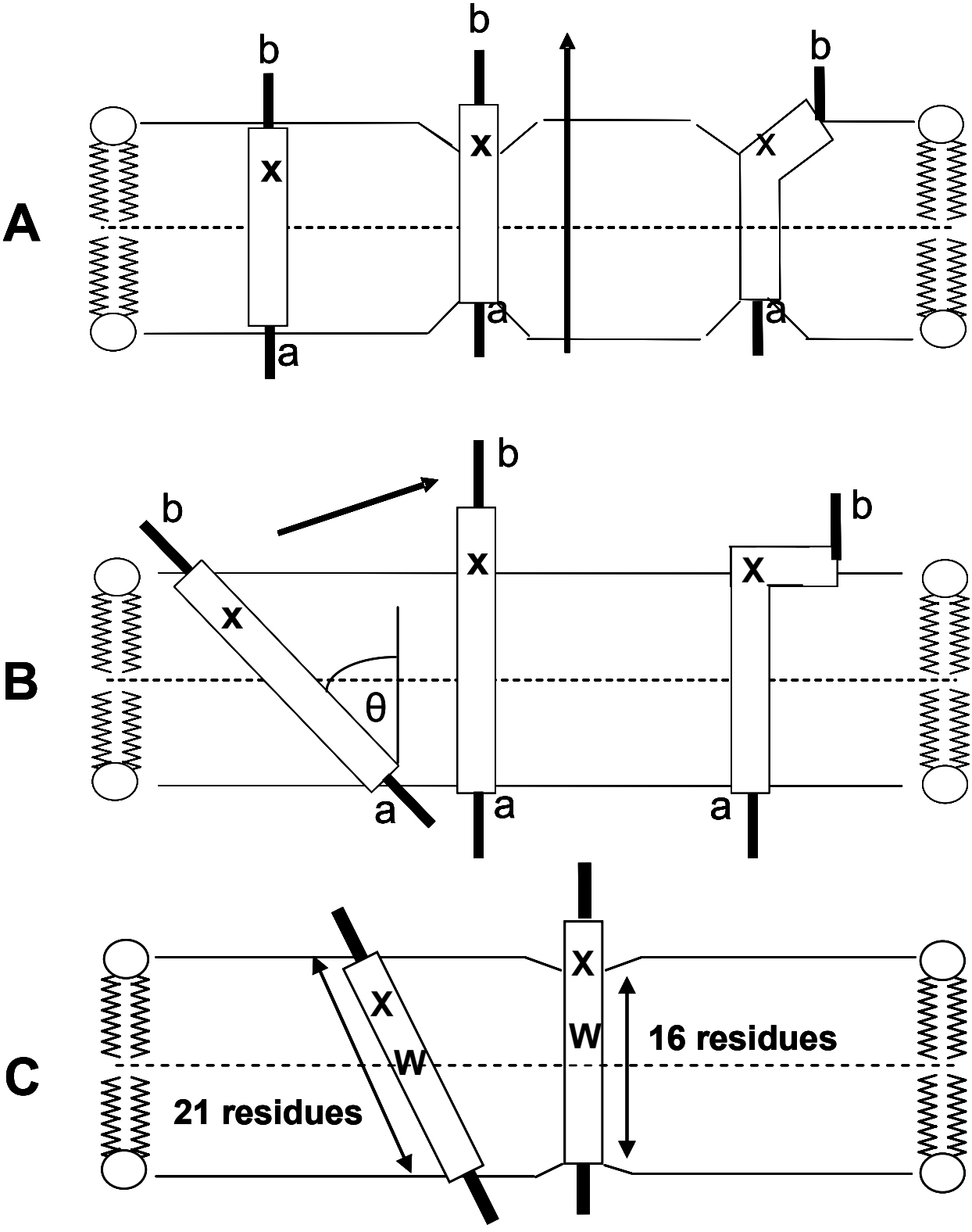
A
b
x
a
b
x
a
b
x
a
B
b
x
θ
a
b
x
a
b
x
a
C
X
W
21 residues
X
W
16 residues

Figure 26: Schematic figure summarizing the consequences of helix length and transverse shifts upon the position of TM helices in membranes. (A) Case in which there is match between the length of the entire hydrophobic sequence (rectangle) and bilayer width. There is negative mismatch when the X residue shifts to the bilayer surface, and a resulting symmetric distortion of the bilayer (48). Notice that in this case the extent of the shift of the X residue is directly transmitted to that of the juxtamembrane sequences (points a and b), unless the extruded sequence tends to lie along the bilayer surface (right) (48). This would decrease the transmission of the shift to point b. (B) Case in which there is positive mismatch between the length of the entire hydrophobic sequence (rectangle) and bilayer width, and in which a shift sufficient to relieve the positive mismatch occurs when the X residue shifts to the bilayer surface. The (maximum) tilt angle in the presence positive mismatch is θ. Notice that in this case the extent of the shift of the X residue is not identical to the shift of the juxtamembrane residues. Instead, the sequence should to pivot around the distal boundary of the TM sequence (point a) reducing the amount of shift of distal juxtamembrane residues. (C) Likely behavior of the pLA peptides. They should show slight positive mismatch in DOPC vesicles if the entire hydrophobic sequence spans the lipid bilayer, but when the X residue shifts to the surface, there should be slight negative mismatch.

TM Helix Transverse Shift Propensities of Different Hydrophilic Amino Acid Residues.

The extent of helix shift was strongly dependent upon the identity of the X residue, with most residues inducing intermediate degrees of shift such that the X residue did not fully move to the membrane surface. Figure 27 summarizes λmax (Figure 27A) and Q-ratio (Figure 27B) for all of the X residues tested, and Figure 28 shows the relationship between $L_{TM\ eff}$ and Trp depth in DOPC vesicles as measured by Q-ratio (a very similar pattern is observed for a graph of $L_{TM\ eff}$ vs. λmax in DOPC vesicles, not shown). Based on these graphs, the transverse shifting properties of different X residues can be compared. This reveals a number of novel and even surprising findings.

Asparagine and Glutamine: Asn and Gln induced very large shifts, as large or larger than most of the charged residues. In fact, at pH 7 Asn induced larger transverse shifts than any residue other than Asp. This probably reflects the strong hydrophilicity of the amide group, and is consistent with the observation that Asn and Gln are the two least abundant uncharged polar residues in TM segments (26, 28). The lesser shifts induced by Gln relative to Asn may be due to its extra methylene, which increases its hydrophobicity and ability to snorkel (see below). Substitution of hydrophobic residues with Asn and Gln may be particularly useful for probing the functional effects of large changes in TM helix position (see below).

Lysine and Arginine: Lys and Arg shifted helix position to a much lesser degree than the Asn or Gln or even other charged residues (see below). The main reason for this is likely to be snorkeling. Arg and Lys with long side chain can snorkel to position their charged groups as close as possible to the membrane surface (75, 127). This explains the small change in Trp depth in the presence of Lys and Arg because the alignment of the Lys or Arg side chains towards the surface would minimize the shift of the entire TM helix necessary to locate charged groups near the membrane surface. Charge delocalization in the Arg side chain may also aid its burial within the lipid bilayer.

It is interesting that even though snorkeling should significantly increase the length of the TM segment (L_{TM}) relative to a non-snorkeling charged residue, $L_{TM\ eff}$ for Arg and Lys was smaller than predicted from Trp depth, as shown by comparison of $L_{TM\ eff}$ and Trp depth for different X residues (Figure 28). The likely explanation for this behavior is that

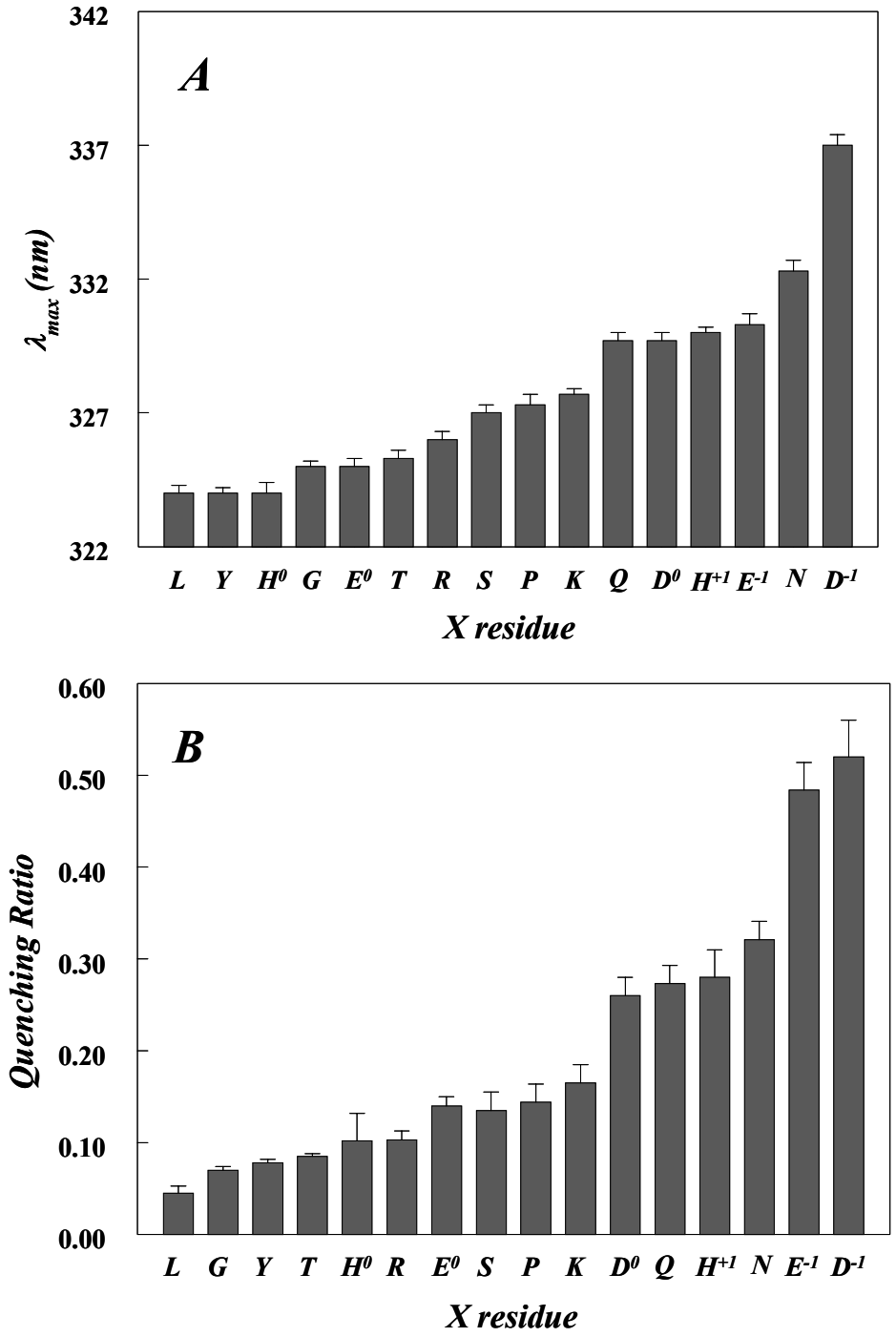

Figure 27: Summary of λmax and quenching ratio for pLA peptides with different residues at position 7. Combined data from Figures 14 and 20 is shown.

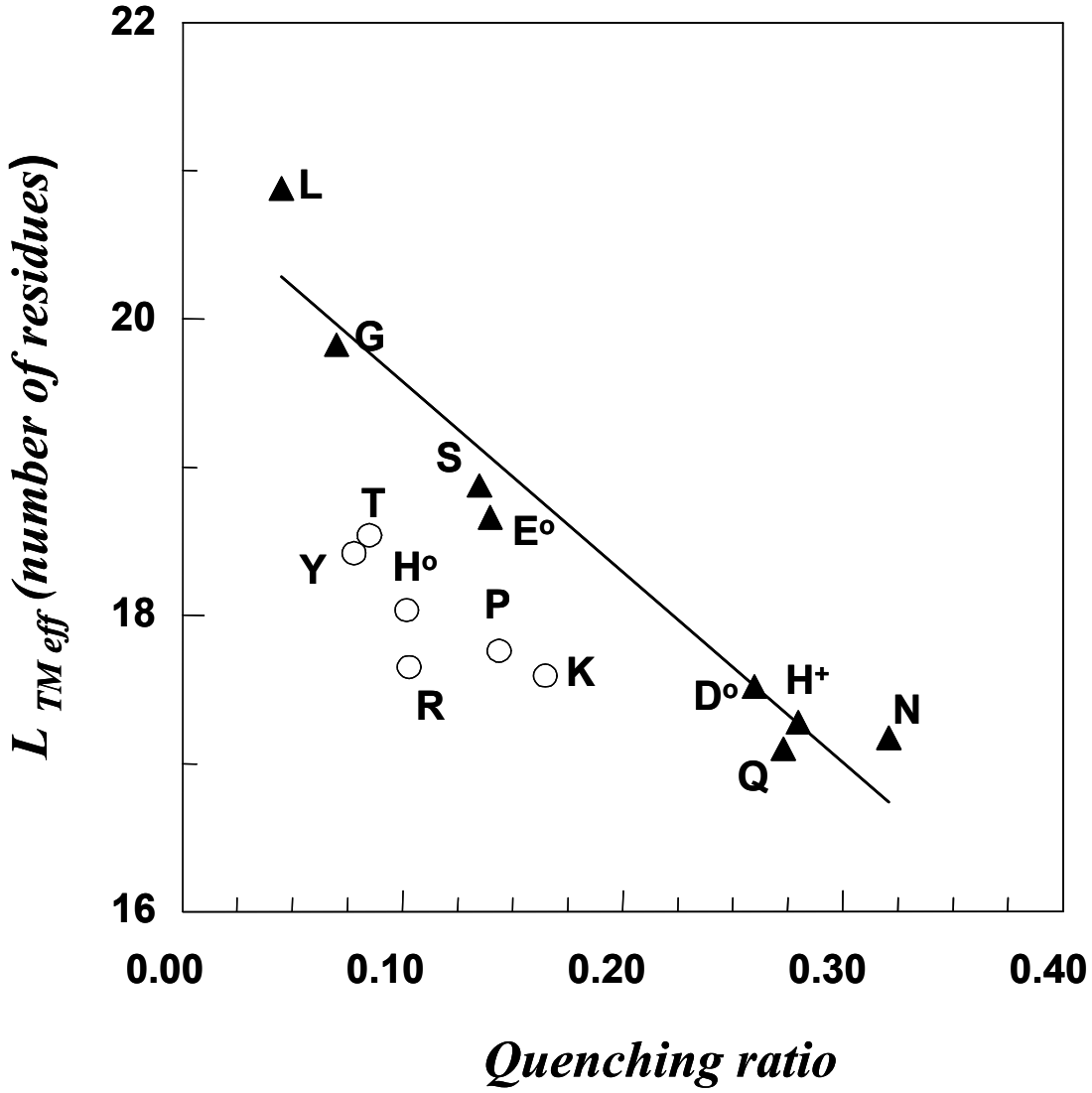

Figure 28. Correlation between Trp depth in DOPC vesicles in the TM state (as reported by the quenching ratio) and $L_{TM\ eff}$. Filled triangles represent residues that define a line with the theoretical slope for the relationship between $L_{TM\ eff}$ and Trp depth for the pLA peptides used in this study (~1Å shift in Trp depth per 2Å decrease in $L_{TM\ eff}$). Open circles represent hydrophilic residues that show a smaller change in Trp depth than predicted from the decrease in $L_{TM\ eff}$ relative to X = L. Note: Values corresponding to E^- and D^- are not shown because the pLA peptides containing these residues form co-existing shifted TM and non-TM states in DOPC vesicles

snorkeling is costly in terms of lost entropy due to the restriction of the side chain orientation required to position the charged group near the surface. As a result, negative mismatch destabilizes the TM state relative to the non-TM state even when TM helix transverse position and length is not much different from that if the parental peptide (when X = L). Thus, when X = Arg or Lys the stability of the TM state and its sensitivity to bilayer width is similar to that of a hydrophobic helix that has a highly hydrophilic X residue that cannot snorkel and so forms a short TM segment.

Histidine, Aspartate and Glutamate: The other ionizable residues had a very strong tendency to shift helix position when charged. This is expected as they are very hydrophilic when charged and have shorter side chains than Lys and Arg. The order of the extent of transverse shifting was X = Asp > Glu > His. The smaller shifts induced by charged Glu and His may reflect their side chains being longer than that of Asp. Thus, they are a bit more hydrophobic and can snorkel to a greater degree than Asp, although not nearly as much as Lys or Arg. The fact that His^+ induces smaller shifts than Glu^- might partly reflect the delocalization of the positive charge on His^+.

Uncharged Glu, Asp and His induced much smaller transverse shifts than when charged, consistent with their lower hydrophilicity in the uncharged state. The extent of shift induced in the uncharged state followed the same order as in the charged state: X = Asp > Glu > His. The uncharged Asp retained the ability to induce very large transverse shifts, while the weaker helix shifting propensity of an uncharged Glu was, at most, no greater than that of a Ser residue. This agrees with hydrophobicity results of Wimley and White (105), who found that an uncharged Glu was slightly more hydrophobic than an uncharged Ser as judged from their relative effects upon binding of a peptide to the non-polar/polar boundary of a bilayer. The weak extent of shift induced by His^o as measured by Trp depth may partly reflect an ability to snorkel, as formation of the His^o tautomer with a proton on the N3 atom would have a hydrophobic side chain three carbon atoms long. An ability of His^o to snorkel is consistent with the disproportionally large decrease in $L_{TM\ eff}$ relative to the shift in Trp depth (Figure 28), a pattern similar to that observed for Lys and Arg residues.

The effects of ionization state upon the transverse position of TM helices containing Asp, Glu and His residues may be biologically important because when

incorporated into TM helices their pKa values fall in a physiologically significant pH range. At pH 7, the overall order of transverse shifting remains X = Asp>Glu>His, but the relative amounts of shift are affected by whether these residues were charged or not. (It should be noted that the difference between Glu and Asp at neutral pH is in agreement with the glycosylation mapping data of Monné *et al* (47).) As we previously observed for Asp residues (30, 49), these ionizable residues have pKa values such that their protonation, and thus effect upon transverse position, could be altered in acidic organelles, and this might have important biological effects, e.g. upon signaling in acidic organelles.

Proline: Pro had a strong tendency to induce transverse shifts at pH 7, but not as much as Lys, Gln, Asn, Glu and Asp. The observation that Pro did not induce shifts larger than Lys, Glu and Asp at neutral pH appears to contrast with previous glycosylation mapping studies which found that Pro residues induced the largest transverse shifts (Asn and Gln were not tested) in the position of the extra-membranous glycosylated sequences (9). However, as noted by Nilsson et al. (9), the large effect of Pro in those studies partly reflects the helix-breaking properties of Pro, which probably results in formation of an extended structure by the sequence extruded from the bilayer (the length of which is what glycosylation mapping measures), and thus a larger shift of sequences outside of the membrane than that occurring within the bilayer.

Local destabilization of helical structure could also explain why Pro was one of the residues that exhibited a disproportionally larger effect on $L_{TM\ eff}$ relative to that it had upon Trp depth in DOPC vesicles (Figure 28). The energetic cost of burial of Pro could have an unusually strong dependence on its depth of burial in the hydrophobic core of the membrane because it destabilizes the helical structure of neighboring residues (9), so that their burial is also energetically unfavorable. This would show up as a decrease in $L_{TM\ eff}$ because the TM state would be destabilized more severely under conditions of negative mismatch, which would tend to bury both the Pro and neighboring residues.

Serine: Ser, a modestly hydrophilic residue, induced an intermediate, but still substantial, extent of transverse shift. There was evidence that this intermediate shift was an average arising from co-existing of shifted and un-shifted populations. The significant shifting ability of Ser is important because it is very common in TM sequences (26, 28).

TM helices with Ser not too far from of one end of the hydrophobic sequence may have an appreciable ability to switch between TM topographies with different TM segment boundaries.

Tyrosine: Tyr induced a rather small shift. This may partly reflect the fact that its lowest free energy location is not in a polar environment, but rather near the polar/non-polar interface (26, 128). Consistent with this explanation it has been found that Trp, the other heteroaromatic residue that prefers to locate at the polar/non-polar interface, has little tendency to induce transverse shifts when located within five residues from the end of a hydrophobic sequence (46). In addition, there may be snorkeling by the large phenyl side chain to place the Tyr OH group close to the bilayer surface. This is consistent with the observation that $L_{TM\ eff}$ for Tyr was smaller than Ser (a residue that cannot snorkel to a significant degree), even though Tyr did not shift helix position as much as Ser.

Threonine: Thr is less hydrophilic than Ser due to its extra methyl group, and had a weaker ability to shift helix position than Ser as judged by Trp depth. However, it had a more significant effect upon $L_{TM\ eff}$, decreasing $L_{TM\ eff}$ slightly more than Ser. We do not understand the origin of this behavior, which cannot be explained by snorkeling.

Glycine: Gly induced the smallest shift of all residues tested, but it was still significant relative to X=Leu. The observation that such a modestly hydrophilic residue as Gly can influence TM helix transverse position emphasizes the strong sensitivity of transverse position to sequence.

The Effect of the Sequence Pushed Out of the Bilayer Core Upon Transverse Helix Shift.

It was also found that modest changes in the hydrophobicity of the sequence extruded from the bilayer core when a hydrophilic residue shifts towards the bilayer surface strongly influences TM helix position. This indicates that there is a considerable change in free energy when a hydrophobic sequence moves from a position slightly below, to slightly above, the formal non-polar/polar boundary, and thus that the actual polarity gradient in the direction perpendicular to the plane of the membrane must be reasonably steep in the interfacial region. This conclusion is consistent with the predictions of recently proposed models for the membrane polarity gradient (129, 130).

Effect Upon Transverse Shift of the Position of the Hydrophilic Residue Within the Hydrophobic Sequence and the Length of the Truncated TM Sequence Formed After a Transverse Shift.

The position of a hydrophilic residue within a hydrophobic sequence also was found to have a significant effect upon the extent of transverse shift, in agreement with glycosylation mapping studies (45, 47, 48). The closer a hydrophilic residue is to the center of a hydrophobic sequence, the more energetically unfavorable its location, which should increase transverse shift. However, if a hydrophilic residue is too close to the center of a hydrophobic sequence then its movement to the surface would be resisted by two factors: having to shift too long a segment of hydrophobic sequence out of the bilayer core, and forming too short a truncated TM sequence upon shifting. Assuming bilayer distortion has a significant energetic cost, strong negative mismatch resulting from the formation of a very short truncated TM helix (Figure 26A) would reduce the degree the movement of a hydrophilic residue to the surface is energetically favorable, and thus reduce the extent of the helix shift relative to a case of a longer hydrophobic sequence in which the shift of the hydrophilic residue to the surface would not result in negative mismatch (Figure 26B).

Additional Factors Likely to Affect Transverse Helix Shifts.

Additional variables may affect transverse shifts of TM helix position. One is interactions between a hydrophilic residue and neighboring residues. Polar interactions between two residues separated by one helical turn away can reduce the unfavorable free energy of burial and thus the tendency to shift helix position (45). Steric effects in which large neighboring residues reduce the exposure of the X residue to its environment could also influence its propensity to shift position (105). Lipid composition may also be an important variable. The positioning of cationic residues might be stabilized by interaction with anionic lipids, and a lipid composition with an especially limited ability to distort to accommodate hydrophobic mismatch could limit the extent of transverse shifts that increase hydrophobic mismatch.

Finally, helix-helix interactions should modulate TM helix positioning. If only one of two transverse positions formed by a TM helix can interact with a second helix,

that position would be stabilized by helix-helix interaction. An important reciprocal concept is that helix positioning could control helix-helix interaction if there is an energetic cost of shifting a TM helix into a transverse position in which it can interact with another helix.

Previous studies have shown that polar residues can drive association of model transmembrane peptides via inter-helical polar interactions (32, 37). However, these measurements were done in presence of detergent and the polar head groups of the detergent molecules can modulate these interactions. Further, long hydrophobic helices (~23 residues) used in these analysis have significant positive mismatch in detergent micelles and positive mismatch tends to promote helix association (16, 24, 30). So the ability of the hydrophilic side chain to promote helix association could have been overstated.

It should be noted that several studies show that electrostatic repulsions between the multiple flanking Lys sequences in our peptides generally prevent helix oligomerization, and even in the absence of electrostatic repulsions, only very weak oligomerization is observed (29, 30, 78). This weak oligomerization can be detected by a dependence of Trp fluorescence properties, or fluorescence resonance energy transfer between labeled peptides, upon peptide concentration within the bilayer (30, 78). With the exception of the X = Lys peptide no effects of peptide concentration upon Trp fluorescence in DOPC vesicles were observed for the peptides used in this report (data not shown). The X = Lys peptide exhibited a blue shift (4 nm) in Trp λmax and a small decrease in Q-ratio when the peptide/DOPC ratio was diluted from 1:100 to 1:500 mol:mol. This indicates that the X = Lys peptide forms weakly-associating oligomers at higher peptide/lipid ratio, and that Lys snorkeling may limit the extent of transverse shift even more strongly in the monomeric state.

Functional Role of Transverse Helix Shifts and Its Investigation Using Mutagenesis to Control Helix Position.

This study shows that TM helix transverse position is very sensitive to sequence. This implies that transverse shifts in TM helix position may be common, and that the

actual boundaries of TM segments may often be different than the values assigned by simple analyses of sequence hydrophobicity. As pointed out above, the constraint peculiar to membrane proteins, that interactions between two domains can require that the domains be properly aligned in a specific plane, implies that shifts in TM helix position represent a unique mechanism for control of membrane protein function. In addition to control of TM helix-TM helix interactions, this mechanism may control function by shifting the position of extra-membranous domains. The behavior of juxtamembrane sequences can affect the degree to which TM sequence shifts are transmitted to domains outside of the membrane [Figure 26 and (48)].

In the most well studied example of such behavior, bacterial TM chemoreceptors, there are very long helices that extend through and far beyond the membrane, and so can directly transmit shifts in TM helix position to domains outside of the membrane (124). Similar transmission of TM helix shifts to non-TM domains has been proposed for integrins (126).

Shifts in TM domain position by polar residues introduced by mutations may be molecular basis for disease states. A hydrophilic mutation (G380R) in the TM domain of FGFR3 receptor results in abnormal bone development (i.e. dysplasias)(131). This mutation leads to slow downregulation of the activated mutant receptors, and is likely to prolong signaling (132, 133). It has recently been shown that this mutation alters the TM helix boundary of FGFR3 receptor (131). It has been proposed that this altered membrane position might affect downregulation by altering the ubiquitination of FGFR3 (131, 133).

Similarly for the ErbB2 receptor, which is involved in cell growth and development, a Val to Glu mutation (V664E) in the TM domain can induce an TM helix shift (44), and this mutation has been linked to the constitutive activation of the tyrosine kinase activity of the receptor, resulting in oncogenicity (44, 134). Although it has been proposed that oligomerization induced by this mutation may be critical for oncogenicity (44, 135, 136), further experimentation is needed to see if the shift in helix position is also functionally important.

In the case of amyloid precursor protein (APP) processing, the membrane position of APP is a major determinant for the cleavage site of γ-secretase (137).

Hydrophilic/polar mutations in and around the TM domain has been shown to affect proteolytic processing of APP by altering the boundary of the TM segment of APP (137, 138).

Functions of membrane proteins that are strongly dependent on TM helix transverse position should be affected by hydrophilic substitutions in a manner that reflects the degree of transverse shift induced more closely than other properties of the substituting residue. Thus, knowledge of how transverse helix shifts depend upon hydrophilic residue structure could be useful in mutagenesis-based studies in which amino acid substitutions are used to probe the functional significance of transverse helix position.

CHAPTER 5

HYDROPHILIC MUTATIONS WITHIN THE TRANSMEMBRANE DOMAIN OF NEU/ERBB2 RECEPTOR ALTER ITS MEMBRANE POSITION

The epidermal growth factor receptor (or ErbB) family of receptor tyrosine kinase (ErbB1-ErbB4) plays a critical role in many physiological processes (139-141). ErbB receptors are composed of a large extracellular ligand-binding domain that is connected, via a single transmembrane helix to a cytoplasmic domain with intrinsic tyrosine kinase activity (139-141). These receptors are activated by extracellular ligands, which contain a conserved epidermal growth factor (EGF) domain (139-141). Typically, these receptors form inactive dimers via lateral association of the TM domains and ligand binding to the extracellular domain induces conformational change in the receptor dimer, activating the receptor (142, 143). The contact between the two cytoplasmic domains in the activated dimer stimulates its catalytic activity and results in transautophosphorylation of the receptor. This activates the tyrosine kinase activity and triggers the signalling cascades that lead to phosphorylation of cytoplasmic substrates (134, 143-145) (Figure 29).

ErbB receptors play a critical role in cell growth and differentiation during embryonic development and in adult life. So, signaling by the ErbB receptors is tightly regulated (139-141). Deregulation of the ErbB signalling system, either by over-expression or gene amplification or by genetic alterations such as deletions and mutations, results in deregulated tyrosine kinase activity (146, 147). Most of these aberrations result in ErbB receptors with constitutive or strongly enhanced signaling capacity, which leads to malignant transformation. Therefore, ErbB receptors are frequently linked to cancer (140, 141).

In most cases, the growth factor signalling of the ErbB receptor is downregulated by ligand-induced receptor endocytosis (148). The ligand-bound dimerized receptors are internalized into endosomes, where the receptors undergo ubiquitination and are subsequently targeted to lysosomes for degradation (149). De-ubiquitination enzymes can abrogate this degradation process, following which the receptor recycles back to the cell surface (150, 151) (Figure 30). This allows the cell to maintain the number of free receptors on the cell surface at a steady state level.

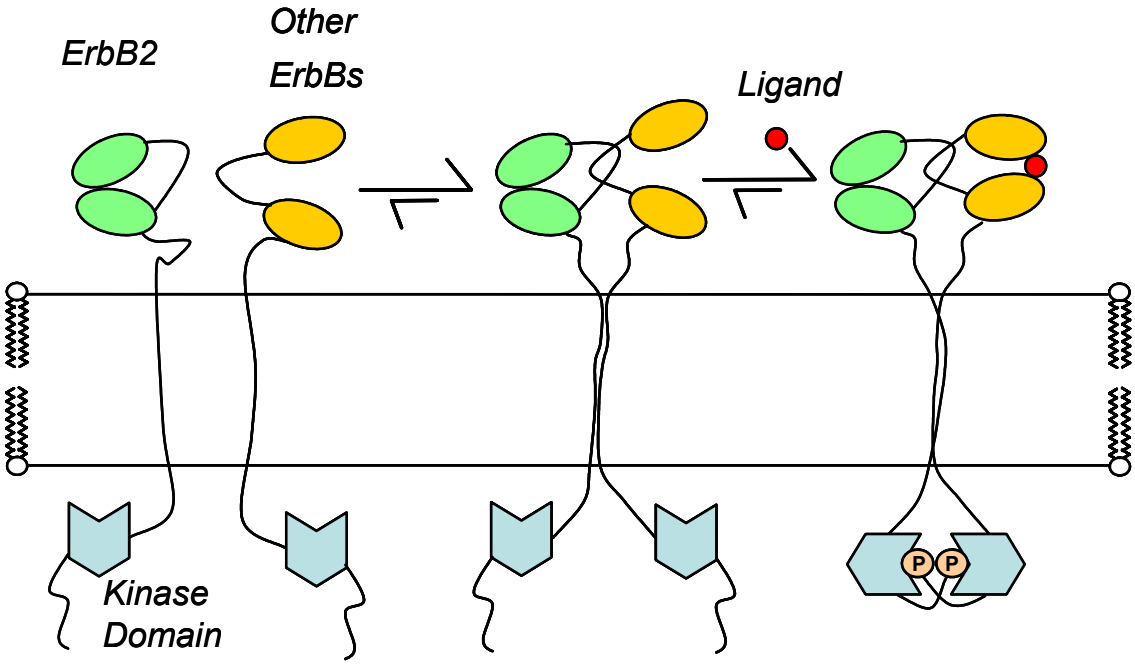

Figure 29. ErbB receptor dimerization and activation. The ErbB receptors exist in a pre-dimerized state on the cell surface (ErbB2-mediated heterodimers are shown here). The inactive dimer is activated by ligand binding to the extracellular domain, which results in structural rearrangement of the catalytic domain, activating the tyrosine kinase activity of the cytoplasmic domain. Adapted from reference (139).

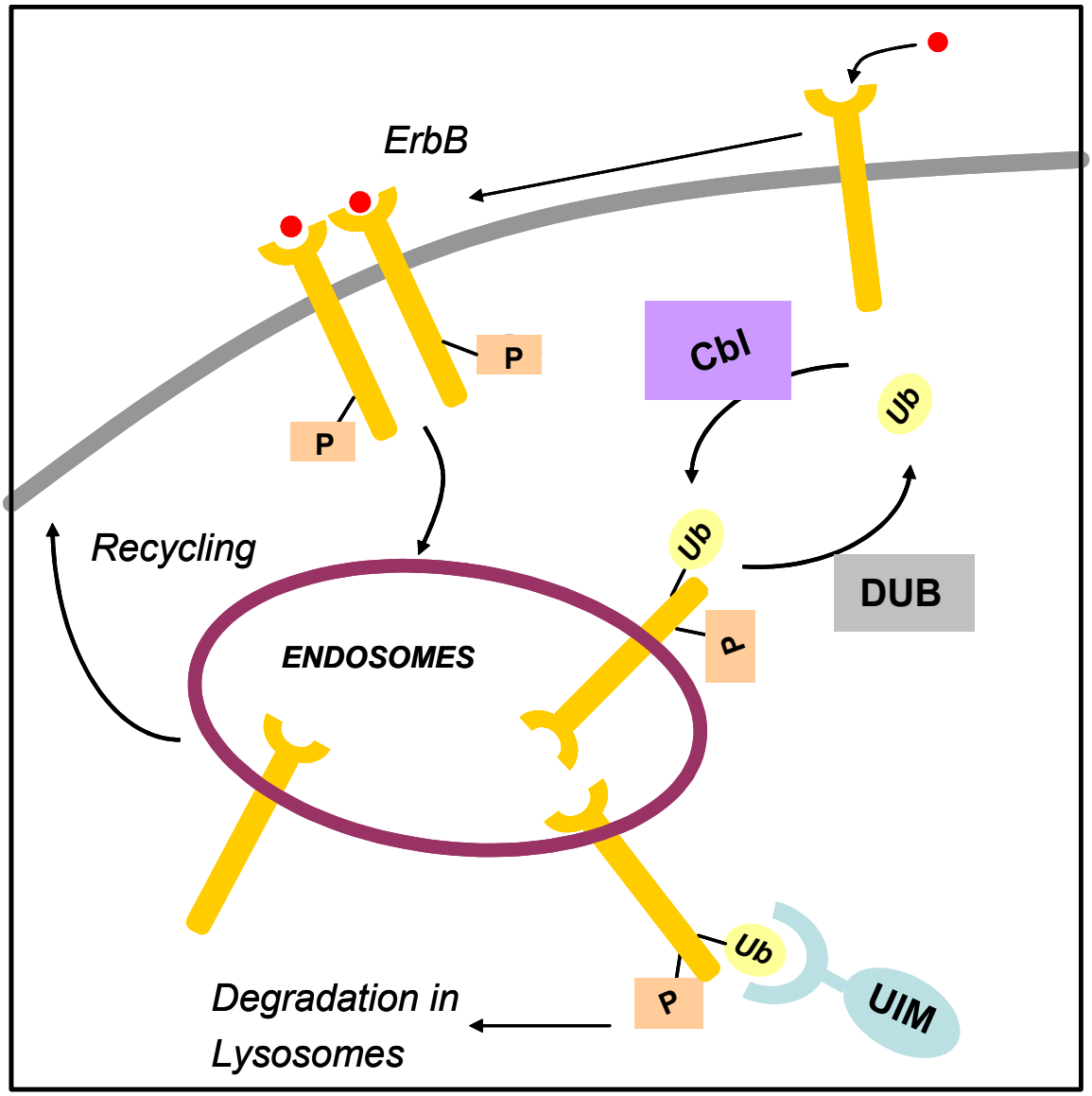

Figure 30. Downregulation of ErbB receptors via endocytosis. Ligand binding to the dimerized receptor induces receptor internalization into endosomes. In the endosomes, the phosphorylated receptor undergoes ubiquitylation (Ub) by E3 ubiquitin ligase (Cbl) and the ubiquitylated receptor recruits adaptors containing ubiquitin-interacting motif (UIM) and is targeted to the lysosomes for degradation. De-ubiquitylation enzymes (DUB) can abrogate this process and target the ErbB receptor to the recycling pathway. Adapted from reference (139).

Cumulative evidence indicates that the ErbB receptors exist in a pre-dimerized state that is not signaling competent (142, 152). Ligand binding to the pre-dimerized state induces rearrangement of the receptor subunits resulting in receptor activation (153-155) (Figure 29). Current information on the ErbB receptors signaling indicates that only ErbB1 and ErbB4 receptors can form functional homodimers as no physiological ligand for the ErbB2 receptor is known and the ErbB3 receptor has defective tyrosine kinase activity (156, 157). However, all members of the ErbB family are capable of initializing signalling cascades as heterodimers (141). It has been shown that the ErbB2 receptor is the preferred dimerization partner for other ErbB receptors (158-160). This is attributed to the structural characteristics of the extracellular domain of the ErbB2 receptor, which is reminiscent of the ligand-bound form of other ErbB extracellular domain. Thus, ErbB2 receptor is constantly primed for interactions with other ErbB receptors (161) (Figure 29). Furthermore, ErbB2-containing-heterodimers are characterized by higher affinity and broader specificity to many ligands compared to other heterodimer partners (160, 161). Also, ErbB2-containing-heterodimers undergo slow endocytosis and recycle back to the cell surface more frequently (162, 163). Thus, the ErbB2 receptor acts as an amplifier of the ErbB signaling network.

Transmembrane domains of the ErbB receptors are not passive membrane anchors and have been implicated in modulation of signaling by the ErbB receptor family. The critical role of TM domain in ErbB signaling is further evident in an oncogenic mutation identified in the TM domain of neu, a rat homologue of the ErbB2 receptor. Mutation of a single valine to glutamic acid at position 664 (V664E) located in the TM domain of neu receptor has been shown to constitutively activate the receptor, turning it into an oncogene (164, 165). It has been demonstrated that the glutamic acid mutation does not affect the membrane association of the sequence, but it rather alters the lateral interaction between the TM helices (136, 166). It has been suggested that the strong hydrogen bonding interactions between protonated Glu side chains in the mutant receptors stabilize the dimer structures, resulting in constitutive activation of the receptor (44). But recent TOXCAT assay with human ErbB2 (HER2) showed that the Glu mutation has very little effect on the dimerizing ability of HER2 TM domain (167). But this analysis was carried in bacterial inner membranes, which may not mimic the eukaryotic membranes.

Furthermore, it has been shown that engineered mutations, which are expected to increase dimer strength, do not result in neu/ErbB2 receptor overactivation (168). Thus, dimerization of the oncogenic form of neu/ErbB2 receptor via its TM domain may be necessary, though not sufficient for its transforming activity (168). Also recent computational studies on isolated TM domain of the neu/ErbB2 receptors have suggested that the wild-type and the mutated ErbB2 receptors have different dimerization motifs, possibly due to different orientation of the TM domains in the ErbB2 WT and the mutant receptors (169, 170). Thus, it is still unclear how the Glu mutation results in increased level of receptor association and constitutive activation of the neu/ErbB2 receptor.

The aim of this study was to understand the structural consequence of the hydrophilic mutation in the TM domain of the neu/ErbB2 receptor. We used fluorescence techniques to define the membrane position of the neu/ErbB2 TM domain with and without the activating mutation. We found that under physiological conditions, the Glu mutation (V664E) alters the membrane position of the TM domain, such that the charged Glu residue locates at the membrane interface and a truncated segment (residues 665-680) spans the bilayer. Other hydrophilic mutations (Gln and Asp) at position 664 were also found to reduce the effective TM length spanning the bilayer and the magnitude of shift in the TM helix position was found to correspond to the hydrophilicity and the ionization state of the hydrophilic residue. This suggests a novel mode of receptor activation in the neu/ErbB2 oncogene.

RESULTS

Defining the Topography of Membrane-Inserted ErbB2 WT and V664E mutant peptides using Fluorescence Spectroscopy

Peptides corresponding to the transmembrane segment of neu/ErbB2 receptor (underlined residues) with a single Trp as position 671, flanking charged residues and with or without the activating mutation [General Sequence: Acetyl-^{649}AEQRASP<u>VTFIIATV**X**^{664}GVLLFL**W**LVVVVGILI</u>KRRRYK^{686}-Amide, where X = V for WT and X = E for V664E mutant] were used to examine the effect of Glu mutation on the membrane topography of the neu/ErbB2 TM domain (Table 9). Fluorescence properties of a Trp residue within the hydrophobic sequence was used to define the topography of the membrane-inserted peptides (16, 24). First, the effect of bilayer width (hydrophobic mismatch effects) on Trp depth was used to define the effective length of the TM helix. Previous studies have shown that the Trp fluorescence is most blue-shifted at the bilayer width where there is hydrophobic matching between the TM segment and the hydrophobic core of the bilayer (16, 24, 29, 49). Red shifts in Trp fluorescence is generally observed in both thinner and wider bilayers due to hydrophobic mismatch. The TM state is destabilized in wider bilayers due to the unfavorable burial of the charged flanking residue into the bilayer resulting in formation of appreciable fractions of non-TM surface state (16, 24). Fluorescence also generally red shifts, although to a lesser degree, in thinner bilayers due to the fact that the distance between a Trp at the center of a bilayer to the membrane surface automatically decreases as bilayer width decreases. In addition, there can be a modest red shift due to (weak) oligomerization under conditions of positive mismatch in thin bilayer (16, 24). Thus, the bilayer width at which the Trp fluorescence is most blue shifted defines the 'effective TM length' ($L_{TM\ eff}$). $L_{TM\ eff}$ is typically expressed as the number of residues that span this bilayer width (Materials and Methods).

Figure 31 shows the effect of bilayer width on neu/ErbB2 WT and V664E mutant peptides at pH 7.0. For the WT sequence, the pattern of λmax as a function of bilayer width (Figure 31) show a minimum with very blue-shifted emission in DEuPC vesicles (c22:1 bilayers), indicative of an $L_{TM\ eff}$ of 23.8 residues (Table 10). This is consistent

Table 9. Neu/ErbB2 Transmembrane Peptides Used in this Study.

Peptide	***Sequence***
WT	AEQRASPVTFIIATVVGVLLFLWLVVVVGILIKRRRYK-Amide
V664E	AEQRASPVTFIIATVEGVLLFLWLVVVVGILIKRRRYK-Amide
V664D	AEQRASPVTFIIATVDGVLLFLWLVVVVGILIKRRRYK-Amide
V664Q	AEQRASPVTFIIATVQGVLLFLWLVVVVGILIKRRRYK-Amide

These peptides were purchased from Keck Peptide Synthesis Facility at Yale University. Peptides were purified via reverse-phase-HPLC using a C4 column using water/ 60% 2-proponal/ 40% Acetonitrile/0.5% v/v TFA as mobile phase. Peptide purity was confirmed using MALDI-TOF mass spectrometry (Proteomics Center, Stony Brook University). We estimated that the final purity was in the order of 95% or better. After drying the HPLC fractions, the peptides were stored in 1:1 (v/v) 2-proponal/water at 4ºC. Peptide concentrations were measured by absorbance spectroscopy on a Beckman DU-650 spectrophotometer using molar extinction coefficient (ε) for Trp of 5560 $M^{-1}cm^{-1}$ at 280 nm.

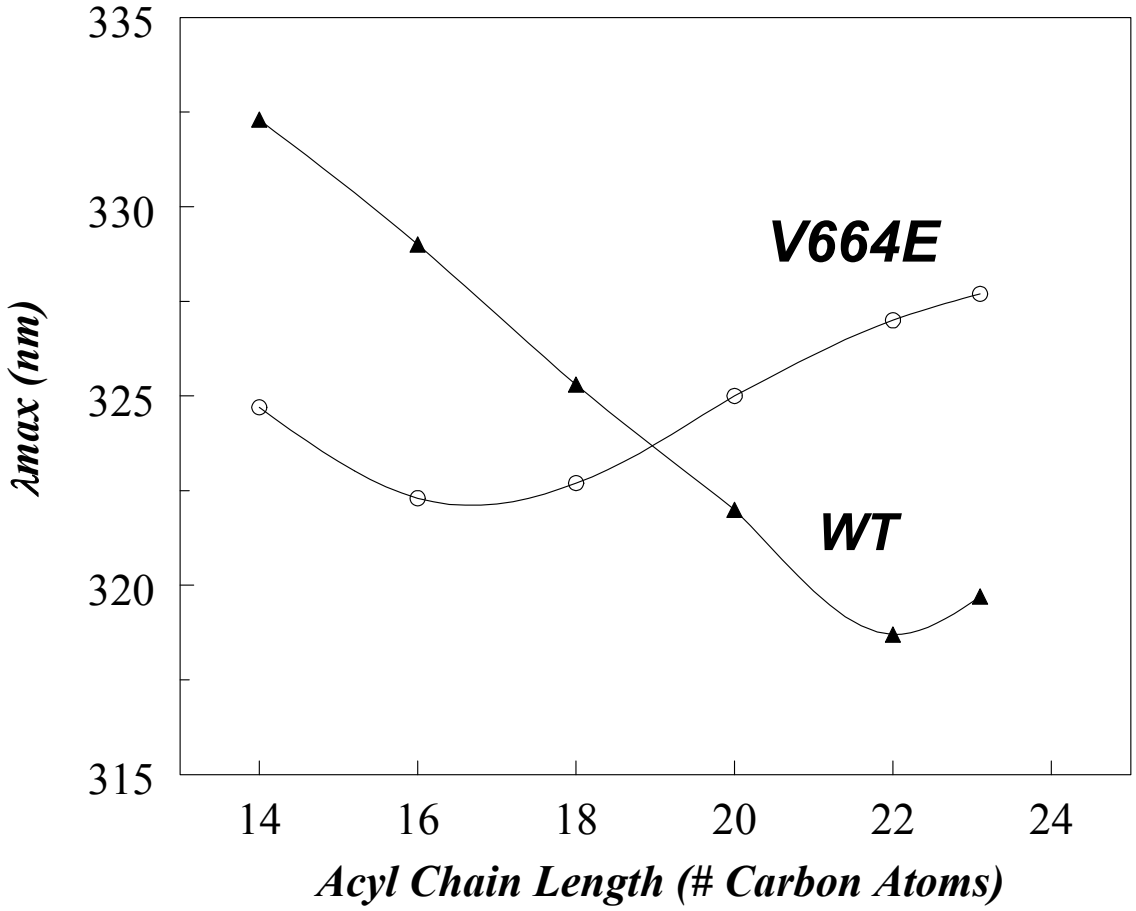

Figure 31. Effect of lipid bilayer width upon Trp emission λmax for neu/ErbB2 WT and V664E mutant peptides at pH 7.0. WT (▲) or V664E peptides (○) were reconstituted into model membrane vesicles composed of monounsaturated PCs with different acyl-chain lengths. Samples contained 2 μM peptide incorporated into 500 μM lipid dispersed in PBS at pH 7.0. The values shown are the average of six samples. The λmax values were generally reproducible to ±1 nm.

Table 10. $L_{TM\ eff}$ values for neu/ ErbB2 WT and V664X mutant peptides at different pH conditions.

Peptide	pH	$L_{TM\ eff}$ [a]
WT	7.0	23.8
V664E	4.0	20.0
	7.0	17.0
	9.0	16.8
V664D	4.0	16.7
	7.0	16.3
	9.0	16.2
V664Q	4.0	18.0

[a] $L_{TM\ eff}$ were calculated from λmax vs. bilayer width curves as described in Experimental Procedures.

with the putative TM segment of 25 residues (residues 656-680) spanning the lipid bilayer. The presence of the activating mutation (V664E) shifts the λmax minimum to a thinner bilayer width (Figure 31). The peptide behaves as a short TM helix with an $L_{TM\ eff}$ of 17 residues (Table 10). It adopts a relatively stable TM structure in DOPC bilayers (c18:1 acyl chains), but is destabilized in wider bilayers due to negative mismatch, with some degree of formation of a non-TM state. This indicates that the hydrophilic mutation alters the TM helix position within the bilayer, such that the Glu-664 locates at the bilayer interface and the TM segment extends from residue 665 to 680 (16 residues).

In addition, the Trp depth was measured directly using a dual quenching method (83). The dual quencher analysis utilizes two quenchers of Trp fluorescence, acrylamide and 10-DN to assess Trp depth. Acrylamide, an aqueous quencher, preferentially quenches Trp residues at or near the membrane surface, while 10-DN, the membrane-inserted quencher, quenches Trp buried in the membrane bilayer. The ratio of acrylamide quenching to 10-DN quenching (Q-ratio) responds nearly linearly to Trp depth in the bilayer, such that a low quenching ratio indicates a deeply located Trp, while a high Q-ratio is indicative of Trp near the bilayer surface (83). Extensive previous studies show that Trp at the bilayer center gives a Q-ratio of < 0.15, while Trp close to the bilayer surface gives a Q-ratio ≥ 1 (29, 49, 83).

The shift in helix position (and the consequent decrease in effective TM length) was confirmed by dual quenching analysis (Figure 32). In medium width DOPC bilayers, both the WT and V664E mutant exhibit low Q-ratio values consistent with a stable TM topography, with the Trp locating relatively deeper in V664E mutant than in the WT sequence (see below). In wider DEuPC bilayers, the V664E mutant shows high Q-ratio value characteristic of a shallow Trp location, consistent with some degree of formation of a non-TM state, but the WT sequence has low Q-ratio indicating that a predominant amount of the WT peptide remains in the TM state, with Trp locating deeply within the bilayer (Figure 32). This data is consistent with the observation that the V664E mutant has a shorter TM segment spanning the bilayer compared to the WT. Further, no significant quencher induced shifts in λmax was observed in both DOPC and DEuPC bilayers indicating that both WT and mutant peptide form homogenous population with single Trp location (Data not shown).

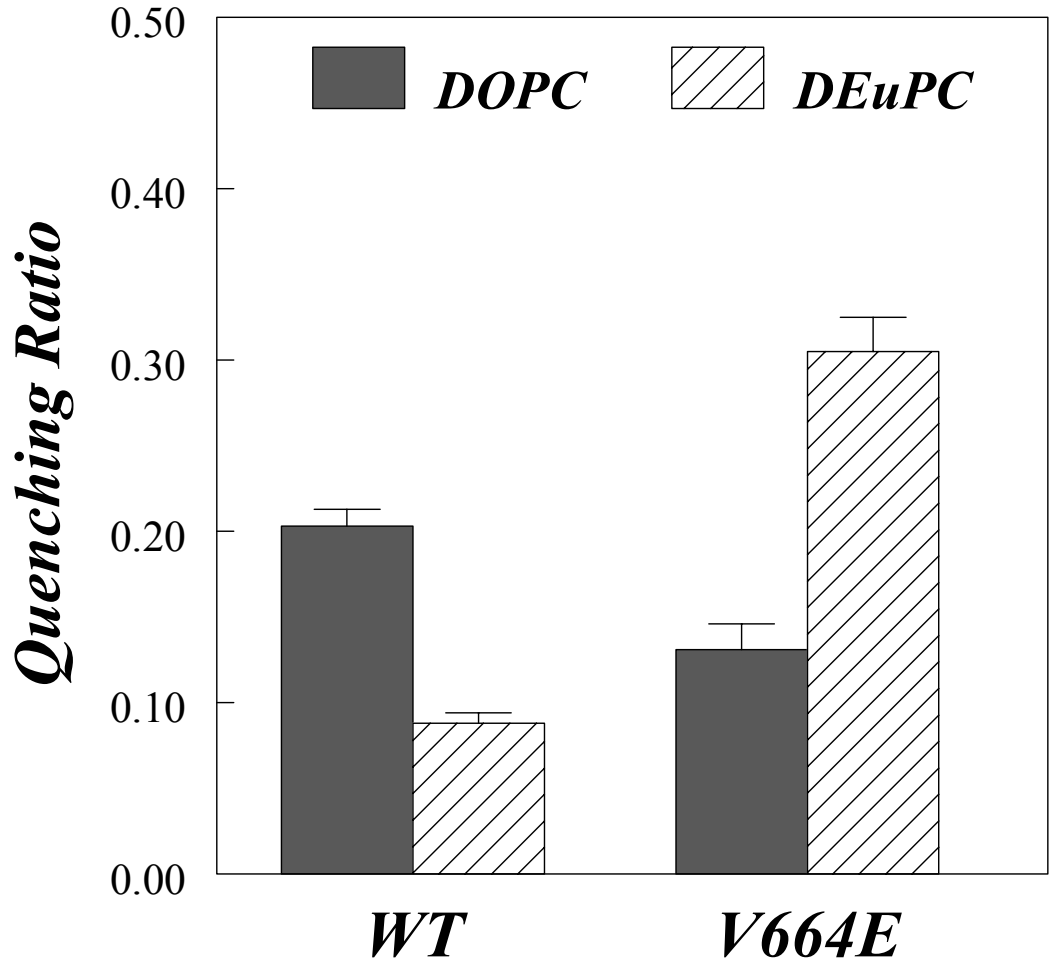

Figure 32. Quenching ratio for neu/ErbB2 WT and V664E mutant peptides when incorporated into DOPC (filled bars) or DEuPC (striped bars) vesicles at pH 7.0. Samples contained 2 μM peptide incorporated into 500 μM lipid dispersed in PBS at pH 7.0. Average values from six samples and standard deviations are shown.

The difference in Trp location between the neu/ ErbB2 WT and V664E mutant in DOPC bilayers is also noteworthy. The Trp at position 671 is closer to the center of the truncated TM sequence (residues 665-680) rather than the entire hydrophobic sequence (residues 656-680). So if the entire hydrophobic segment adopts a stable TM structure in DOPC vesicles, as it would be in case of the WT sequence, then the Trp would locate shallowly since it is off-center (Figure 33). But a shift in helix position, such that only truncated segment spans the DOPC bilayers, would result in Trp locating closer to the bilayer center (Figure 33). So the fact that the mutant peptide shows blue-shifted λmax and lower Q-ratio in DOPC vesicles compared to the WT sequence (Figures 31 & 32), indicating that the Trp is closer to the bilayer center in the V664E mutant than in the WT, further supports the idea that the hydrophilic mutation alters the TM helix position within the lipid bilayers and results in a truncated segment spanning the lipid bilayer. Furthermore, WT sequence with Trp at position 669 (closer to the center of the entire hydrophobic sequence) behaves qualitatively similar to WT peptide with Trp at position 67, with a $L_{TM\ eff}$ of 24 residues (data not shown). So, Trp position does not appear to affect the behavior of the WT sequence.

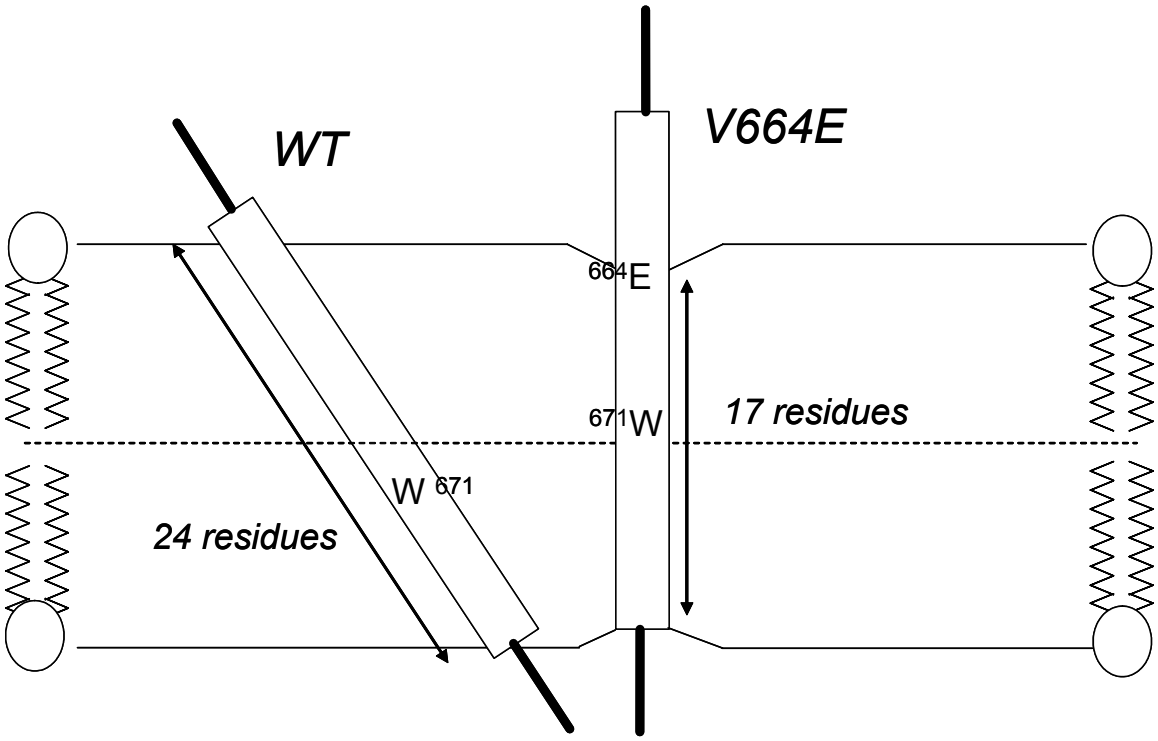

Figure 33. Schematic figure summarizing the change in Trp^{671} position within the bilayer upon helix shifting in DOPC bilayer at pH 7.0. The position of Trp^{671} in the neu/ErbB2 WT and V664E mutant sequences is shown. The dashed line represents the plane of the center of the bilayer. Even though the WT sequence adopts a TM structure, Trp^{671} locates slightly shallow as it is off-center in the hydrophobic sequence. Shift in helix position induced by the Glu^{664} mutation results in a truncated segment spanning the bilayer with Trp^{671} locating closer to the bilayer center.

Effect of Other Hydrophilic Mutations at Position 664 upon Membrane Positioning of neu/ErbB2 Receptor

We also examined whether other hydrophilic residues known to alter neu/ErbB2 receptor function (165), when located at position 664, could alter TM helix position within the bilayer. To do this, neu/ErbB2 TM sequences with a Gln or Asp substitution at position 664 were compared to the WT sequence (General Sequence: Acetyl-^{649}AEQRASPVTFIIATV**X**^{664}GVLLFL**W**LVVVVGILIKRRRYK^{686}-Amide, where X = Q for V664Q and X = D for V664D mutant peptides) (Table 9). Figure 34 shows the effect of bilayer width upon Trp λmax for the V664Q and the V664D mutant peptides at pH 7.0. Qualitatively, both V664Q and V664D mutants exhibit λmax profile similar to the V664E mutant (Figure 34). This pattern corresponds to a truncated TM segment spanning the bilayer and forming relatively stable TM structures in DOPC bilayers, but is destabilized in wider bilayers due to negative mismatch. The estimated $L_{TM\ eff}$ values of 18 residues and 16.3 residues for V664Q and V664D peptide respectively is comparable to the effective TM segment of 17 residues observed for the V664E peptide (Table 10)

These conclusions were confirmed by fluorescence quenching data (Figure 35). All mutant peptides exhibit low Q-ratios in DOPC vesicles (Figure 35) corresponding to either fully or almost fully TM configurations, with the Trp near the bilayer center and higher Q-ratios in wider DEuPC vesicles (Figure 35) indicating a shallower Trp depth, consistent with a some degree of formation of a non-TM state.

The cumulative data indicates that a strong hydrophilic residue at position 664 induces a shift in helix position, such that the hydrophilic residue locates at or closer to the bilayer surface and only a truncated segment spans the bilayer. Trp λmax and Q-ratio values (Figures 34 & 35) show that the magnitude of shift in helix position depends on the identity of hydrophilic residue at position 664 and it increases in the order: $Q < E \leq D$. This is supported by the $L_{TM\ eff}$ values derived from the effect of bilayer width upon λmax (Table 10). The effective TM length decreases by 5.8 residues, 6.8 residues and 7.5 residues for V664Q, V664E and V664D mutants respectively relative to the WT sequence (Table 10). This order of 'helix shifting potential' for hydrophilic residue is similar to that we observed in simple model hydrophobic peptide sequences (Chapter 4).

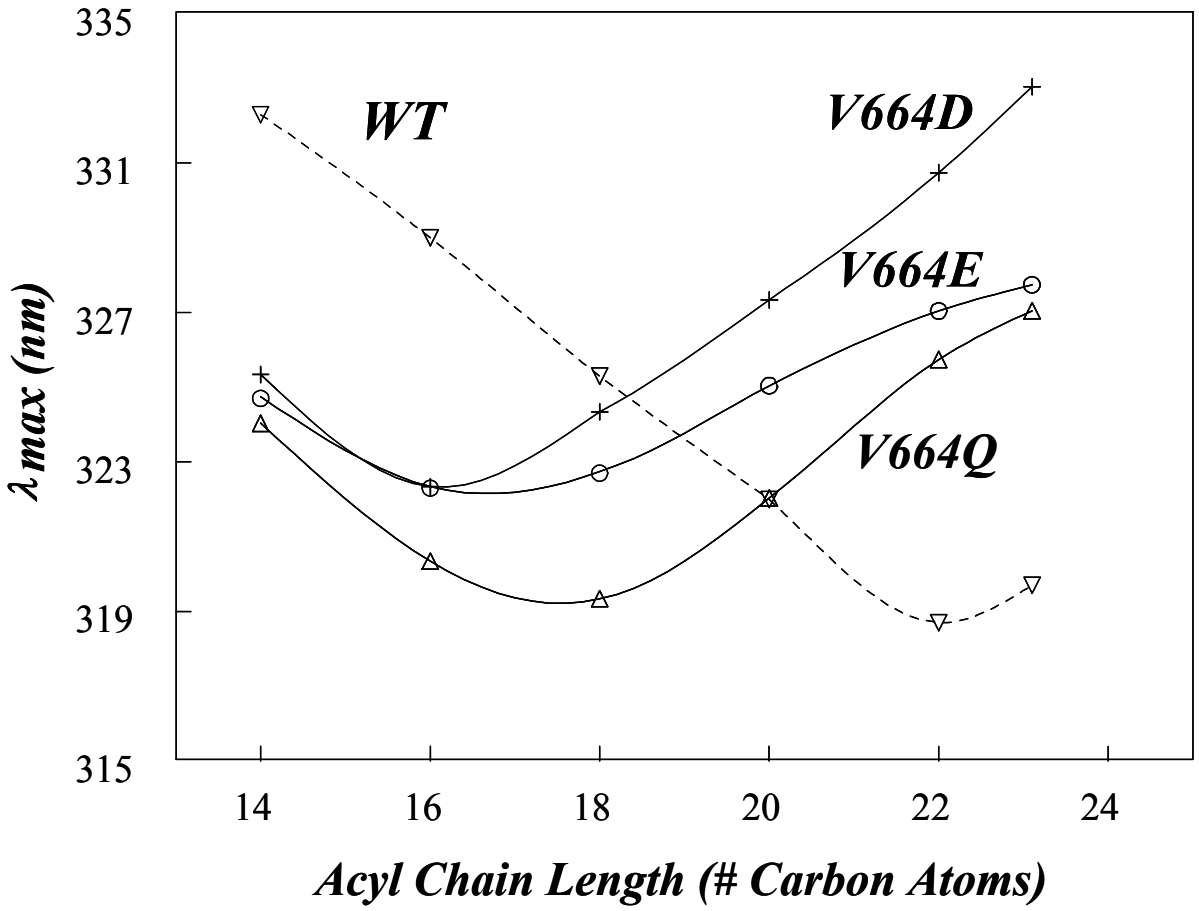

Figure 34. Effect of lipid bilayer width upon Trp emission λmax for neu/ErbB2 V664Q and V664D mutant peptides at pH 7.0. The WT and V664E data from Figure 31 are shown for comparison. The ErbB2 peptides WT (∇), V664E (○), V664Q (Δ) or V664D (+) were reconstituted into model membrane vesicles composed of monounsaturated PCs with different acyl-chain lengths. Samples contained 2 μM peptide incorporated into 500 μM lipid dispersed in PBS at pH 7.0. The values shown are the average of three to six samples. The λmax values were generally reproducible to ±1 nm

.

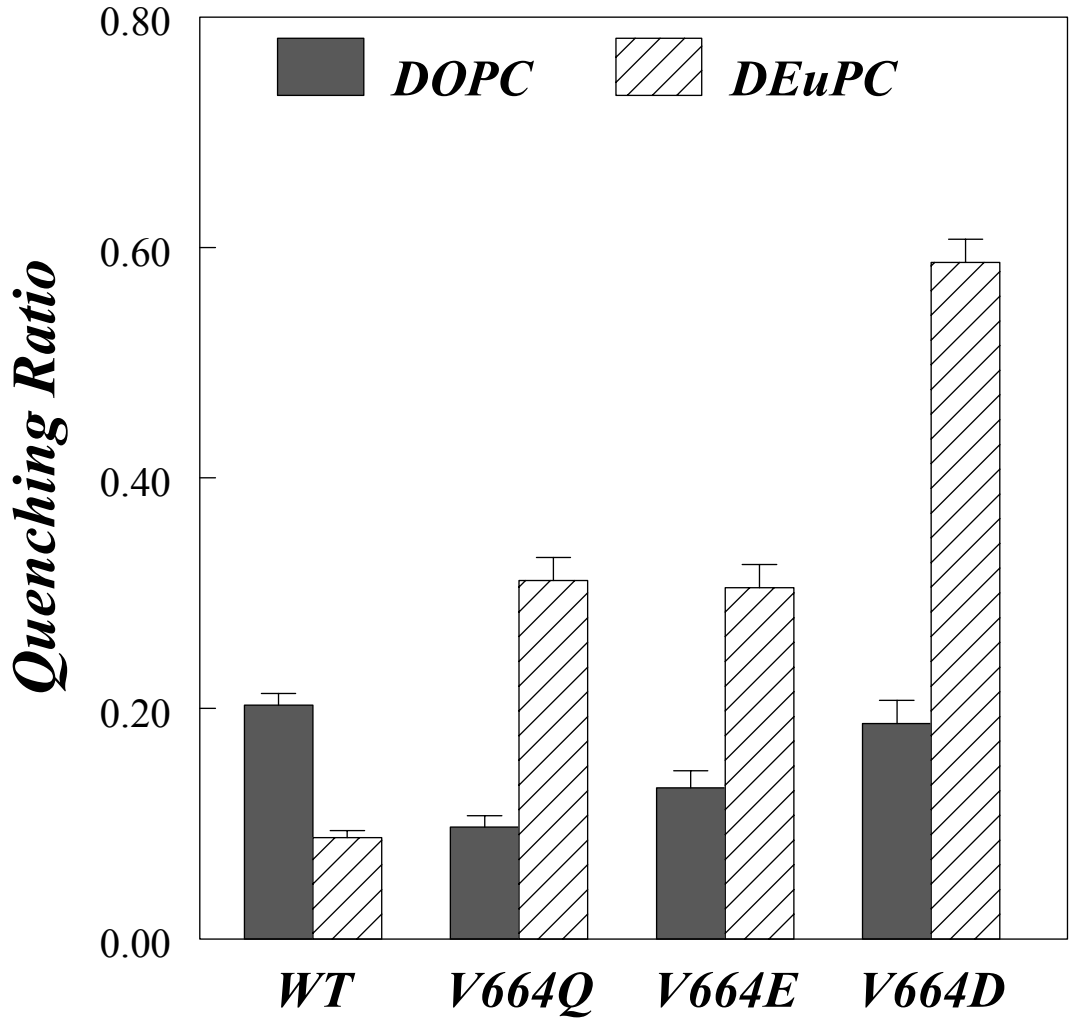

Figure 35. Quenching ratio for neu/ErbB2 V664Q and V664D mutant peptides when incorporated into DOPC (filled bars) or DEuPC (striped bars) vesicles at pH 7.0. Quenching ratio for the ErbB2 WT and V664E peptides from Figure 32 are shown for comparison. Samples contained 2 μM peptide incorporated into 500 μM lipid dispersed in PBS at pH 7.0. Average value from three to six samples and standard deviation are shown.

How pH Affects Topography of ErbB2 TM segments with Ionizable Residue Mutations.

In order to investigate the effect of charge on the ionizable residues (Glu and Asp) on ErbB2 TM helix behavior, their pKa's were measured. To do this, samples containing peptides inserted into vesicles prepared at low pH were titrated with base as described previously (49). Changes in ionization were detected by pH-induced changes on Trp emission (49). The pKa values for V664E and V664D peptides in DOPC vesicles were 6.94 and 6.12 respectively (data not shown). The pKa values were very similar in DEuPC vesicles (data not shown). The pKa value agrees well with previous work, which estimated the pKa of V664E peptide to be ~ 6.5 using NMR measurements (44). [Note: pH titration for the WT sequence revealed no measurable pKa value and no pH-induced change in Trp depth or fluorescence quenching was observed for the WT sequence (data not shown). Hence the fluorescence values of the WT sequence at pH 7.0 are used as reference for all pH conditions].

Fluorescence measurements were then performed under conditions under which Glu and Asp residues would be fully protonated (pH 4.0) or fully deprotonated (pH 9.0), based on their pKa values. Figure 36 shows the Trp λmax and Q-ratio values for V664E and V664D peptides at various pH in DOPC and DEuPC bilayers. At pH 9.0, when Glu and Asp are fully ionized, the Trp locates shallowly as shown by red-shifted Trp fluorescence and high Q-ratio values. This indicates that the D^- and E^- residues resist burial within the lipid bilayer and locate at or closer to the bilayer surface, resulting in a truncated TM segment spanning the bilayer.

This is confirmed by the $L_{TM\ eff}$ values derived from λmax vs. bilayer width curves (Figure 37). At pH 9.0, the $L_{TM\ eff}$ for V664E and V664D peptides were 16.8 and 16.2 residues respectively, much shorter than the 23.8 residues observed for the WT sequence (Table 10). Interestingly, the $L_{TM\ eff}$ value estimates for V664E and V664D at pH 9.0 are very similar to the $L_{TM\ eff}$ estimates at pH 7.0 [17.0 and 16.3 residues respectively] (Table 10). This indicates that even under physiological pH conditions, Glu and Asp residues are primarily in an ionized state.

Under low pH conditions (pH 4.0), when Glu and Asp residues were protonated, the mutant peptides adopts a TM topography in DOPC bilayers, but with different Trp depth compared to the charged state and the WT, as judged by its blue-shifted Trp λmax

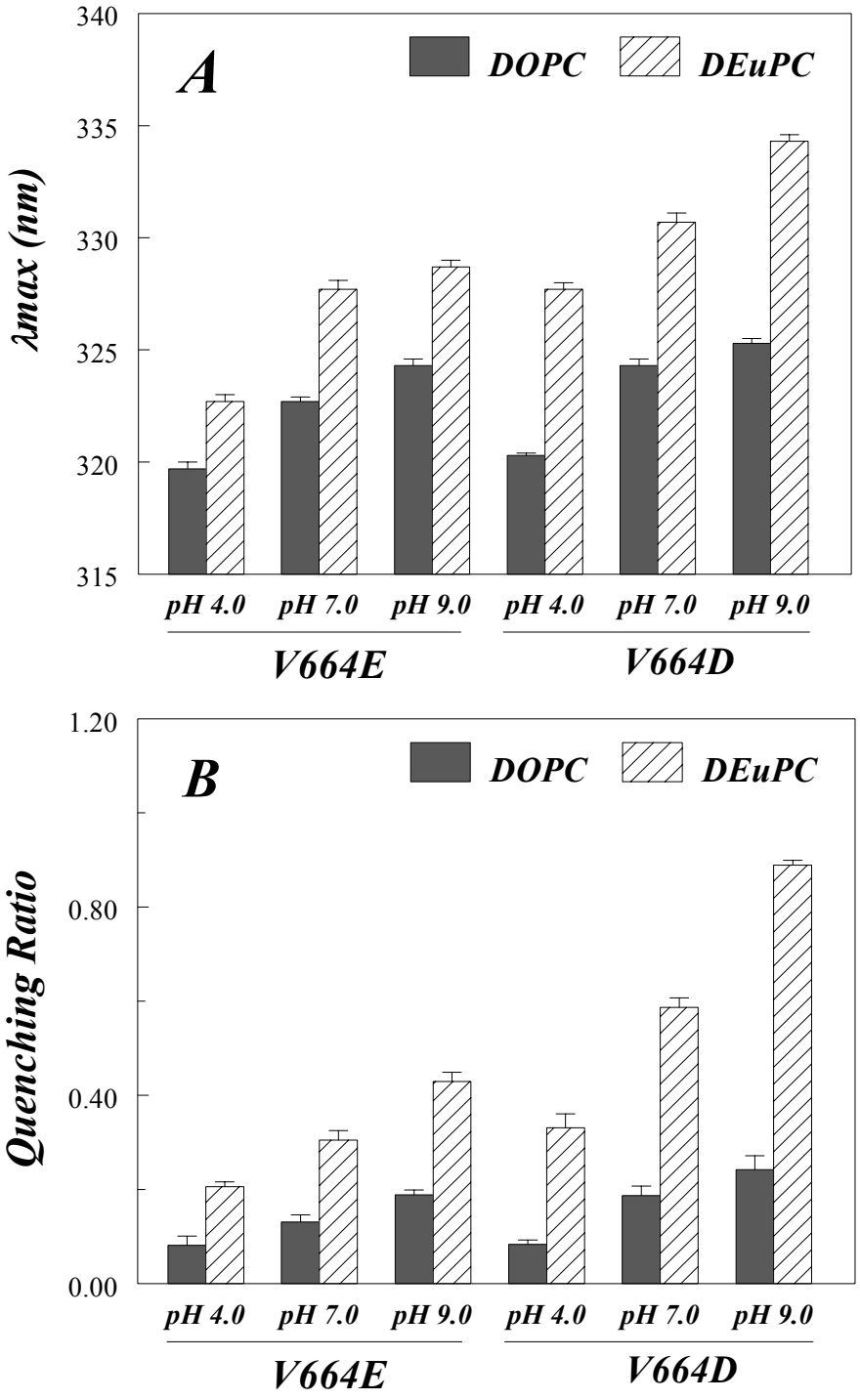

Figure 36. Trp λmax and quenching ratio for neu/ErbB2 V664E and V664D mutant peptides when incorporated into DOPC (filled bars) or DEuPC (striped bars) vesicles at different pH. Samples contained 2 μM peptide incorporated into 500 μM lipid dispersed in pH adjusted PBS buffer. Average values from three to six samples and standard deviations are shown.

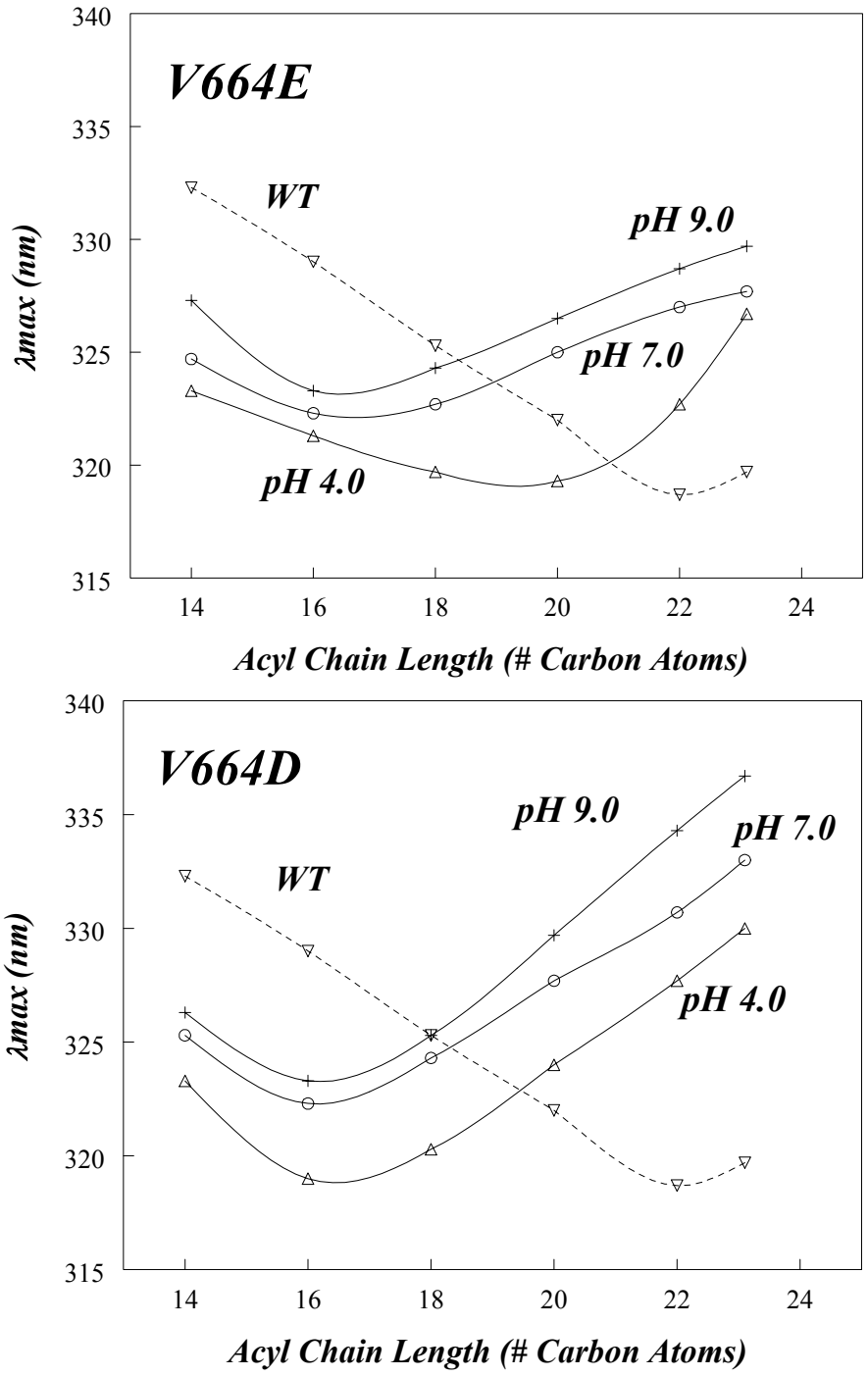

Figure 37. Effect of lipid bilayer width upon Trp emission λmax for neu/ErbB2 V664E and V664D mutant peptides at different pH. Data at pH 4.0 (Δ), pH 7.0 (○) and pH 9.0 (+) are shown. The curve for the ErbB2 WT sequence is shown for comparison. The samples contained 2 μM peptide incorporated into 500 μM lipid dispersed in pH-adjusted PBS. Average values of three to six samples are shown.

values and low Q-ratios (Figure 36). The data shows that the Glu and Asp residues induce smaller shifts in helix position in the uncharged state than in the charged state. But even the uncharged residues induces a substantial shift in TM helix position, as shown by the decrease in $L_{TM\ eff}$ to 20 residues and 16.8 residues for V664E and V664D respectively relative to the WT sequence (23.8 residues) (Table 10). The observation that the E^0 did not induce as much shift as the as the D^0 correlates well with our earlier observations that D^0 residue is more hydrophilic than an E^0 (Chapter 4).

Secondary Structure of neu/ErbB2 TM peptides – CD measurements

In order to evaluate the secondary structure of the neu/ErbB2 peptides, CD measurements were carried out (Table 11). The α-helical content was estimated to be 72 % for wild-type sequence. The α-helical content decreased by a small amount for V664X mutant peptides. The estimated α-helical content was 67% for V664E peptide, 65% for V664D peptide and 68% for V664Q peptide (Table 11). Furthermore, the ionization state of the Glu^{664} and Asp^{664} did not affect the helical content by more than 2 % (Table 11). The helical content was also similar for peptides incorporated into DOPC and DEuPC vesicles (Table 11).

Table 11. Estimated secondary structure for neu/ErbB2 WT and V664X mutant peptides incorporated into DOPC or DEuPC vesicles under various pH conditions. Samples contained 2 μM peptide incorporated into 500 μM lipid dispersed in PBS.

Peptide	pH	% Helix [a]	
		DOPC	DEuPC
WT	7.0	72	72
V664E	4.0	68	67
	7.0	67	67
	9.0	66	65
V664D	4.0	66	66
	7.0	65	65
	9.0	65	64
V664Q	7.0	68	69

[a] Remainder were predominantly random structure with <10% β-structure.

DISCUSSION

In this study, using a model membrane system, we found that the activating mutation (V664E) within the TM domain of the neu/ErbB2 receptor alters the membrane boundary of the TM helix. Under physiological conditions, the Glu residue is partially charged and induces a shift in the TM helix position, such that the hydrophilic Glu residue locates at or closer to the membrane surface. As a result, the effective length of the TM segment decreases from 24 residues in WT to 17 residues in V664E mutant peptide. Furthermore, the extent of the shift in helix position correlates with the ionization state of the Glu-residue. A fully charged Glu residue induces a greater amount of shift in helix position compared to the protonated Glu residue.

Our data partially agrees with that of Smith et al. (44) who showed that the Glu^{664} in the neu/ErbB2 TM domain does not partition into the bilayer at physiological pH in dimyristoylphosphatidylcholine (DMPC) bilayers, while protonation of Glu^{664} allowed the sequence to fold into a long α-helix spanning the bilayer (44). However, they suggested that the charged Glu residue leads to unfolding of the sequence N-terminal to the Glu^{664} residue, thereby shortening the length of TM helix, but we observe only a 2 % decrease in α-helical content of the neu/ErbB2 mutant peptide when Glu is charged compared to when Glu is protonated (Table 11). Hence, local unfolding does not appear to accommodate the decrease in effective TM length in our system.

Our finding that the Glu^{664} shifts the TM helix position (whatever its ionization state) raises the possibility that the Glu^{664} mutation alters the configuration of the existing TM domain interactions. For example, the transverse shift in the TM helix position induced by the Glu^{664} mutation could alter the relative orientation of the TM helices in the dimer and perhaps promotes the adoption of an 'active' configuration (Figure 38C). It has been proposed that HER2, human ErbB2 receptor, has two distinct dimerization modes: one mediated via a N-terminal dimerization motif and other via a C-terminal dimerization motif (167, 171). Using computational analysis, Ben-Tal and colleagues (171) have proposed a molecular-switch mechanism for HER2 receptor activation wherein the dimer mediated via the C-terminal motif represents the inactive conformation and the transition to the active state would involve a switch to dimerization via the N-terminal motif (171).

A

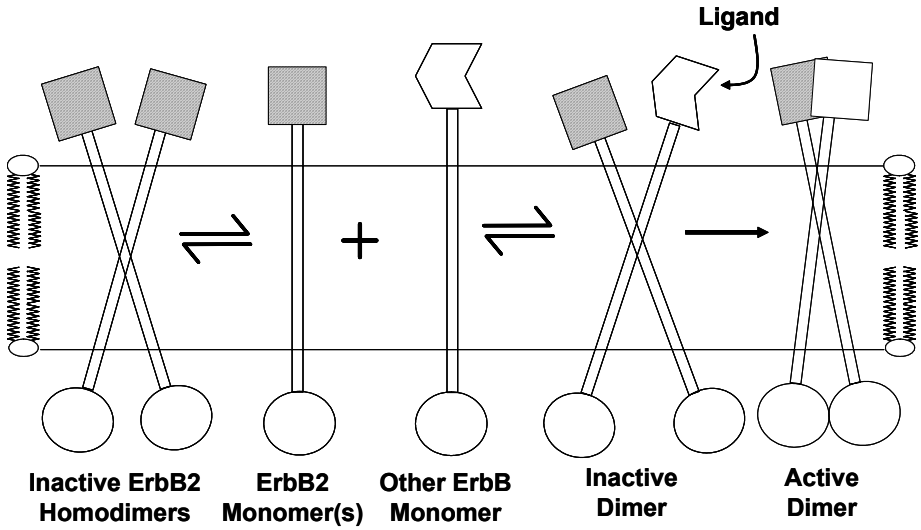
Ligand
Inactive ErbB2 Homodimers
ErbB2 Monomer(s)
Other ErbB Monomer
Inactive Dimer
Active Dimer

B

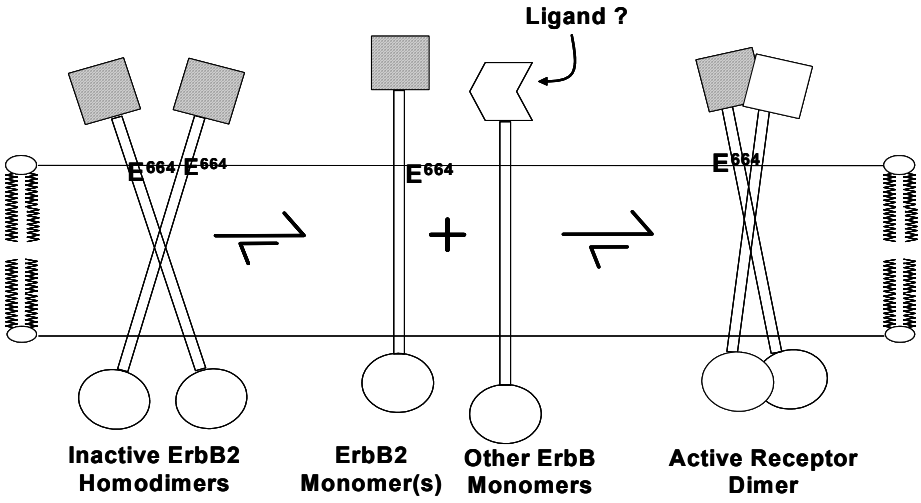
Ligand ?
E664
E664
E664
E664
Inactive ErbB2 Homodimers
ErbB2 Monomer(s)
Other ErbB Monomers
Active Receptor Dimer

C

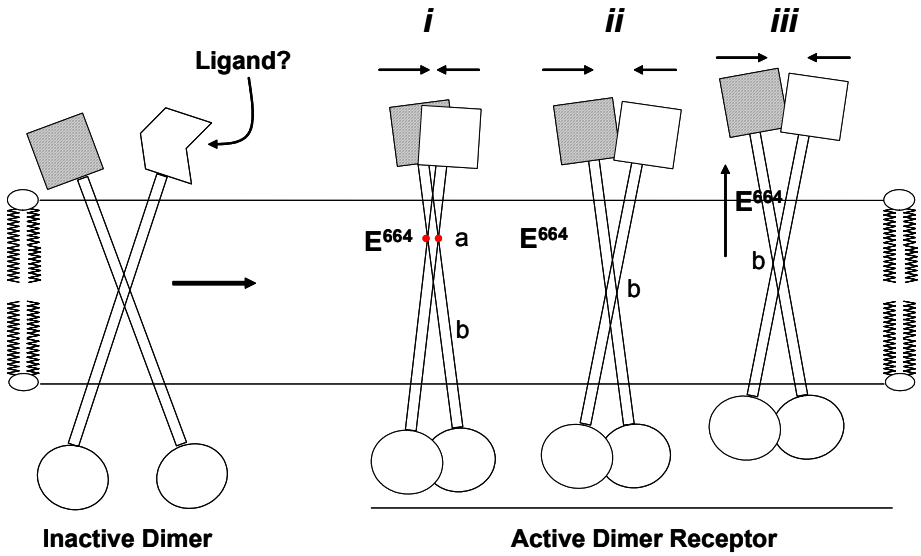
i
ii
iii
Ligand?
E664
a
b
E664
b
E664
b
Inactive Dimer
Active Dimer Receptor

Figure 38. Schematic Representation of Possible Mechanism for Receptor Activation in wild-type and mutant neu/ErbB2 Receptor. (A) Activation of the wild-type ErbB2 receptor. The neu/ErbB2 receptor exists in steady state equilibrium between the inactive homodimers and the monomeric neu/ErbB2 receptor. The monomeric receptor could associate with other ErbB receptors to form inactive heterodimers. The inactive heterodimers are activated by ligand binding, which results in structural rearrangement of the cytoplasmic (catalytic) domain stimulating the tyrosine kinase activity (B) Glu^{664} mutation upregulates the neu/ErbB2 receptor by altering the equilibrium between the homodimers and the heterodimers. The Glu^{664} mutation destabilizes the neu/ErbB2 homodimers and shifts the equilibrium towards the monomeric ErbB2 receptor and thereby promoting the formation of the functional heterodimers. The shift in TM helix position alters the dimer configuration, which can result in constitutive activation of the receptor. (C) Possible mechanism for receptor upregulation in the V664E mutant neu/ErbB2 receptors. (i) The Glu^{664} residue is directly involved in stabilizing the dimer structure formed possibly via hydrogen bonding interactions with the neighboring helix. (ii) The Glu^{664} alters the dimerization mode by changing the relative orientation of the receptor in the dimer. The alternate dimerization mode can result in a more stable dimer structure. (iii) The transverse shift induced by the Glu^{664} mutation changes the spatial arrangement of the cytoplasmic catalytic domain, resulting in activation of the kinase activity. The schematic shown here depicts an altered dimerization mode, but receptor activation can happen with or without altering the dimerization mode. It is possible that a combination of these modes is involved in receptor upregulation.

Similar alternative dimerization modes are possible in neu receptor and the activating mutation could shift the equilibrium towards the active form. In fact, a consensus sequence in the N-terminal has been shown to be involved in neu TM domain dimerization (172, 173), although no other dimerization motifs has been identified. Further evidence that the Glu^{664} mutation activates the neu/ErbB2 receptor by altering the pre-dimerized state comes from Sharpe et al. (135), who showed that the Glu^{664} mutation induces significant structural rearrangement in the neu/ErbB2 TM domain extending over four helix turns downstream of the mutation, arguing that it could alter the lateral association of the TM helix with other helices within the membrane. (135).

Another possible outcome of altering the dimerization mode is that it could change the equilibrium between the neu/ErbB2 homodimers and neu/ErbB2-containing-heterodimers. No physiological ligand for neu/ErbB2 receptor is known and it is believed the neu/ErbB2 receptor typically signals as a heterodimer with other ErbB receptors (139, 140). Perhaps, by altering the orientation of the dimer structure, the Glu^{664} mutation promotes the formation of functional heterodimers over inactive ErbB2 homodimers by either destabilizing the ErbB2 homodimers or by stabilizing the ErbB2-containing heterodimers (Figure 38B).

An alternate possibility is that the shift in the TM domain could move the cytoplasmic catalytic domain closer to the bilayer and alter the spatial arrangement of the catalytic domains such that it activates the receptor dimer. This mode of receptor activation may or may not be accompanied with a change in the dimerization mode of the receptor (Figure 38C). Further, this could result in constitutive activation of the receptor as the structural rearrangement induced by the transverse shift could mimic the activated dimer structure.

In a recent report, McLaughlin et al. (174) have proposed an electrostatic engine model for activation of the ErbB family receptor. They postulated that the juxtamembrane (JM) region and the tyrosine kinase domain of ErbB family members bind electrostatically to acidic lipids in the inner leaflet of the plasma membrane and this result in autoinhibition. Upon ligand activation, the Ca^{2+}/calmodulin complex binds to the JM region, reversing its net charge and this allows the JM and the kinase domains of the ErbB protein to move off the membrane, at which time, the latter becomes catalytically

active. We find that the hydrophilic mutation shifts the TM helix position and thus moves the catalytic domain towards the membrane. This appears to contradict the electrostatic engine model, where the catalytic domain moves away from the bilayer. However, this is not necessarily true. If the JM region and the kinase domain interact with the inner leaflet, then a shift in TM helix location could move the charged residues in the N-terminus of the JM sequence such that the interaction of the JM sequence with the bilayer surface is weakened and this could move the JM/kinase domains away from the bilayer, resulting in removing the inhibition.

Heterodimers containing neu/ErbB2 receptor undergo slow downregulation and recycle back to the cell surface more efficiently (162, 163). The altered membrane position of the mutated neu/ErbB2 TM domain could further compromise the downregulation of the mutant receptor. This is supported by studies showing that the TM domain of other receptor tyrosine kinases play a critical role in ligand-induced receptor internalization (131, 134, 175). For example, Yamada et al. (175) have shown that replacing the charged residues flanking the TM domain of insulin receptor to uncharged residues and thus changing the TM domain membrane position, results in impaired internalization of the receptor. Also, a TM domain shift induced by achondroplasia Arg380 mutation in FGFR3 receptor is believed to impair ubiquitination of the receptor and its subsequent degradation of the receptor (131, 134). So, a similar mechanism may apply to mutant neu/ErbB2 receptor.

In other experiments, we found that the Gln or Asp mutations at position 664 also alter the membrane position of the TM domain and the extent of shift in helix position correlates with the hydrophilicity of the residue. The order of extent of transverse shift is $Asp^{-1} > Glu^{-1} \sim Asp^{0} > Gln > Glu^{0}$. This data is consistent by our earlier findings that the magnitude of shift is controlled by hydrophilicity and ionization state of the hydrophilic residue (Chapter 4).

It has been shown that only certain hydrophilic mutation at position 664 in TM domain of neu/ErbB2 receptor have the ability to constitutively activate the receptor (165). Of all hydrophilic mutation tested, Glu^{664} had the maximum transforming ability, followed by Gln^{664}, which had about 70% transforming ability of Glu^{664}, and then Asp^{664}, which had about 10 % transforming ability of the Glu^{664} mutation (165). Other

hydrophilic mutations, like Gly, His and Lys, at position 664 showed no transforming ability (165). Interestingly, the transforming ability of a hydrophilic residue correlates with the ability of these residues to induce a shift in the TM helix position under physiological pH conditions (Chapter 4). For example, at physiological pH, Glu, Gln and Asp residues have high propensity to alter TM helix position compared to Gly, His and Lys residues (Chapter 4). The high degree of specificity required for the activating mutation suggests that a precise arrangement of the dimerized state is required for neu/ErbB2 receptor activation.

Further support for the idea that a charged residue mutation in a natural TM sequence can alter the protein function by shifting helix position comes from a recent study on FGFR3, a tyrosine kinase receptor involved in skeletal system development (131). Using neutron diffraction, Hristova and colleagues showed that a hydrophilic mutation (G380R) within the TM domain of the FGFR3 receptor induces a shift in the TM segment embedded in the membrane (131). They proposed that the structural change in the TM domain plays a role in slow downregulation of the activated mutant receptors, resulting in abnormal bone development (dysplasias) (131, 134). Shifts in TM helix position have also been shown to functionally relevant in bacterial chemoreceptors (124, 125). Ligand binding to the extracellular domain has been shown to induce a piston-type sliding of signaling TM helix towards the cytoplasm, which modulates the kinase activity inside the cell (124, 125). Recent study shows that signal enhancing substitutions typically drive the piston displacement of the signaling helix (124).

CHAPTER 6

MEMBRANE TOPOGRAPHY OF THE HYDROPHOBIC ANCHOR SEQUENCE OF POLIOVIRUS 3A AND 3AB PROTEINS

After poliovirus (PV) enters the host cell its plus strand RNA genome is translated into a polyprotein that contains one structural (P1) and two nonstructural domains (P2, P3; Figure 39A). There is an efficient and regulated cascade of protein processing that produces cleavage products with function distinct from those of the precursor proteins (Figure 39A). A variety of precursor and mature proteins are released from the PV polyprotein by cleavage with proteinases $2A^{pro}$, $3C^{pro}$/$3CD^{pro}$. The proteins of the P1 domain (VP1-VP4) assemble to form the capsid while those derived from P2 ($2A^{pro}$, 2B, 2BC, $2C^{ATPase}$) are primarily responsible for the biochemical and structural changes that occur in the infected cell. The proteins of the P3 domain are those most directly involved in RNA synthesis. These include two important and relatively stable precursors, proteinase $3CD^{pro}$ and 3AB, which were shown to specifically interact with a cloverleaf-like structure at the 5' end of the viral RNA in a reaction that required for RNA replication. The two precursors are slowly processed to the mature polypeptides, 3A, 3B, $3C^{pro}$, and $3D^{pol}$ (176).

Shortly after infection of susceptible cells with PV, dramatic changes take place in the host cell. There is a striking rearrangement of the cellular membranes and vesicles accumulate in the cytoplasm *(*177-179*)*. These vesicles are mostly derived from the endoplasmic reticulum, Golgi apparatus, and lysosomes of the host cell. Recent studies indicate that many of the vesicles are autophagosomes, which carry virus-specific proteins, for example 2BC and 3A (180). The viral non-structural proteins and their precursors, as well as some cellular proteins and the viral RNA assemble to form a replication complex on the cytoplasmic surface of the vesicles that appear as rosette-like structures (178, 181). Such structures are believed to provide a suitable environment for RNA replication by increasing the local concentrations of viral proteins or by providing a scaffold for the assembly of the members of the complex. Some of the viral nonstructural proteins (2B, $2C^{ATPase}$ and 3A) associate with the replication complex via their own membrane binding domains while others are recruited to the complex by protein/protein or protein/RNA interactions (176, 182). The PV RNA polymerase $3D^{pol}$ is an example of a soluble protein that interacts with another protein, 3AB, whose hydrophobic domain, located in 3A, anchors the complex to membranes (183, 184).

(A)

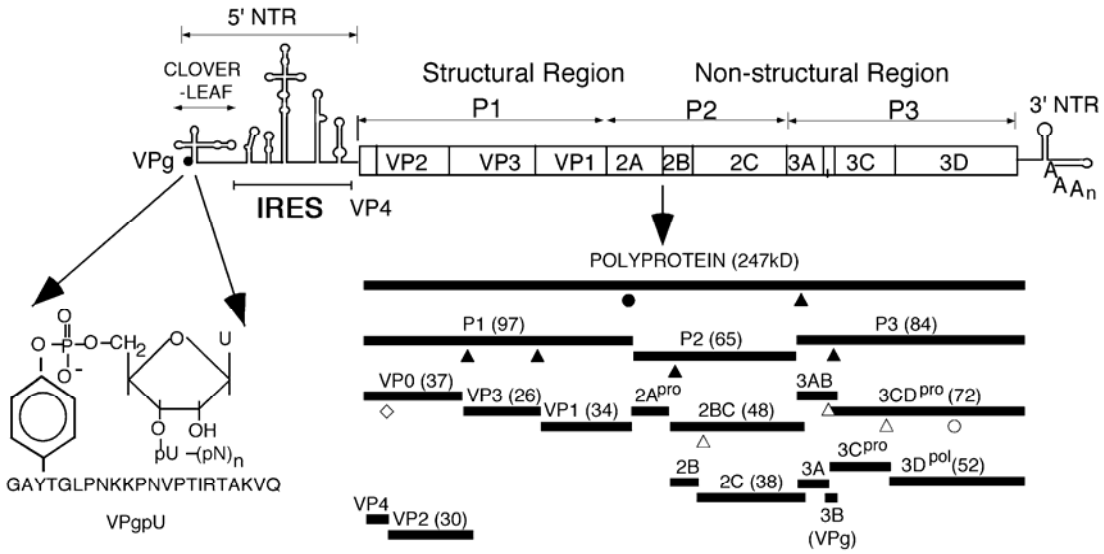

(B)

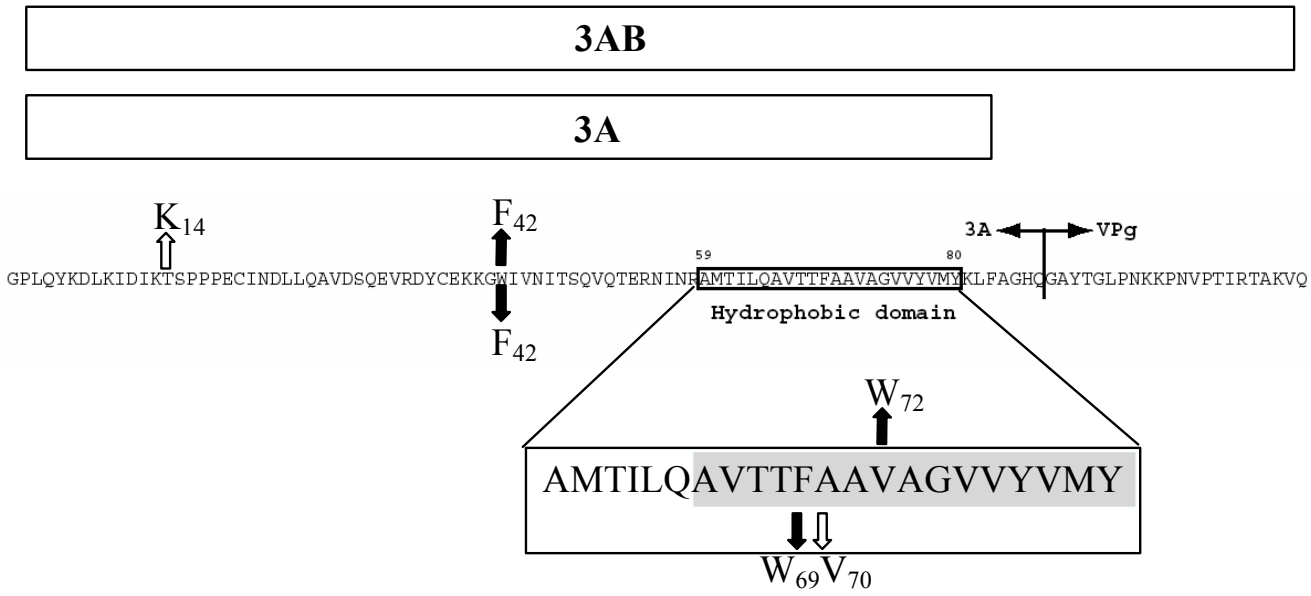

RAMTILQAVTT**WV**AVAGVVYVMYK **Anchor peptide 1**

RAMTILQAVTTFAA**W**AGVVYVMYK **Anchor peptide 2**

Figure 39. Genomic organization of poliovirus, processing of the polyprotein and amino acid sequences of protein 3AB. (A) The single-stranded RNA genome is covalently linked to the viral-encoded protein VPg at the 5' end of the non-translated region (5'NTR). The linkage of the 5' terminal UMP to the hydroxyl group of tyrosine in VPg is shown on the left. The 5'NTR consists of two *cis*-acting domains. The cloverleaf is involved in genome replication, and the internal ribosomal entry site (IRES), controls translation of a 247 kDa polyprotein (open box). The polyprotein is processed by the virus encoded proteinases $2A^{pro}$ and $3C^{pro}/3CD^{pro}$ into structural proteins (P1) and nonstructural (P2 and P3), the latter specifying the proteins involved in replication. Triangles indicate cleavages by $3C^{pro}/3CD^{pro}$ and circles cleavage by $2A^{pro}$. Filled symbols indicate fast cleavages and open symbols indicate slow cleavages. The open diamond marks the VP0 capsid maturation cleavage. The 3'NTR contains a structured heteropolymeric region and is polyadenylylated. The open arrow indicates one of two suppressor mutations resulting from the W42F/F69W mutations in 3AB (see below). (B). Presentation of 3AB and its cleavage product 3A. Shown is the amino acid sequence of 3AB with the Q/G cleavage site between 3A and 3B(VPg). The hydrophobic anchor domain of 3A, starting at amino acid 59, is indicated in a box, which is enlarged below. The shaded area represents the TM segment as defined in this report. Downward or upward arrows indicate two separate sets of mutations. Filled arrows depict mutations engineered into the protein, open arrows the suppressor mutations that rapidly emerged during the first cycle of virus replication. Anchor peptide-1 and anchor peptide-2 delineate the peptides used for membrane binding studies.

3AB is a small basic protein that contains a hydrophobic and membrane-binding region near the C-terminus of its 3A domain. It was shown to possess the biochemical characteristics of an integral membrane protein (185). Yeast two hybrid and biochemical analyses have indicated that the 3AB protein strongly interacts with $3D^{pol}$ and the sequences primarily responsible for this interaction are located in the 3B domain of the protein (184, 186). Four amino acids in a hydrophobic patch on the surface of $3D^{pol}$ were recently identified as binding partners of 3AB (183). Protein 3AB also has the propensity to dimerize and form higher oligomers in solution in the absence of detergent. Both the N-terminal region and the hydrophobic domain of 3A were found to be involved in these interactions (184, 187). In vitro studies have suggested that 3AB has multiple functions in RNA replication: (*i*) 3AB is a nonspecific RNA binding protein but in a complex with proteinase $3CD^{pro}$ it specifically binds to both the 5' cloverleaf and the 3'NTR of the PV genome (188-190) *(ii)* 3AB stimulates the elongation activity of $3D^{pol}$ on a poly(A) template with an oligonucleotide primer (188-194) (*iii)* 3AB stimulates the autoprocessing of $3CD^{pro}$ (195) (*iv)* the membrane bound form of 3AB is required for processing by $3CD^{pro}$ (191). In vitro the N-terminal domain of 3AB can be glycosylated but the biological significance of this observation is not known *(*196*)*.

Proteolytic cleavage of 3AB by $3C^{pro}$/$3CD^{pro}$ yields 3A and 3B (VPg). The 3A protein is 87 amino acids long (Figure 39B), consisting of a soluble cytosolic N-terminus (58 residues) *(*197*)*, which exists as a symmetric dimer *(187)*, a 22-residue long hydrophobic domain (aa 59-81) followed by 7 additional residues at the C-terminus. Part of the hydrophobic domain has been subdivided into two domains (I: aa 64-72 and II: aa 73-80), the latter of which was shown to be the primary determinant of membrane binding in the context of 3AB *(185)*. The first 15 amino acids of the hydrophobic domain (aa 59-73) were predicted to form an amphipathic helix (185). Amino acid changes in the hydrophobic domain of 3A were shown to result in impaired RNA replication and virus death (198). The site of action of enviroxime, an antiviral drug which blocks PV RNA replication, maps to the 3A sequences, supporting a critical role for 3A in the replication complex (199*)*. The 3A protein itself possesses additional functions beside those that are in the context of 3AB. In vivo 3A inhibits ER-to Golgi membrane and secretory protein traffic and induces specific translocation of different members of the ARF family (ADP-

ribosylation factor) to membranes *(*200-203*)*. Both a mammalian and a yeast two-hybrid system showed that 3A multimerizes and interacts with 2B and $2C^{ATPase}$ (184, 204) (Yin, Paul and Wimmer, unpublished observations). Studies with an in vitro translation/replication system indicated that a mutation in 3A (M97A or M97T) affected only plus strand synthesis and not minus strand RNA synthesis *(*205*)*.

The second product derived from 3AB is VPg, a small basic peptide consisting of 22 amino acids, which is covalently linked to the 5' end of the genomic RNA *(206)*. PV RNA synthesis is initiated by the covalent linkage of a UMP to the hydroxyl group of a tyrosine in VPg yielding VPgpU(pU), the primer for both minus and plus strand RNA synthesis *(*207*)*. In vitro, both poly(A) and a small RNA hairpin cre(2C), located in the coding sequences of $2C^{ATPase}$, function as templates for the uridylylation reaction (207, 208). It has been proposed that in vivo the VPgpU synthesized on the cre(2C) RNA is used for plus strand RNA synthesis while the poly(A) tail of the genomic RNA serves as template for VPgpU synthesis prior to minus strand synthesis (207, 209). This claim, however, has been recently challenged *(*210*)*.

Studies of 3AB and 3A function in vitro have been hampered by their low solubility in aqueous solutions, and purified preparations of these proteins always contain detergent. However, it has been shown before that detergents are detrimental to PV RNA replication. The uridylylation of VPg is totally blocked when crude replication complexes, isolated from poliovirus-infected cells, or in vitro translation/RNA replication reactions, are treated with detergent (211, 212). In addition, 3AB can be processed by $3CD^{pro}$ only when membrane-bound and not in the presence of detergents *(*191*)*.

Therefore, studies of 3A and 3AB in model membrane vesicles might be of more relevance than studies in detergents. However, although the membrane association of 3A and 3AB has been known for years, the precise arrangement of these proteins in the hydrophobic environment of a lipid bilayer is obscure. In this study, we exploited the fluorescence properties of a Trp residue placed in the center of the hydrophobic anchor sequence to determine the topology of the anchor sequence when incorporated into model membrane vesicles, using both a peptide containing the anchor sequence and intact 3A and 3AB proteins. Our results indicate that the anchor sequence has the intrinsic ability to form a TM topography, and adopts a mixture of a transmembrane and non-

transmembrane topography in the context of the intact 3A protein. The hydrophobic anchor of intact polypeptide 3AB, however, assumes only a non-transmembrane configuration.

RESULTS

Construction of 3A/3AB Mutants Suitable for Membrane-Association Studies.

To analyze the properties of the hydrophobic domain when 3A and 3AB are membrane associated, we adopted the method of measuring Trp fluorescence. For these fluorescence experiments, a Trp is most useful when placed at the center of the hydrophobic sequence (16, 24, 29, 30). In that case, Trp location can distinguish whether the hydrophobic segment within which it is located forms a transmembrane helix, in which case the Trp locates at the bilayer center, or forms a non-transmembrane structure, in which case the Trp locates near the bilayer surface (16, 24, 29, 30, 83). Because the hydrophobic anchor domain of 3A does not contain Trp, a single Trp residue was introduced by a substitution mutation into a position we thought to be at the center of the hydrophobic region (F69W; Figure 39B). To render the spectroscopic measurements specific to the hydrophobic sequence, the Trp residue in the hydrophilic region of 3A was replaced with a Phe residue (W42F; Figure 39B). It was then determined to what extent these mutations influence the function of 3A/3AB by assaying the ability of corresponding variant RNAs to produce cytopathogenic effects (CPE) on HeLa cell monolayers. Mutants did not disrupt the polio virus function, but it revealed two unexpected suppressor mutations. One mutation (A70V) mapped to the 3A hydrophobic region next to the new Trp residue (Figure 39B), the other to the membrane-associated viral protein 2B (I47V; Figure 39A).

The replication kinetics of the 2B/3A mutant virus, assayed by one-step growth curve experiments in HeLa cell monolayers, revealed slightly slower growth phenotypes as compared to WT PV (Figure 40). Nevertheless, these growth phenotypes indicated satisfactory function of 3A/3AB in the context of the poliovirus genome and thus the 3A/3AB (W42F/F69W/A70V) polypeptides were used in the following studies.

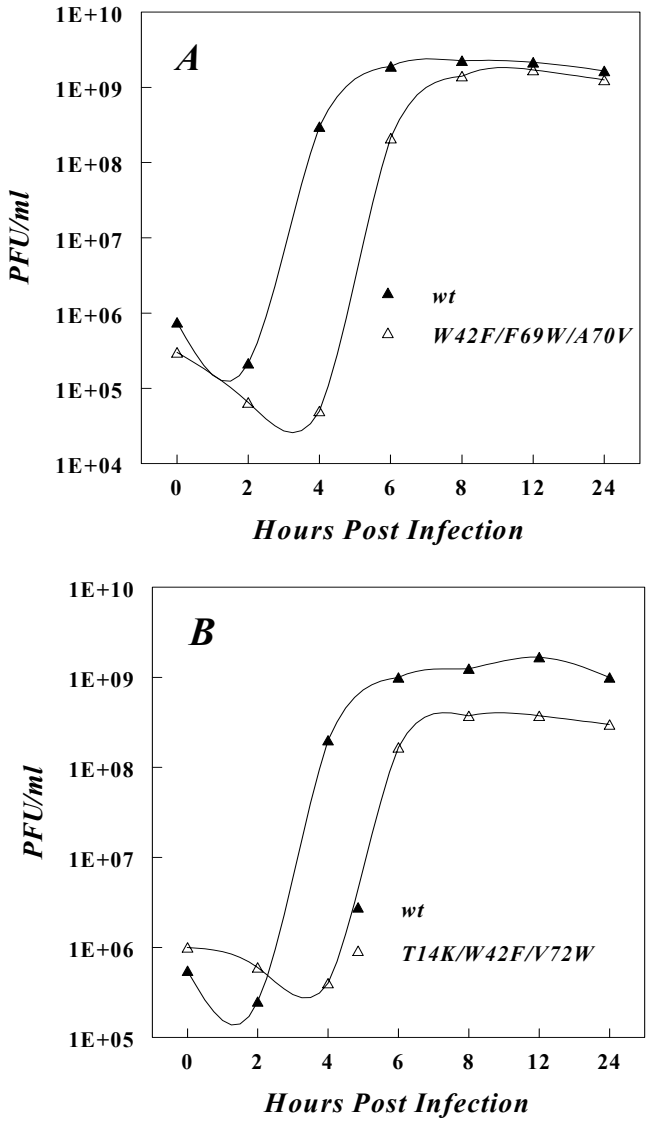

Figure 40. One step growth curves of WT poliovirus and a 3A mutants at 37 ºC. (A) WT poliovirus compared to 3A mutant (W42F/F69W/A70V). (B) WT poliovirus and 3A mutant (T14K/W42F/V72W). Growth curves were carried out as follows: HeLa cell monolayers in 35-mm culture dishes were washed with Dulbecco's minimal essential medium (DMEM) and inoculated with each virus at a multiplicity of infection of 10. After adsorption for 30 min at room temperature, the cells were extensively washed to remove unbound virus, and then incubated at 37°C or 39°C. The dishes were harvested at 0, 2, 4, 6, 8, 12, and 24 h post-infection, and subjected to three cycles of freezing/thawing. The viral titers of the supernatants were determined by plaque assay, as described previously (213).

Ability of the Polio 3A Hydrophobic Sequence to Span Lipid Bilayers in TM form: *Behavior of the Anchor Peptide-1*.

A peptide corresponding to the hydrophobic anchor sequence (underlined) of protein 3A carrying the Trp-Val mutation at positions 69-70 plus the flanking charged residues (acetyl^{58}R<u>AMTILQAVTT***WV***AVAGVVYVMY</u>K^{81}amide) (Figure 39B) was used to study the ability of the hydrophobic sequence to span lipid bilayers. Fluorescence methods we developed previously were used to define the topography of the bilayer-inserted sequences (16, 24, 29, 30, 49, 83). The first assay involved measurement of Trp emission λmax to evaluate approximate Trp depth. When a 20 residue long hydrophobic sequence with a Trp near the center of its hydrophobic sequence adopts a TM orientation, the Trp locates near the bilayer center, and gives highly blue shifted emission (λmax = 315-325 nm) (16, 24). If the sequence adopts a non-TM topography located close to the surface of the bilayer Trp λmax red shifts strongly (335-340 nm) (16, 24). Additional information was derived from the Trp λmax vs. bilayer width curve. A highly hydrophobic peptide with a Trp at the center of the hydrophobic sequence exhibits a minimum λmax value at the maximum width bilayer in which the peptide maintains a fully TM structure. In wider bilayers, due to negative mismatch (i.e. bilayer width exceeding hydrophobic helix length) there is formation of an appreciable fraction of a non-TM, surface topography which gives more red shifted Trp emission (16, 24, 83). The bilayer widths in which Trp emission red shifts can reveal the length of the TM sequence (16, 24).

To measure Trp depth directly, a dual fluorescence quenching method was used (83). In this method the ratio of quenching of Trp by acrylamide, which resides in the aqueous solution, to quenching by the membrane-inserted quencher 10-doxylnonadecane is measured. This quenching ratio (Q-ratio) responds nearly linearly to Trp depth in the bilayer, such that a low quenching ratio (<0.15) indicates a deeply located Trp near the center of the bilayer, while a high Q-ratio (>1) is indicative of a Trp near the bilayer surface (29, 83).

Figure 41 and Table 12 show values for anchor peptide-1 Trp λmax and how it is affected by bilayer width (varied by using lipids with different length acyl chains). Even in vesicles in which the λmax was most highly blue-shift, e.g. those vesicles composed of DOPC (diC18:1PC), anchor peptide-1 exhibited a somewhat red shifted λmax (332 nm), although the λmax red shift increased considerably (to 339 nm) in wider bilayers (Figure 41, filled triangles). The somewhat red shifted λmax observed in DOPC vesicles indicates that the Trp was not located at the bilayer center in these vesicles. However, there was at least some formation of a TM configuration in DOPC vesicles, as the λmax even more red-shifted in wider bilayers, under which conditions a non-TM form would predominate. When quenching was measured, results in agreement with the λmax data were obtained. The Q-ratio was 0.35 in DOPC (C18:1 acyl chains) and 0.82 in DEuPC (C22:1 acyl chains) (Table 12). This behavior indicates that anchor peptide-1 forms, at least to some degree, a TM structure when incorporated into DOPC bilayers and adopts a shallow, non-TM topography in wider bilayers.

The fluorescence properties of anchor peptide-1 incorporated into DOPC vesicles do not distinguish between the peptide forming a homogeneous configuration, in which the Trp has a single intermediate depth, and a case in which the peptide exists in a mixture of two populations: one with a TM topography, and thus a deep Trp depth, and another population with a non-TM topography having a Trp near the bilayer surface. The effect of quenchers on the λmax of Trp emission can distinguish between these alternatives. When deep and shallow Trp populations co-exist, intermediate λmax values are observed because the two populations have overlapping blue and red-shifted spectra. In such samples, there is selective acrylamide quenching of the shallow Trp population because it is closer to the acrylamide than the deep Trp. This induces a blue shift in λmax, because the deeper Trp population is only weakly quenched. In contrast, 10-DN quenching induces red shifts due to selective quenching of deep Trp, which is closer to 10-DN than shallow Trp. In such heterogeneous populations, these shifts can result in a λmax value in the presence of acrylamide that differs from that in the presence of 10-DN by 5-15 nm. In populations with a homogeneous Trp depth, the quencher-induced shifts

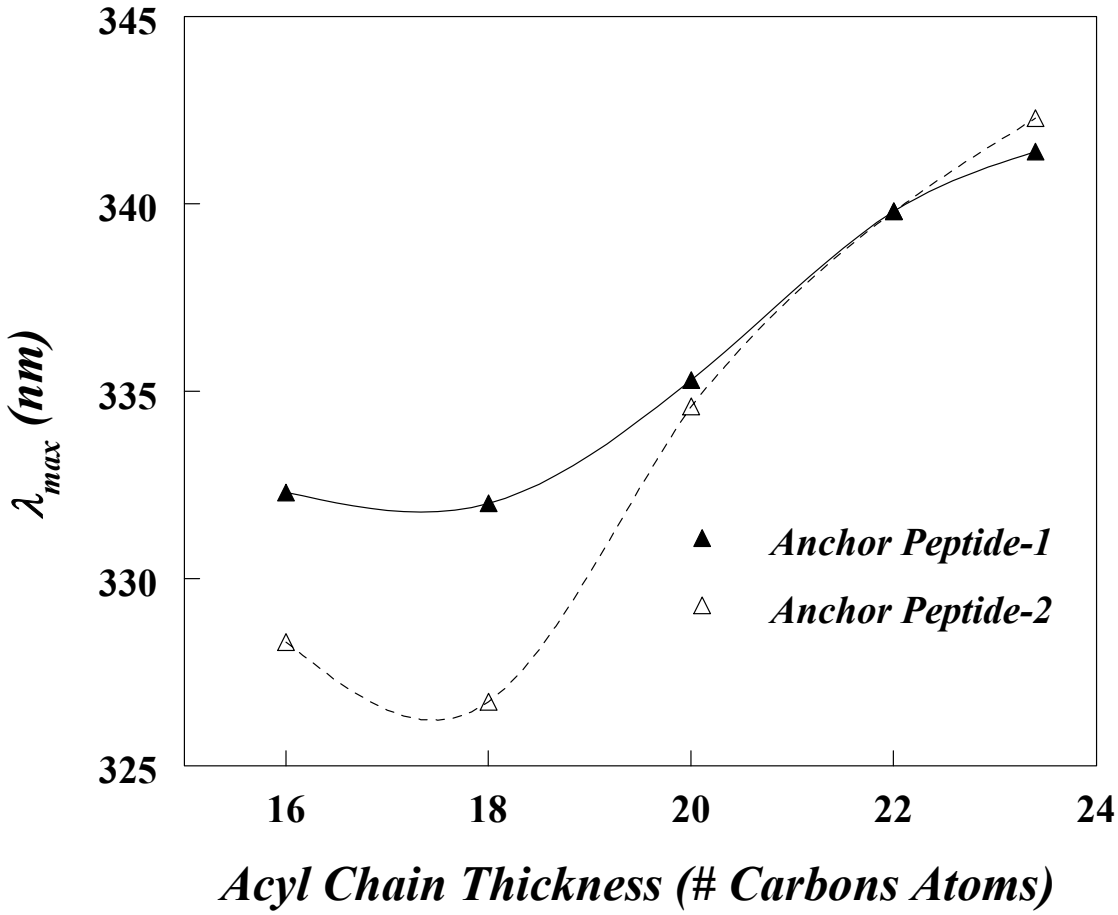

Figure 41. Effect of lipid bilayer width upon Trp emission λmax for anchor peptide-1 and anchor peptide-2. Anchor peptide-1 (▲) or anchor peptide-2 (Δ) were reconstituted into model membrane vesicles composed of monounsaturated PCs with different acyl-chain lengths. Samples contained 2 μM peptide incorporated into 500 μM lipid dispersed in PBS at pH 7.0. The values shown are the average of six samples. The λmax values are generally reproducible to ±1 nm.

Table 12. Quenching of Membrane-Inserted Anchor Peptide-1 and Anchor Peptide-2 by Acrylamide and 10-Doxylnonadecane.

Peptide	Fo/F Acrylamide	Fo/F 10-DN	Q-Ratio	λmax (nm)
Peptide inserted into DOPC vesicles (C18:1 acyl chains) [a]				
Anchor Peptide -1	1.31 ± 0.02	1.88 ± 0.01	0.352 ± 0.02	332± 0.2
Anchor Peptide-2	1.25 ± 0.01	2.33 ± 0.14	0.192 ± 0.21	327± 0.25
Peptide inserted into DEuPC vesicles (C22:1 acyl chains)				
Anchor Peptide-1	2.11 ± 0.11	2.29 ± 0.13	0.82 ± 0.15	339.8± 0.4
Anchor Peptide-2	1.91 ± 0.02	1.99 ± 0.04	0.92 ± 0.05	340± 0.3

[a] F_o/F is the ratio of fluorescence in the absence of quencher to the that in the presence of quencher. The ratio of quenching by acrylamide to that by 10-DN, the Q-ratio, is defined in Experimental Procedures. Average values and standard deviations derived from six samples are shown.

are much smaller (29, 83). For anchor peptide-1 in DOPC vesicles we observed very little difference between Trp λmax in the presence of acrylamide and 10-DN (1.5 nm) indicating that it adopts a homogeneous state in which the Trp is not at the center of the bilayer.

The observation that the Trp was not located at the bilayer center suggested that the TM was not 22 residues long. This was supported by the observation that emission was significantly more red-shifted in diC20:1PC bilayers than in DOPC vesicles. This is indicative of a partial loss of TM topography in diC20:1PC bilayers and previous studies shows that this behavior corresponds to that expected for a TM sequence <18-19 residues long (16, 24)(and see below).

Recovery of recombinant polioviruses harboring mutations at different positions within the hydrophobic domain of 3A.

To confirm that TM sequence was shorter than expected, and that as a result the center of the transmembrane sequence was at a position closer to the C-terminus of the hydrophobic sequence than originally estimated, we decided to introduce a Trp at a position closer to the C-terminus of the hydrophobic sequence than Phe69. In order to determine at what positions Trp could be introduced while maintaining PV viability, several mutant cDNA clones containing both a Trp substitution in the hydrophobic sequence and the W42F mutation in the hydrophilic region were constructed. Genome sequence analysis of revealed that PV could tolerate a Trp only at positions 72, although one suppressor mutation (T14K) in the hydrophilic region of 3A emerged. This mutant (T14K/W42F/V72W) grew moderately well at 37ºC although somewhat slower than WT PV (Figure 40B). But 3A/3AB polypeptides containing the T14K/W42F/V72W mutations are functional in the context of the replicating PV genome (data not shown).

Behavior of Anchor Peptide-2 in Model Membranes.

Since viruses containing Trp at position 72 grew well in HeLa cells, a synthetic peptide carrying a Trp at position 72 (anchor peptide-2; acetyl-^{58}RAMTILQAVTTFAA **W**AGVVYVMYK^{81}-NH_2) was synthesized and subjected to the fluorescence analysis. In DOPC vesicles, the values of both λmax and Q ratio for the Trp of anchor peptide-2 were

just slightly above those expected for a Trp exactly at the bilayer center, and this indicated a significantly deeper Trp depth than measured for anchor peptide-1, and (Figure 41 and Table 12). These results show that anchor peptide-2 predominantly forms the TM state in DOPC bilayers, and confirm that the Trp in anchor peptide-1 was not located at the bilayer center.

The fact that the Trp of anchor peptide-2 is close to the bilayer center, while the Trp of anchor peptide-1 is not as close to the bilayer center, indicates residue 72 is closer to the center of the TM sequence than residue 69. The TM sequence cannot end beyond Lys81, which is the last residue in the peptide, and it is far more likely to end at residue Tyr80. If residue 72 is at the bilayer center of the TM sequence, the TM sequence must start at, or very near, Gln64, which would mean the TM sequence is 16 residues long (Figure 39B; shaded area in the hydrophobic domain).

This conclusion is supported by the shape of the Trp λmax vs. bilayer width curve, which shows that the minimum λmax value (observed in lipids forming bilayers with widths that are close to the point where there is no mismatch between TM helix length and bilayer width) occurs in liposomes formed from lipids with acyl chains that are 17-18 carbon atoms long (Figure 41). We previously found that 19-20 residue long TM sequences exhibit a λmax minimum in liposomes composed of lipids with acyl chains that are 20 carbon atoms long (16). Since bilayer width increases by about 1.8 angstroms per acyl chain carbon atom (0.9 angstroms per lipid molecule) (214), and the length of a helix increases by 1.5 angstroms per residue, the difference between the acyl chain lengths at which a 16 and 19-20 residue-long TM helix experience no mismatch should be about that 3 carbon atoms, close to what is observed.

Fluorescence studies with intact polio $3A^m$ and $3AB^m$ proteins.

We next wished to study the membrane configuration of the anchor sequence in the context of the intact proteins 3A and 3AB. Since the mutant virus containing three mutations within the 3A sequence (T14K/W42F/V72W) grows similarly compared to WT virus (data not shown), indicating that 3A/3AB was functional, we proceeded to purify the mutant 3A and 3AB proteins with these mutations (referred to as $3A^m$ and $3AB^m$) for further studies. The purified $3A^m$ or $3AB^m$ proteins were then incorporated

into preformed liposomes as described in the Experimental Procedure section. This process mimics insertion in vivo (see Discussion).

Trp fluorescence was again used to characterize the topography of the hydrophobic anchor sequence within the membrane-incorporated full length proteins. The behavior of the anchor sequence might differ in peptide and intact 3AB protein because intact 3AB protein has large hydrophilic N- and C-terminal domains which should not be able to cross membranes. This would prevent the formation of a TM state by the anchor sequence upon binding of 3AB to membranes. In contrast, the 3A protein has only a short C-terminal hydrophilic sequence that might be able cross membranes (Figure 39B), and so the anchor sequence in 3A protein might form a TM state when added to membranes. Table 13 shows that Trp λmax values support these hypotheses. In DOPC vesicles, the $3A^m$ protein exhibited a more blue-shifted λmax (328 nm) and lower Q-ratio (0.39) than was observed for the $3AB^m$ protein (λmax 331 nm, Q-ratio 0.67). This suggests that a significant fraction of the hydrophobic sequence of the $3A^m$ protein formed a state with a deep Trp, i.e. a TM configuration, while the hydrophobic sequence of the $3AB^m$ protein formed a greater degree of a shallow, non-TM state in which Trp is near the surface of the bilayer. The latter conclusion is confirmed by the observation that the $3AB^m$ protein incorporated into wider DEuPC bilayers, in which a non-TM form would be expected to be present to a significant degree because the length of the hydrophobic segment is too short to span the DEuPC bilayer, showed λmax and Q ratios (λmax 332 nm and Q-ratio = 0.69, Table 13) that were very similar to those in DOPC bilayers. As noted above, this insensitivity to mismatch between hydrophobic helix length and bilayer width is characteristic of a sequence that is fully non-TM. In contrast, $3A^m$ protein in DEuPC vesicles showed a higher λmax and Q-ratio (λmax 331 nm and Q-ratio = 0.62, Table 13) than it did in DOPC vesicles. Furthermore, λmax and Q-ratios for $3A^m$ in DEuPC vesicles were similar to those for $3AB^m$ protein in DEuPC vesicles, indicating that negative mismatch affects the topography of the $3A^m$ hydrophobic segment, such that it converts from the TM to non-TM state, as expected This type of sensitivity to mismatch is indicative of a TM state in the absence of mismatch (i.e. in the DOPC vesicles).

Table 13. Quenching of Membrane-Inserted Polio 3AB and Polio 3A Protein by Acrylamide and 10-Doxylnonadecane.

Protein	Fo/F Acrylamide	Fo/F 10-DN	Q-Ratio	λmax (nm)
Protein inserted into DOPC vesicles (C18:1 acyl chains) [a]				
Polio 3AB	1.84 ± 0.12	2.26 ± 0.17	0.67 ± 0.20	330.8 ± 0.4
Polio 3A	1.45 ± 0.03	2.16 ± 0.04	0.39 ± 0.04	328 ± 0.3
Protein inserted into DEuPC vesicles (C22:1 acyl chains)				
Polio 3AB	1.40 ± 0.03	1.57 ± 0.02	0.69 ± 0.03	331.7 ± 0.3
Polio 3A	1.54 ± 0.03	1.88 ± 0.04	0.62 ± 0.05	330.8 ± 0.2

[a] F_o/F is the ratio of fluorescence in the absence of quencher to the that in the presence of quencher. The ratio of quenching by acrylamide to that by 10-DN, the Q-ratio, is defined in Experimental Procedures. Average values and standard deviations derived from six samples are shown

Thus, a number of internally consistent fluorescence parameters support the TM assignment for the topography of the hydrophobic segment in the $3A^m$ protein (at least for some population of $3A^m$ molecules, see below), and non-TM topography in $3AB^m$ protein.

However, there are some differences between the fluorescence behavior of the hydrophobic sequences in the isolated peptides and intact protein. One difference is that the Trp depth in DOPC for $3A^m$ protein is significantly shallower than for the isolated peptide as judged by Q-ratio. This suggests that in the case of the intact protein not all of the hydrophobic sequence is in a TM state. The second difference is that in the DEuPC vesicles, in which the non-TM state predominates, Trp fluorescence is more red-shifted and Q ratios are much higher in the isolated anchor peptide than in the intact protein. This suggests that the hydrophilic portion of the $3A^m$ domain affects how deeply the hydrophobic anchor sequence penetrates the bilayer in the non-TM state.

DISCUSSION

Tryptophan mutations in 3A highlight intra and intermolecular interaction between PV proteins.

In this study, we used tryptophan-specific fluorescence measurements to determine the topography of the 3A and 3AB proteins inserted into pre-formed model membrane vesicles. In order to make fluorescence measurements specific to the 3A-hydrophobic domain, we placed a Trp at position 69 within the hydrophobic domain of 3A (F69W) and replaced a Trp residue in the hydrophilic region of 3A with a Phe residue (W42F). The effects of these mutations upon viral replication are interesting. Although it has been reported that the substitution of the well-conserved Trp at position 42 to Arg resulted in a lethal phenotype (215) and aberrant protein processing, the Trp to Phe substitution yielded a viable virus. Other previous studies have shown that a Phe 69 to His substitution leads to a quasi-infectious virus, which acquired a second-site mutation at the adjacent amino acid at position 70 to either Val or Thr (216). We found a similar second-site mutation at position 70 to Val in the virus recovered from the W42F/F69W mutant. Furthermore, we observed a suppressor mutation within the first hydrophobic

domain of 2B (I47V) in the virus recovered from the W42F/F69W clone. This result suggested that the hydrophobic domains of 3A/3AB and 2B/2BC functionally interact during poliovirus replication, in agreement with previous studies by Towner et al. (217). Interestingly, no second-site reversions were observed either in 3A or in 2B in the virus derived from the W42F or F69W single mutants. One possible explanation of this finding is that the mutation in the N-terminal hydrophilic region of 3A affects the structure of the C-terminal hydrophobic domain, which results in inefficient interaction of the hydrophobic domain of 3A with itself or with those of other viral proteins (e.g. 2B). Interestingly, we found second-site mutations within the hydrophilic domain of 3A (T14K or P17A) when we introduced a Trp mutation at position 72. These results support the hypothesis that the hydrophilic and the hydrophobic domains of 3A structurally affect each other.

Topography and membrane-interactions of the 3A hydrophobic anchor domain in intact 3A and 3AB proteins.

Based on the information above, single-Trp mutants were designed to test the configuration of membrane-associate 3A and 3AB proteins. The model membrane interaction of the isolated hydrophobic sequence of 3A, and that 3A and 3AB proteins with single Trp were then used to evaluate the topography in membranes. The studies using peptides containing the hydrophobic sequence within the 3A protein clearly demonstrated that it had the capacity to form a TM configuration, but that did not answer whether it does so in intact protein. To do that we devised a membrane-interaction protocol that would mimic the post-translational interaction of 3AB and 3A with membranes that occurs *in vivo***.** This method resulted in a membrane insertion that was about as efficient as that used to incorporate peptide into membranes, as demonstrated by the observation that membrane-bound 10-DN quenched peptide and intact protein fluorescence to similar degrees (compare Tables 12 & 13).

Using this protocol we found that the hydrophobic anchor domain of 3A adopts a membrane-bound non-TM configuration in the context of the 3AB protein, wherein both the 3A and VPg domains of 3AB are cytosolic. A similar non-TM arrangement of a potentially-TM sequence has seen in other proteins such as cytochrome *b5* and caveloin,

under at least some conditions (218, 219). The non-TM configuration is not a surprise, as formation of a TM configuration would have required either the large hydrophilic domain of 3A or that of 3B to translocate across the membrane. However, although translocation of a large hydrophilic domain would be very unusual, certain bacterial toxin proteins do catalyze self-translocation of hydrophilic domains, so this could not be ruled out *a priori* (220, 221).

In contrast to the behavior in the 3AB protein, the hydrophobic domain in 3A adopts both a TM and a non-TM structure. In order for a TM state to form, the sequence flanking the C-terminal tail of the hydrophobic domains (KLFAGHQ) must cross the bilayer, despite the presence of several hydrophilic residues. It is possible that the residual non-TM configuration is an artifact of the use of model membrane liposomes that do not adequately mimic natural membranes. The difference in hydrophobic anchor configuration in 3A and 3AB proteins is interesting because it illustrates one physical mechanism by which precursor (3AB) and mature (3A) proteins can have different structures that might lead to different functions. In this context it is also interesting to note that based on biochemical studies, Towner et al. (185) have suggested that the primary membrane anchor domain of 3A in the context of 3AB contains only the C-terminal 13 amino acids of the hydrophobic domain, which is too short to form an α–helical structure that spans the lipid bilayer.

It should also be noted that when we incorporated the anchor peptides or the intact 3A or 3AB proteins into vesicles composed of 70mol% DOPC/ 30mol% DOPG we obtained Trp λmax and quenching data that was very similar to that obtained in DOPC, indicating that the presence of the anionic DOPG did not affect the topography of the hydrophobic sequence (data not shown).

It is plausible that a fraction of the 3A hydrophobic anchors form TM helices once 3A is cleaved off from 3AB by $3C^{pro}$ or $3CD^{pro}$. It has been previously reported that the hydrophobic domain of the RNA polymerase (NS5B) of HCV forms a TM helix (222), and we have recently shown that this hydrophobic domain of NS5B can be replaced with that of poliovirus 3A without abrogating replication of an HCV replicon (223). This result can be easily rationalized if the hydrophobic anchor of 3A also has the ability to form a TM helix.

As discussed above, our results are in agreement with those of Towner et al. (217) , in terms of suggesting that the hydrophobic domains of 2B and 3A interact with each other during poliovirus replication. Because of the precursor/mature protein relationships multiple interacting partners are possible: 3A/2B, 3A/2BC, 3AB/2BC, and 3AB/2B. In addition, if one of the interacting partners is 3A then two forms of the membrane bound protein (TM and non-TM) are available for these interactions. Whether one or more of these interactions are required for creating the correct environment for RNA replication is not known. It should be noted that any such effects could be exerted at different stages in the replication process. Previous studies with the 2B(C) protein of enteroviruses indicated that its membrane binding ability affects RNA replication at two different stages (177, 224). One of these involves the induction of vesicles, which are required for RNA replication (225). The second step involves RNA replication more directly and requires an interaction with one or more viral or cellular proteins (224).

Our studies using peptides containing the hydrophobic domain of 3A and liposomes with different acyl chain lengths indicated that the hydrophobic domain of 3A behaves as a short transmembrane helix consisting of approximately 16 amino acids. Based on the putative hydrophobic domain sequence, Phe at position 69 was originally believed to be near the center of the TM segment. However, λmax and Q-ratio of F69W peptide (anchor peptide-1) was higher compared to the V72W peptide (anchor peptide-2), indicating that the Val at position 72 is closer to the center of the transmembrane helix than the Phe at position 69. Therefore, the TM segment is most likely to be formed by residues 65-80, rather than by the entire hydrophobic sequence (residues 59-80), with Q64 forming the N-terminal boundary of the buried sequence (Figure 39B; shaded area of the hydrophobic sequence). This is further supported by our findings that Gln has a strong tendency to locate at the membrane surface rather than being buried in the bilayer (Chapter 4)

Proposed model for the association of 3A/3AB with membranes and the initiation of PV RNA synthesis.

The major cleavage products originating from the P3 region are 3AB and $3CD^{pro}$, which are slowly processed to the final mature proteins (Figure 42). The 3AB protein

associates with intracellular membranes via the hydrophobic domain of 3A and adopts a non-TM structure. Its soluble, cytosolic VPg domain then interacts with $3D^{pol}$ and recruits it to the membranes. Once 3AB is cleaved into 3A and VPg by $3C^{pro}$/$3CD^{pro}$ the hydrophobic domain of 3A can adopt both a TM and a non-TM structure. Whether the TM and/or non-TM forms of 3A derived from membrane-bound 3AB, have a subsequent function in replication remains to be determined. Since cleavage of 3AB by $3CD^{pro}$ does not take place in detergent (191), and the uridylylation reaction in HeLa cell extracts is abolished in the presence of detergent (211), reconstitution of proteoliposomes containing 3AB is a useful tool for studying the role of 3AB in poliovirus replication. In the future, it might be possible to reconstitute the entire poliovirus replication complex in vitro using proteoliposomes. Such a system might enhance our understanding of the protein network within the poliovirus replication complex and also the difference in the mechanism of negative- and positive-strand RNA synthesis.

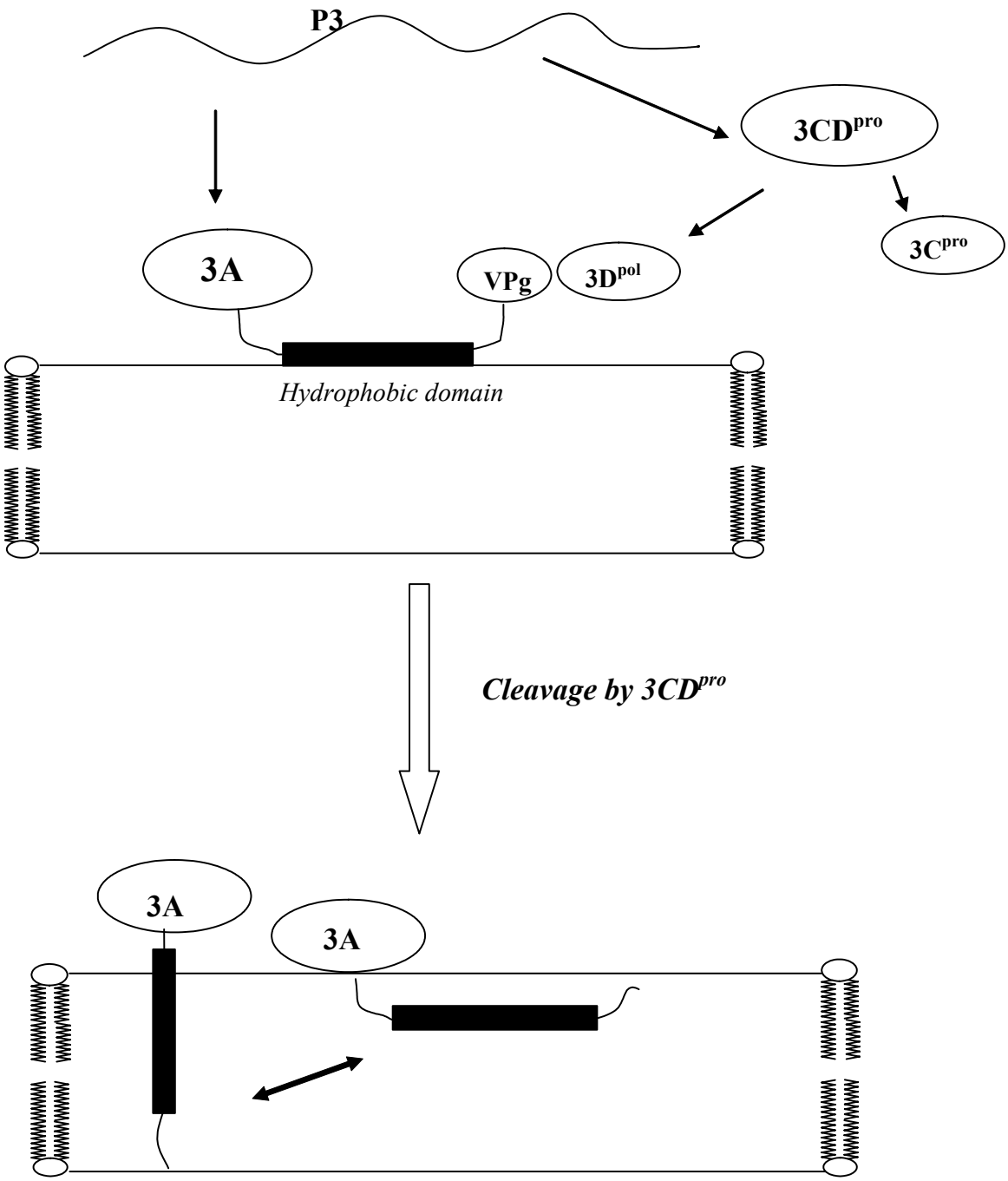

Figure 42. Proposed model for the structures of 3AB and 3A on membranes and initiation of poliovirus replication. The P3 precursor is processed by proteinase $3CD^{pro}$ to yield 3AB and $3CD^{pro}$. 3AB interacts with membranes forming a non-TM configuration and its VPg domain binds $3D^{pol}$ to the membranes. Protein $3CD^{pro}$ cleaves off VPg releasing the 3A protein, which then assumes both a TM and a non-TM form.

CHAPTER 7

SUMMARY & FUTURE DIRECTIONS

SUMMARY

In this report, we used membrane-inserted hydrophobic α-helices to understand the sequence to topography relationship in TM helices. Fluorescence methods developed in our lab were used to define the various topographical states and understand the equilibrium describing these topographical states. Using this model membrane system, the minimum hydrophobic length necessary to form a TM helix in membranes was investigated. The fluorescence of a Trp at the center of the sequence and its sensitivity to quenching were used to ascertain helix position within the membrane. Peptides with hydrophobic cores composed of polyLeu were compared to sequences containing a poly 1:1 Leu:Ala core (which have a hydrophobicity typical of natural TM helices). Studies varying bilayer width revealed that the polyLeu core peptides predominately formed a TM state when the bilayer width exceeded hydrophobic sequence length by (i.e. when negative mismatch was) ~11-12Å (e.g. the case of a 11-12 residue hydrophobic sequence in bilayers with a biologically relevant width, i.e. DOPC bilayers), while polyLeuAla core peptides formed predominantly TM state with negative mismatch of up to 9Å (a 13 residue hydrophobic sequence in DOPC bilayers). This indicates that minimum length necessary to form a predominating amount of a TM state (minimum TM length) is only modestly hydrophobicity-dependent for the sequences studied here, and a formula that defines the minimum TM length as a function of hydrophobicity for moderately-to-highly hydrophobic sequences was derived. The minimum length to form a stable TM helix for alternating LeuAla sequences and that for sequences with a Leu block followed by an Ala block was similar, suggesting that the hydrophobicity gradient along the sequence may not be an important factor in TM stability. TM stability was also similar for sequences flanked by different charged ionizable residues (Lys, His, Asp). However, ionizable flanking residues destabilized the TM configuration much more when charged than when uncharged. The ability of short hydrophobic sequences to form TM helices in membranes in the presence of substantial negative mismatch implies that lipid bilayers have a considerable ability to adjust to negative mismatch, and that short TM helices may be more common than generally believed. Factors that modulate the ability of bilayers to adjust to mismatch may strongly affect the configuration of short hydrophobic helices.

In addition, the ability of hydrophilic residues to shift the transverse position of

TM helices within bilayers was studied in model membrane vesicles. Transverse shifts were detected by fluorescence measurements of the membrane depth of a Trp residue at the center of a hydrophobic sequence. They were also estimated from the effective length of the TM-spanning sequence, derived from the stability of the TM configuration under conditions of negative hydrophobic mismatch. Hydrophilic residues (at the fifth position in a 21-residue hydrophobic sequence composed of alternating Leu and Ala residues and flanked on both ends by two Lys) induced transverse shifts in the TM helix moving the hydrophilic residue closer to the membrane surface. At pH 7.0, the dependence of the extent of shift upon the identity of the hydrophilic residue increased in the order L<G~Y~T<R~H<S<P<K<E~Q<N<D. By varying pH, shifts with ionizable residues fully charged or uncharged were measured, and the combined extent of shift data increased in the order: $L<G\sim Y\sim H^{o}\sim T<E^{o}\sim R<S<P<K^{+}<Q\sim D^{o}\sim H^{+}<N\sim E^{-}<D^{-}$. The dependence of transverse shifts upon hydrophilic residue identity was consistent with the hypothesis that shift magnitude is largely controlled by the combination of side chain hydrophilicity, ionization state and the ability of the side chains to position the polar groups near the bilayer surface (snorkeling). Additional experiments showed that shift was also modulated by the position of the hydrophilic residue in the sequence and the hydrophobicity of the sequence that moves out of the bilayer core upon shifting. Combined, these studies show that the insertion boundaries of TM helices are very sensitive to sequence and can be altered even by weakly hydrophilic residues. Thus, many TM helices may have the capacity to exist in more than one transverse position. Knowledge of the magnitudes of transverse shifts induced by different hydrophilic residues should be useful for design of mutagenesis studies measuring the effect of transverse TM helix position upon function.

Furthermore, we used hydrophobic peptides corresponding to the transmembrane domain of neu (rat homologue of ErbB2) receptor to understand the structural consequence of the hydrophilic mutation in the TM domain. Fluorescence properties of a Trp residue introduced near the center of the hydrophobic segment was used to define the membrane position of the neu/ErbB2 TM domain. The activating Glu^{664} mutation (charged or uncharged) induced a shift in TM domain, such that the Glu residue located at or close to membrane bilayer surface and a truncated segment spanned the bilayer.

Other activating hydrophilic mutations (Gln and Asp), at position 664, also reduced the effective TM length spanning the bilayer and the magnitude of shift in TM helix position was found to correspond to the hydrophilicity and the ionization state of the hydrophilic residue. This data suggests that the transforming ability of a hydrophilic residue at position 664 could depend on the ability of the hydrophilic residues to induce a shift in TM helix position under physiological conditions. The altered membrane position of the mutant neu/ErbB2 TM domain raises the possibility that the hydrophilic mutation upregulates the receptor function by either altering the dimerization mode of the receptor or by shifting the equilibrium towards active heterodimers or by spatial rearrangement of the catalytic domain resulting in constitutive activation.

Finally, in collaboration with Dr. Eckard Wimmer in Department of Molecular Genetics and Microbiology, we used fluorescence and fluorescence quenching methods to define the topography of the anchor sequence in context of Polio virus 3A and 3AB proteins inserted in model membranes. Mutants with a single tryptophan near the center of the anchor sequence but lacking Trp elsewhere in 3A/3AB were constructed, which after the emergence of suppressor mutations, replicated well in HeLa cells. When a peptide containing the mutant anchor sequence was incorporated in model membrane vesicles, measurements of Trp depth within the lipid bilayer indicated formation of a transmembrane topography. However, rather than the 22 residue length predicted from hydrophobicity considerations, the transmembrane segment had an effective length of 16 residues, such that the Gln^{64} likely formed the N-terminal boundary. Analogous experiments using full length proteins bound to pre-formed model membrane vesicles showed that the anchor sequence formed a mixture of TM and non-TM topographies in the 3A protein but adopted only the non-TM configuration in the context of 3AB protein.

FUTURE DIRECTIONS

Additional Hydrophobic Peptide Studies – Other Properties Influencing the Minimum Length Threshold and Helix Shifting Potential of Hydrophilic Residues

All work presented in this report were done in zwitterionic PC vesicles in ordinary fluid state. In order to accurately predict TM helix behavior in cellular membranes, it will be important to determine how lipid composition influences the TM helix behavior. The effects of lipid headgroup charge would be particularly important to consider. Lipid headgroup charge could stabilize or destabilize the TM structure via interactions with the ionizable flanking residues and thus alter the minimum length threshold. In preliminary studies, our lab has found that negatively charged lipids could facilitate deep insertion of Lys-flanked peptides through favorable electrostatic interactions with the flanking charges (K. Shahidullah and E. London, unpublished observations). Similarly, lipid headgroup charge could alter the shifting potential of hydrophilic residues. Favorable interactions between the hydrophilic residue and the lipid headgroup at the interfacial region would increase the amount of shift. In contrast, unfavorable interactions might prevent the TM helix from shifting. In addition, interactions between the ionizable flanking residues and the lipid headgroup charge could influence the magnitude of transverse shift in TM helix position. A favorable electrostatic interaction between the flanking ionizable residue and the lipid headgroup charge would anchor the peptide strongly in the bilayer, resisting shift, even in the presence of strong hydrophilic residue within the TM sequence. In addition, the effect of cholesterol-containing mixtures on TM helix stability would be of interest because the eukaryotic plasma membranes are rich in cholesterol (nearly 30 %). Previous work from our lab has shown that addition of cholesterol tends to increase the thickness of the lipid bilayer (24). This means that the minimum length of the hydrophobic sequence necessary to form a stable structure would be different in cholesterol-containing bilayers. Also, wider bilayers could limit the extent of transverse shift in TM helices in presence of hydrophilic residue since negative mismatch would significantly destabilize the truncated TM segments formed when the hydrophilic residue moves towards the bilayer surface.

Another variable that could affect TM helix behavior is helix-helix interaction.

Helix association would help TM helix compensate for hydrophobic mismatch and thereby stabilize the formation of very short TM segments. Thus, helix association could decrease the minimum length threshold. Electrostatic interaction between oppositely charged flanking residues could promote helix association such that otherwise metastable TM helices with hydrophobic sequence less than 13 residues could form. Helix association could also modulate TM helix positioning. Helix association, such that the hydrophilic residues interact, would decrease the energetic cost of burying a hydrophilic residue in the lipid bilayer and thus reduce the extent of shift in TM helix position.

Oligomerization of hydrophobic peptides could be altered using flanking residue charges. Previous work has shown that LysAsp-flanked or $LysAsp_3$- flanked peptides strongly associate at neutral pH, but oligomerization is largely lost when pH is decreased (78). So by altering the flanking residue charge, the oligomerization of hydrophobic could be controlled. A variety of fluorescence based methods could be used to study helix association. One possibility is to use the rhodamine self-quenching assay. The basis for this method is that the rhodamine fluorescence is typically quenched when rhodamine in close proximity of another rhodamine molecule, as would be the case in TM oligomers. The flanking Lys residue could be labeled with rhodamine dye and rhodamine self-quenching can be used to monitor helix association (16). Another alternative is to use the di-bromo tyrosine quenching assay (78). This technique involves peptides with a central Tyr residue (instead of central Trp), which is subsequently brominated. Di-bromo Tyr is a efficient quencher of Trp fluorescence at short range (~8 Å) and extent of Trp quenching could be used to assess TM oligomerization. An advantage of this method is that it could be easily adapted for hetero-oligomerization studies. So we could use the flanking residue charge and fluorescence quenching methods to study the effect of helix association on minimum length threshold and on helix shifting ability of hydrophilic residues.

Additional Polio Virus 3A Protein Membrane Topography Studies

As described in Chapter 5, we found that the hydrophobic segment of Polio 3A protein can adopt a stable TM topography, but discovered an unexpected positioning of TM segment within the bilayer. A continuation of this work is to confirm, as the model predicts, that the Gln-residue lies at the boundary of the lipid bilayer. One way to confirm

this truncated topography is to substitute the Gln residue with another hydrophilic residue, like Asp. If the Gln residue does form the insertion boundary, then its substitution with a charged Asp would not affect the depth of Trp (at position 72) within the bilayer and the λmax vs. bilayer width profile will be similar for Gln and Asp substitutions. Alternatively, Gln could be replaced with a hydrophobic residue, like Leu or Val. If Gln locates at the boundary due to its hydrophilicity, then this substitution would allow the entire 22-residue hydrophobic sequence to bury in the bilayer, and the Trp at position 69 would locate closer to the center of the bilayer compared to Trp at position 72.

In addition, the functional significance of the TM topography of 3A anchor domain could be studied by examining whether membrane anchoring of 3A is sufficient for normal function. The hydrophobic segment could be forced to adopt a membrane-bound non-TM state by introducing charged hydrophilic residue in the middle of the hydrophobic sequence. Previous studies have shown that charged residue in the middle of the hydrophobic sequence tends to destabilize the TM state, promoting formation of membrane-bound non-TM state (29, 49). We could measure the effect of the hydrophilic substitution upon ability of 3A protein to support polio virus replication. If the any type of membrane anchoring is sufficient for 3A function, then such a mutation would not affect the normal function. However, if TM topography is important for function, then this mutation would abolish the normal function. If TM topography is required for normal function, then we could substitute Gln residue at the membrane boundary, with a hydrophilic Asp or hydrophobic Leu or Val residue to see if the different TM position of the hydrophobic anchor domain could affect the normal function of the 3A protein.

Furthermore, we observed a suppressor mutation within the first hydrophobic domain of 2B (I47V) in the virus recovered from the W42F/F69W clone. This result suggests that the hydrophobic domains of 3A/3AB and 2B/2BC may interact during poliovirus replication. This helix-helix association could alter the TM stability of the 3A hydrophobic domain and also be functionally important. We could test for *in vitro* helix-helix association between 3A and 2B hydrophobic domain using FRET measurements. As described above, rhodamine self-quenching assay or di-bromo tyrosine quenching assay could be used to test for helix-helix interactions.

Additional neu/ErbB2 Receptor Studies – Effect of Hydrophilic Mutation in TM Domain

We found that the hydrophilic mutation (Glu, Gln and Asp) at position 664 in the neu/ErbB2 TM domain alters its membrane position, such that the hydrophilic residue locates at or close to the membrane surface. The magnitude of shift in the TM position was dependent on the hydrophilicity and the ionization state of the hydrophilic residue. We propose that the transforming ability of a hydrophilic residue correlates with the ability of the hydrophilic residues to induce a shift in TM helix position under physiological conditions. One way to verify this hypothesis is to test the ability of other hydrophilic residues, like Gly, Lys and His, which have no transforming ability (165), to induce a shift in the membrane position of neu/ErbB2 TM helix. If these residues do not change the membrane position, then it would support the hypothesis that the transforming ability of a hydrophilic mutation is linked to its helix shifting ability.

All experiments on the neu/ErbB2 receptor were done in zwitterionic PC lipids and it is imperative to understand the effect of hydrophilic mutations in neu/ErbB2 receptor under physiological conditions. As described earlier, membrane surface charge (negative lipid) and cholesterol content could alter the shifting ability of hydrophilic residues. Thus, understanding how lipid composition influences the behavior of neu/ErbB2 TM domain would be important.

Since neu/ErbB2 receptors functions as dimers, the effect of hydrophilic mutation on dimerization has to be considered. Di-bromo tyrosine quenching assay would be an ideal choice for these experiments, as it could be applied to both homodimerization and heterodimerization. One of the hypotheses for receptor upregulation is that the mutant neu/ErbB2 sequence forms relatively stable dimers compared to WT sequence and the Glu^{664} residue is directly involved in stabilizing these dimers. We could measure the relatively stability of the WT and the mutant neu/ErbB2 dimers at physiological pH to confirm this hypothesis. Furthermore, we could assess the stability of the mutant dimers under low and high pH conditions to identify the ionization state of the Glu^{664} involved in stabilizing the dimers. If dimer structures are relatively more stable at low pH compared to high pH, then it would indicate that a protonated Glu^{664} is involved in stabilizing the dimer structure and vice versa.

In addition, we could test the possibility that the Glu^{664} mutation shifts the equilibrium between neu/ErbB2 homodimers and neu/ErbB2-containing heterodimers. We could do a competition assay with ErbB1 or ErbB3 TM helix to see if mutant neu/ErbB2 preferentially forms heterodimers over neu/ErbB2 homodimers. Control experiments with other TM helices, like glycophorin-A TM helix or Tar receptor TM helix, could be done to test the specificity of these interactions.

Furthermore, we could test for alternative mode for receptor dimerization in WT and mutant neu/ErbB2 receptor using NMR (in collaboration with Dr. Smith, Department of Biochemistry and Cell Biology). Dr. Smith's lab has used linewidth broadening in ^{2}HNMR to identify the inter-helical contacts in oligomers (226). This should help us identify any change in helical contacts or change in oligomeric state when truncated TM state is formed.

In this study, we introduced a Trp residue in the middle of the TM sequence (position 671) as a fluorescence probe. It is unlikely that the Trp mutation will strongly perturb the equilibrium between the TM and shifted state. A control experiment to rule out any perturbation effect of Trp is to compare the localization and EGF-induced internalization of full length neu/ErbB2 receptor with and without the Trp mutation in mammalian cells. The cell surface localization of neu/ErbB2 protein and EGF- induced internalization could be followed using fluorescently-labeled antibodies against neu/ErbB2 receptor. These experiments will be carried out in collaboration with Dr. Brown's lab in Department of Biochemistry and Cell Biology. In preliminary studies, we found that in COS cells, the full-length human ErbB2 protein, with and without Trp mutation, have similar cell surface expression indicating that the Trp mutation does not significantly perturb ErbB2 behavior.

The ionization state of the Glu residue associated with overactivation of the neu/ErbB2 receptor is still unclear. We could test for the transforming ability of Glu mutation at lower pH and higher pH conditions using a soft agar growth assay. Normal cells must be attached to a surface before they can divide and hence fail to grow when suspended in viscous fluid or gel. But transformed cells can grow in suspension as they become anchorage-independent. This phenotypic change is closely related to *in vivo* carcinogenesis (227). If an uncharged Glu is involved in receptor overactivation, then the

cells will be transformed to a greater degree under low pH conditions, but if a charged Glu is necessary for transformation, then the anchorage-independent growth will be more prevalent under high pH conditions. Transformation assays using Gln^{664} mutant could be carried out as a control. It would be interesting if Asp and Glu showed opposite pH dependences. Since Asp^{0} and Glu^{-1} shift about the same degree, this might indicate that a very specific amount of shifting is involved in activation of neu/ErbB2 receptor.

CHAPTER 8

REFERENCES

1. Wallin, E., and von Heijne, G. (1998) Genome-wide analysis of integral membrane proteins from eubacterial, archaean, and eukaryotic organisms, *Protein Sci* 7, 1029-1038.
2. Caffrey, M. (2003) Membrane protein crystallization, *J Struct Biol* 142, 108-132.
3. Opella, S. J., Ma, C., and Marassi, F. M. (2001) Nuclear magnetic resonance of membrane-associated peptides and proteins, *Methods Enzymol* 339, 285-313.
4. Wiener, M. C. (2004) A pedestrian guide to membrane protein crystallization, *Methods* 34, 364-372.
5. Hong, M. (2007) Structure, Topology, and Dynamics of Membrane Peptides and Proteins from Solid-State NMR Spectroscopy, *J Phys Chem B*.
6. Jiang, Y., Lee, A., Chen, J., Cadene, M., Chait, B. T., and MacKinnon, R. (2002) Crystal structure and mechanism of a calcium-gated potassium channel, *Nature* 417, 515-522.
7. Jiang, Y., Lee, A., Chen, J., Ruta, V., Cadene, M., Chait, B. T., and MacKinnon, R. (2003) X-ray structure of a voltage-dependent K+ channel, *Nature* 423, 33-41.
8. Klein, O., Polack, G. W., Surti, T., Kegler-Ebo, D., Smith, S. O., and DiMaio, D. (1998) Role of glutamine 17 of the bovine papillomavirus E5 protein in platelet-derived growth factor beta receptor activation and cell transformation, *J Virol* 72, 8921-8932.
9. Nilsson, I., Saaf, A., Whitley, P., Gafvelin, G., Waller, C., and von Heijne, G. (1998) Proline-induced disruption of a transmembrane alpha-helix in its natural environment, *J Mol Biol* 284, 1165-1175.
10. Hessa, T., Kim, H., Bihlmaier, K., Lundin, C., Boekel, J., Andersson, H., Nilsson, I., White, S. H., and von Heijne, G. (2005) Recognition of transmembrane helices by the endoplasmic reticulum translocon, *Nature* 433, 377-381.
11. Russ, W. P., and Engelman, D. M. (1999) TOXCAT: a measure of transmembrane helix association in a biological membrane, *Proc Natl Acad Sci U S A* 96, 863-868.
12. DeGrado, W. F., Gratkowski, H., and Lear, J. D. (2003) How do helix-helix interactions help determine the folds of membrane proteins? Perspectives from the study of homo-oligomeric helical bundles, *Protein Sci* 12, 647-665.

13. Lemmon, M. A., Flanagan, J. M., Hunt, J. F., Adair, B. D., Bormann, B. J., Dempsey, C. E., and Engelman, D. M. (1992) Glycophorin A dimerization is driven by specific interactions between transmembrane alpha-helices, *J Biol Chem* 267, 7683-7689.
14. Simmerman, H. K., Kobayashi, Y. M., Autry, J. M., and Jones, L. R. (1996) A leucine zipper stabilizes the pentameric membrane domain of phospholamban and forms a coiled-coil pore structure, *J Biol Chem* 271, 5941-5946.
15. Ladokhin, A. S. (1999) Analysis of protein and peptide penetration into membranes by depth-dependent fluorescence quenching: theoretical considerations, *Biophys J* 76, 946-955.
16. Ren, J., Lew, S., Wang, J., and London, E. (1999) Control of the transmembrane orientation and interhelical interactions within membranes by hydrophobic helix length, *Biochemistry* 38, 5905-5912.
17. Rosconi, M. P., and London, E. (2002) Topography of helices 5-7 in membrane-inserted diphtheria toxin T domain: identification and insertion boundaries of two hydrophobic sequences that do not form a stable transmembrane hairpin, *J Biol Chem* 277, 16517-16527.
18. Runnels, L. W., and Scarlata, S. F. (1995) Theory and application of fluorescence homotransfer to melittin oligomerization, *Biophys J* 69, 1569-1583.
19. You, M., Li, E., Wimley, W. C., and Hristova, K. (2005) Forster resonance energy transfer in liposomes: measurements of transmembrane helix dimerization in the native bilayer environment, *Anal Biochem* 340, 154-164.
20. Eftink, M. R., and Ghiron, C. A. (1981) Fluorescence quenching studies with proteins, *Anal Biochem* 114, 199-227.
21. London, E. (1982) Investigation of membrane structure using fluorescence quenching by spin-labels. A review of recent studies, *Mol Cell Biochem* 45, 181-188.
22. London, E., and Ladokhin, A.S. (2002) Investigation of membrane structure using fluorescence quenching by spin-labels. A review of recent studies, *Current Topics in Membranes*, 89-115.
23. Heuck, A. P., and Johnson, A. E. (2002) Pore-forming protein structure analysis

in membranes using multiple independent fluorescence techniques, *Cell Biochem Biophys* 36, 89-101.

24. Ren, J., Lew, S., Wang, Z., and London, E. (1997) Transmembrane orientation of hydrophobic alpha-helices is regulated both by the relationship of helix length to bilayer thickness and by the cholesterol concentration, *Biochemistry* 36, 10213-10220.
25. Wang, J., Rosconi, M. P., and London, E. (2006) Topography of the hydrophilic helices of membrane-inserted diphtheria toxin T domain: TH1-TH3 as a hydrophilic tether, *Biochemistry* 45, 8124-8134.
26. Landolt-Marticorena, C., Williams, K. A., Deber, C. M., and Reithmeier, R. A. (1993) Non-random distribution of amino acids in the transmembrane segments of human type I single span membrane proteins, *J Mol Biol* 229, 602-608.
27. Ulmschneider, M. B., and Sansom, M. S. (2001) Amino acid distributions in integral membrane protein structures, *Biochim Biophys Acta* 1512, 1-14.
28. Zhao, G., and London, E. (2006) An amino acid "transmembrane tendency" scale that approaches the theoretical limit to accuracy for prediction of transmembrane helices: relationship to biological hydrophobicity, *Protein Sci* 15, 1987-2001.
29. Caputo, G. A., and London, E. (2003) Cumulative effects of amino acid substitutions and hydrophobic mismatch upon the transmembrane stability and conformation of hydrophobic alpha-helices, *Biochemistry* 42, 3275-3285.
30. Lew, S., Ren, J., and London, E. (2000) The effects of polar and/or ionizable residues in the core and flanking regions of hydrophobic helices on transmembrane conformation and oligomerization, *Biochemistry* 39, 9632-9640.
31. Zhou, F. X., Cocco, M. J., Russ, W. P., Brunger, A. T., and Engelman, D. M. (2000) Interhelical hydrogen bonding drives strong interactions in membrane proteins, *Nat Struct Biol* 7, 154-160.
32. Zhou, F. X., Merianos, H. J., Brunger, A. T., and Engelman, D. M. (2001) Polar residues drive association of polyleucine transmembrane helices, *Proc Natl Acad Sci U S A* 98, 2250-2255.
33. Choma, C., Gratkowski, H., Lear, J. D., and DeGrado, W. F. (2000) Asparagine-mediated self-association of a model transmembrane helix, *Nat Struct Biol* 7, 161-

166.

34. Dawson, J. P., Melnyk, R. A., Deber, C. M., and Engelman, D. M. (2003) Sequence context strongly modulates association of polar residues in transmembrane helices, *J Mol Biol* 331, 255-262.

35. Dawson, J. P., Weinger, J. S., and Engelman, D. M. (2002) Motifs of serine and threonine can drive association of transmembrane helices, *J Mol Biol* 316, 799-805.

36. Gratkowski, H., Dai, Q. H., Wand, A. J., DeGrado, W. F., and Lear, J. D. (2002) Cooperativity and specificity of association of a designed transmembrane peptide, *Biophys J* 83, 1613-1619.

37. Gratkowski, H., Lear, J. D., and DeGrado, W. F. (2001) Polar side chains drive the association of model transmembrane peptides, *Proc Natl Acad Sci U S A* 98, 880-885.

38. Lear, J. D., Gratkowski, H., Adamian, L., Liang, J., and DeGrado, W. F. (2003) Position-dependence of stabilizing polar interactions of asparagine in transmembrane helical bundles, *Biochemistry* 42, 6400-6407.

39. Russ, W. P., and Engelman, D. M. (2000) The GxxxG motif: a framework for transmembrane helix-helix association, *J Mol Biol* 296, 911-919.

40. Eilers, M., Shekar, S. C., Shieh, T., Smith, S. O., and Fleming, P. J. (2000) Internal packing of helical membrane proteins, *Proc Natl Acad Sci U S A* 97, 5796-5801.

41. Smith, S. O., Song, D., Shekar, S., Groesbeek, M., Ziliox, M., and Aimoto, S. (2001) Structure of the transmembrane dimer interface of glycophorin A in membrane bilayers, *Biochemistry* 40, 6553-6558.

42. Partridge, A. W., Therien, A. G., and Deber, C. M. (2004) Missense mutations in transmembrane domains of proteins: phenotypic propensity of polar residues for human disease, *Proteins* 54, 648-656.

43. Therien, A. G., Grant, F. E., and Deber, C. M. (2001) Interhelical hydrogen bonds in the CFTR membrane domain, *Nat Struct Biol* 8, 597-601.

44. Smith, S. O., Smith, C. S., and Bormann, B. J. (1996) Strong hydrogen bonding interactions involving a buried glutamic acid in the transmembrane sequence of

the neu/erbB-2 receptor, *Nat Struct Biol* 3, 252-258.

45. Chin, C. N., and von Heijne, G. (2000) Charge pair interactions in a model transmembrane helix in the ER membrane, *J Mol Biol* 303, 1-5.
46. Braun, P., and von Heijne, G. (1999) The aromatic residues Trp and Phe have different effects on the positioning of a transmembrane helix in the microsomal membrane, *Biochemistry* 38, 9778-9782.
47. Monne, M., Nilsson, I., Johansson, M., Elmhed, N., and von Heijne, G. (1998) Positively and negatively charged residues have different effects on the position in the membrane of a model transmembrane helix, *J Mol Biol* 284, 1177-1183.
48. Monne, M., and von Heijne, G. (2001) Effects of 'hydrophobic mismatch' on the location of transmembrane helices in the ER membrane, *FEBS Lett* 496, 96-100.
49. Caputo, G. A., and London, E. (2004) Position and ionization state of Asp in the core of membrane-inserted alpha helices control both the equilibrium between transmembrane and nontransmembrane helix topography and transmembrane helix positioning, *Biochemistry* 43, 8794-8806.
50. Bechinger, B. (2001) Membrane insertion and orientation of polyalanine peptides: a (15)N solid-state NMR spectroscopy investigation, *Biophys J* 81, 2251-2256.
51. Lewis, R. N., Zhang, Y. P., Hodges, R. S., Subczynski, W. K., Kusumi, A., Flach, C. R., Mendelsohn, R., and McElhaney, R. N. (2001) A polyalanine-based peptide cannot form a stable transmembrane alpha-helix in fully hydrated phospholipid bilayers, *Biochemistry* 40, 12103-12111.
52. Wimley, W. C., Creamer, T. P., and White, S. H. (1996) Solvation energies of amino acid side chains and backbone in a family of host-guest pentapeptides, *Biochemistry* 35, 5109-5124.
53. Chen, H., and Kendall, D. A. (1995) Artificial transmembrane segments. Requirements for stop transfer and polypeptide orientation, *J Biol Chem* 270, 14115-14122.
54. Kuroiwa, T., Sakaguchi, M., Mihara, K., and Omura, T. (1991) Systematic analysis of stop-transfer sequence for microsomal membrane, *J Biol Chem* 266, 9251-9255.
55. Whitley, P., Grahn, E., Kutay, U., Rapoport, T. A., and von Heijne, G. (1996) A

12-residue-long polyleucine tail is sufficient to anchor synaptobrevin to the endoplasmic reticulum membrane, *J Biol Chem* 271, 7583-7586.

56. Adams, G. A., and Rose, J. K. (1985) Structural requirements of a membrane-spanning domain for protein anchoring and cell surface transport, *Cell* 41, 1007-1015.
57. Hildebrand, P. W., Preissner, R., and Frommel, C. (2004) Structural features of transmembrane helices, *FEBS Lett* 559, 145-151.
58. van Meer, G. (1989) Lipid traffic in animal cells, *Annu Rev Cell Biol* 5, 247-275.
59. de Planque, M. R., Boots, J. W., Rijkers, D. T., Liskamp, R. M., Greathouse, D. V., and Killian, J. A. (2002) The effects of hydrophobic mismatch between phosphatidylcholine bilayers and transmembrane alpha-helical peptides depend on the nature of interfacially exposed aromatic and charged residues, *Biochemistry* 41, 8396-8404.
60. Killian, J. A. (1998) Hydrophobic mismatch between proteins and lipids in membranes, *Biochim Biophys Acta* 1376, 401-415.
61. Duong-Ly, K. C., Nanda, V., Degrado, W. F., and Howard, K. P. (2005) The conformation of the pore region of the M2 proton channel depends on lipid bilayer environment, *Protein Sci* 14, 856-861.
62. Koehorst, R. B., Spruijt, R. B., Vergeldt, F. J., and Hemminga, M. A. (2004) Lipid bilayer topology of the transmembrane alpha-helix of M13 Major coat protein and bilayer polarity profile by site-directed fluorescence spectroscopy, *Biophys J* 87, 1445-1455.
63. Kovacs, F. A., Denny, J. K., Song, Z., Quine, J. R., and Cross, T. A. (2000) Helix tilt of the M2 transmembrane peptide from influenza A virus: an intrinsic property, *J Mol Biol* 295, 117-125.
64. Park, S. H., Mrse, A. A., Nevzorov, A. A., Mesleh, M. F., Oblatt-Montal, M., Montal, M., and Opella, S. J. (2003) Three-dimensional structure of the channel-forming trans-membrane domain of virus protein "u" (Vpu) from HIV-1, *J Mol Biol* 333, 409-424.
65. Park, S. H., and Opella, S. J. (2005) Tilt angle of a trans-membrane helix is determined by hydrophobic mismatch, *J Mol Biol* 350, 310-318.

66. Ozdirekcan, S., Rijkers, D. T., Liskamp, R. M., and Killian, J. A. (2005) Influence of flanking residues on tilt and rotation angles of transmembrane peptides in lipid bilayers. A solid-state 2H NMR study, *Biochemistry* 44, 1004-1012.

67. London, E. (1992) How bacterial protein toxins enter cells; the role of partial unfolding in membrane translocation, *Mol Microbiol* 6, 3277-3282.

68. Montecucco, C., Smith, G. A., Dabbeni-sala, F., Johannsson, A., Galante, Y. M., and Bisson, R. (1982) Bilayer thickness and enzymatic activity in the mitochondrial cytochrome c oxidase and ATPase complex, *FEBS Lett* 144, 145-148.

69. Perozo, E., Kloda, A., Cortes, D. M., and Martinac, B. (2002) Physical principles underlying the transduction of bilayer deformation forces during mechanosensitive channel gating, *Nat Struct Biol* 9, 696-703.

70. Caffrey, M., and Feigenson, G. W. (1981) Fluorescence quenching in model membranes. 3. Relationship between calcium adenosinetriphosphatase enzyme activity and the affinity of the protein for phosphatidylcholines with different acyl chain characteristics, *Biochemistry* 20, 1949-1961.

71. Goforth, R. L., Chi, A. K., Greathouse, D. V., Providence, L. L., Koeppe, R. E., 2nd, and Andersen, O. S. (2003) Hydrophobic coupling of lipid bilayer energetics to channel function, *J Gen Physiol* 121, 477-493.

72. Mitra, K., Ubarretxena-Belandia, I., Taguchi, T., Warren, G., and Engelman, D. M. (2004) Modulation of the bilayer thickness of exocytic pathway membranes by membrane proteins rather than cholesterol, *Proc Natl Acad Sci U S A* 101, 4083-4088.

73. Harroun, T. A., Heller, W. T., Weiss, T. M., Yang, L., and Huang, H. W. (1999) Experimental evidence for hydrophobic matching and membrane-mediated interactions in lipid bilayers containing gramicidin, *Biophys J* 76, 937-945.

74. Harroun, T. A., Heller, W. T., Weiss, T. M., Yang, L., and Huang, H. W. (1999) Theoretical analysis of hydrophobic matching and membrane-mediated interactions in lipid bilayers containing gramicidin, *Biophys J* 76, 3176-3185.

75. Killian, J. A., and von Heijne, G. (2000) How proteins adapt to a membrane-water interface, *Trends Biochem Sci* 25, 429-434.

76. von Heijne, G. (1994) Membrane proteins: from sequence to structure, *Annu Rev Biophys Biomol Struct* 23, 167-192.

77. de Planque, M. R., Goormaghtigh, E., Greathouse, D. V., Koeppe, R. E., 2nd, Kruijtzer, J. A., Liskamp, R. M., de Kruijff, B., and Killian, J. A. (2001) Sensitivity of single membrane-spanning alpha-helical peptides to hydrophobic mismatch with a lipid bilayer: effects on backbone structure, orientation, and extent of membrane incorporation, *Biochemistry* 40, 5000-5010.

78. Lew, S., Caputo, G. A., and London, E. (2003) The effect of interactions involving ionizable residues flanking membrane-inserted hydrophobic helices upon helix-helix interaction, *Biochemistry* 42, 10833-10842.

79. Strandberg, E., Ozdirekcan, S., Rijkers, D. T., van der Wel, P. C., Koeppe, R. E., 2nd, Liskamp, R. M., and Killian, J. A. (2004) Tilt angles of transmembrane model peptides in oriented and non-oriented lipid bilayers as determined by 2H solid-state NMR, *Biophys J* 86, 3709-3721.

80. van der Wel, P. C., Strandberg, E., Killian, J. A., and Koeppe, R. E., 2nd. (2002) Geometry and intrinsic tilt of a tryptophan-anchored transmembrane alpha-helix determined by (2)H NMR, *Biophys J* 83, 1479-1488.

81. Strandberg, E., Morein, S., Rijkers, D. T., Liskamp, R. M., van der Wel, P. C., and Killian, J. A. (2002) Lipid dependence of membrane anchoring properties and snorkeling behavior of aromatic and charged residues in transmembrane peptides, *Biochemistry* 41, 7190-7198.

82. Killian, J. A., and Nyholm, T. K. (2006) Peptides in lipid bilayers: the power of simple models, *Curr Opin Struct Biol* 16, 473-479.

83. Caputo, G. A., and London, E. (2003) Using a novel dual fluorescence quenching assay for measurement of tryptophan depth within lipid bilayers to determine hydrophobic alpha-helix locations within membranes, *Biochemistry* 42, 3265-3274.

84. Whitmore, L., and Wallace, B. A. (2004) DICHROWEB, an online server for protein secondary structure analyses from circular dichroism spectroscopic data, *Nucleic Acids Res* 32, W668-673.

85. Fujita, K., Krishnakumar, S. S., Franco, D., Paul, A. V., London, E., and

Wimmer, E. (2007) Membrane topography of the hydrophobic anchor sequence of poliovirus 3A and 3AB proteins and the functional effect of 3A/3AB membrane association upon RNA replication, *Biochemistry* 46, 5185-5199.

86. Dalley, J. A., and Bulleid, N. J. (2003) The endoplasmic reticulum (ER) translocon can differentiate between hydrophobic sequences allowing signals for glycosylphosphatidylinositol anchor addition to be fully translocated into the ER lumen, *J Biol Chem* 278, 51749-51757.
87. Jeong, S. Y., Gaume, B., Lee, Y. J., Hsu, Y. T., Ryu, S. W., Yoon, S. H., and Youle, R. J. (2004) Bcl-x(L) sequesters its C-terminal membrane anchor in soluble, cytosolic homodimers, *Embo J* 23, 2146-2155.
88. Kienker, P. K., Qiu, X., Slatin, S. L., Finkelstein, A., and Jakes, K. S. (1997) Transmembrane insertion of the colicin Ia hydrophobic hairpin, *J Membr Biol* 157, 27-37.
89. Ladokhin, A. S., Isas, J. M., Haigler, H. T., and White, S. H. (2002) Determining the membrane topology of proteins: insertion pathway of a transmembrane helix of annexin 12, *Biochemistry* 41, 13617-13626.
90. Qiu, X. Q., Jakes, K. S., Kienker, P. K., Finkelstein, A., and Slatin, S. L. (1996) Major transmembrane movement associated with colicin Ia channel gating, *J Gen Physiol* 107, 313-328.
91. Rosconi, M. P., Zhao, G., and London, E. (2004) Analyzing topography of membrane-inserted diphtheria toxin T domain using BODIPY-streptavidin: at low pH, helices 8 and 9 form a transmembrane hairpin but helices 5-7 form stable nonclassical inserted segments on the cis side of the bilayer, *Biochemistry* 43, 9127-9139.
92. Wattenberg, B., and Lithgow, T. (2001) Targeting of C-terminal (tail)-anchored proteins: understanding how cytoplasmic activities are anchored to intracellular membranes, *Traffic* 2, 66-71.
93. Bretscher, M. S., and Munro, S. (1993) Cholesterol and the Golgi apparatus, *Science* 261, 1280-1281.
94. Munro, S. (1995) An investigation of the role of transmembrane domains in Golgi protein retention, *Embo J* 14, 4695-4704.

95. Webb, R. J., East, J. M., Sharma, R. P., and Lee, A. G. (1998) Hydrophobic mismatch and the incorporation of peptides into lipid bilayers: a possible mechanism for retention in the Golgi, *Biochemistry* 37, 673-679.

96. Brandizzi, F., Frangne, N., Marc-Martin, S., Hawes, C., Neuhaus, J. M., and Paris, N. (2002) The destination for single-pass membrane proteins is influenced markedly by the length of the hydrophobic domain, *Plant Cell* 14, 1077-1092.

97. Karsten, V., Hegde, R. S., Sinai, A. P., Yang, M., and Joiner, K. A. (2004) Transmembrane domain modulates sorting of membrane proteins in Toxoplasma gondii, *J Biol Chem* 279, 26052-26057.

98. Masibay, A. S., Balaji, P. V., Boeggeman, E. E., and Qasba, P. K. (1993) Mutational analysis of the Golgi retention signal of bovine beta-1,4-galactosyltransferase, *J Biol Chem* 268, 9908-9916.

99. Aisenbrey, C., Goormaghtigh, E., Ruysschaert, J. M., and Bechinger, B. (2006) Translocation of amino acyl residues from the membrane interface to the hydrophobic core: thermodynamic model and experimental analysis using ATR-FTIR spectroscopy, *Mol Membr Biol* 23, 363-374.

100. Liu, F., Lewis, R. N., Hodges, R. S., and McElhaney, R. N. (2004) Effect of variations in the structure of a polyleucine-based alpha-helical transmembrane peptide on its interaction with phosphatidylethanolamine Bilayers, *Biophys J* 87, 2470-2482.

101. Mall, S., Broadbridge, R., Sharma, R. P., Lee, A. G., and East, J. M. (2000) Effects of aromatic residues at the ends of transmembrane alpha-helices on helix interactions with lipid bilayers, *Biochemistry* 39, 2071-2078.

102. van Duyl, B. Y., Meeldijk, H., Verkleij, A. J., Rijkers, D. T., Chupin, V., de Kruijff, B., and Killian, J. A. (2005) A synergistic effect between cholesterol and tryptophan-flanked transmembrane helices modulates membrane curvature, *Biochemistry* 44, 4526-4532.

103. Lew, S., and London, E. (1997) Simple procedure for reversed-phase high-performance liquid chromatographic purification of long hydrophobic peptides that form transmembrane helices, *Anal Biochem* 251, 113-116.

104. Zhang, Y. P., Lewis, R. N., Henry, G. D., Sykes, B. D., Hodges, R. S., and

McElhaney, R. N. (1995) Peptide models of helical hydrophobic transmembrane segments of membrane proteins. 1. Studies of the conformation, intrabilayer orientation, and amide hydrogen exchangeability of Ac-K2-(LA)12-K2-amide, *Biochemistry* 34, 2348-2361.

105. Wimley, W. C., and White, S. H. (1996) Experimentally determined hydrophobicity scale for proteins at membrane interfaces, *Nat Struct Biol* 3, 842-848.

106. Davis, J. H., Clare, D. M., Hodges, R. S., and Bloom, M. (1983) Interaction of a Synthetic Amphiphilic Polypeptide and Lipids in a Bilayer Structure *Biochemistry* 22, 5298-5305.

107. Hammond, K., Caputo, G. A., and London, E. (2002) Interaction of the membrane-inserted diphtheria toxin T domain with peptides and its possible implications for chaperone-like T domain behavior, *Biochemistry* 41, 3243-3253.

108. Dumas, F., Tocanne, J. F., Leblanc, G., and Lebrun, M. C. (2000) Consequences of hydrophobic mismatch between lipids and melibiose permease on melibiose transport, *Biochemistry* 39, 4846-4854.

109. Johannsson, A., Keightley, C. A., Smith, G. A., Richards, C. D., Hesketh, T. R., and Metcalfe, J. C. (1981) The effect of bilayer thickness and n-alkanes on the activity of the (Ca2+ + Mg2+)-dependent ATPase of sarcoplasmic reticulum, *J Biol Chem* 256, 1643-1650.

110. Johannsson, A., Smith, G. A., and Metcalfe, J. C. (1981) The effect of bilayer thickness on the activity of (Na+ + K+)-ATPase, *Biochim Biophys Acta* 641, 416-421.

111. Pilot, J. D., East, J. M., and Lee, A. G. (2001) Effects of bilayer thickness on the activity of diacylglycerol kinase of Escherichia coli, *Biochemistry* 40, 8188-8195.

112. Mouritsen, O. G., and Bloom, M. (1984) Mattress model of lipid-protein interactions in membranes, *Biophys J* 46, 141-153.

113. Grinthal, A., and Guidotti, G. (2007) Bilayer mechanical properties regulate the transmembrane helix mobility and enzymatic state of CD39, *Biochemistry* 46, 279-290.

114. Fernandez-Vidal, M., Jayasinghe, S., Ladokhin, A. S., and White, S. H. (2007)

Folding amphipathic helices into membranes: amphiphilicity trumps hydrophobicity, *J Mol Biol* 370, 459-470.

115. Bechinger, B. (1996) Towards membrane protein design: pH-sensitive topology of histidine-containing polypeptides, *J Mol Biol* 263, 768-775.
116. Hunt, J. F., Rath, P., Rothschild, K. J., and Engelman, D. M. (1997) Spontaneous, pH-dependent membrane insertion of a transbilayer alpha-helix, *Biochemistry* 36, 15177-15192.
117. Popot, J. L., and Engelman, D. M. (2000) Helical membrane protein folding, stability, and evolution, *Annu Rev Biochem* 69, 881-922.
118. Fleming, K. G., and Engelman, D. M. (2001) Specificity in transmembrane helix-helix interactions can define a hierarchy of stability for sequence variants, *Proc Natl Acad Sci U S A* 98, 14340-14344.
119. Hermansson, M., and von Heijne, G. (2003) Inter-helical hydrogen bond formation during membrane protein integration into the ER membrane, *J Mol Biol* 334, 803-809.
120. Harzer, U., and Bechinger, B. (2000) Alignment of lysine-anchored membrane peptides under conditions of hydrophobic mismatch: a CD, 15N and 31P solid-state NMR spectroscopy investigation, *Biochemistry* 39, 13106-13114.
121. Vogt, B., Ducarme, P., Schinzel, S., Brasseur, R., and Bechinger, B. (2000) The topology of lysine-containing amphipathic peptides in bilayers by circular dichroism, solid-state NMR, and molecular modeling, *Biophys J* 79, 2644-2656.
122. Borochov, H., and Shinitzky, M. (1976) Vertical displacement of membrane proteins mediated by changes in microviscosity, *Proc Natl Acad Sci U S A* 73, 4526-4530.
123. Boldog, T., and Hazelbauer, G. L. (2004) Accessibility of introduced cysteines in chemoreceptor transmembrane helices reveals boundaries interior to bracketing charged residues, *Protein Sci* 13, 1466-1475.
124. Falke, J. J., and Hazelbauer, G. L. (2001) Transmembrane signaling in bacterial chemoreceptors, *Trends Biochem Sci* 26, 257-265.
125. Miller, A. S., and Falke, J. J. (2004) Side chains at the membrane-water interface modulate the signaling state of a transmembrane receptor, *Biochemistry* 43, 1763-

1770.

126. Armulik, A., Nilsson, I., von Heijne, G., and Johansson, S. (1999) Determination of the border between the transmembrane and cytoplasmic domains of human integrin subunits, *J Biol Chem* 274, 37030-37034.

127. Chamberlain, A. K., Lee, Y., Kim, S., and Bowie, J. U. (2004) Snorkeling preferences foster an amino acid composition bias in transmembrane helices, *J Mol Biol* 339, 471-479.

128. Kachel, K., Asuncion-Punzalan, E., and London, E. (1995) Anchoring of tryptophan and tyrosine analogs at the hydrocarbon-polar boundary in model membrane vesicles: parallax analysis of fluorescence quenching induced by nitroxide-labeled phospholipids, *Biochemistry* 34, 15475-15479.

129. Senes, A., Chadi, D. C., Law, P. B., Walters, R. F., Nanda, V., and Degrado, W. F. (2007) E(z), a depth-dependent potential for assessing the energies of insertion of amino acid side-chains into membranes: derivation and applications to determining the orientation of transmembrane and interfacial helices, *J Mol Biol* 366, 436-448.

130. Ulmschneider, M. B., Sansom, M. S., and Di Nola, A. (2005) Properties of integral membrane protein structures: derivation of an implicit membrane potential, *Proteins* 59, 252-265.

131. Han, X., Mihailescu, M., and Hristova, K. (2006) Neutron diffraction studies of fluid bilayers with transmembrane proteins: structural consequences of the achondroplasia mutation, *Biophys J* 91, 3736-3747.

132. Monsonego-Ornan, E., Adar, R., Feferman, T., Segev, O., and Yayon, A. (2000) The transmembrane mutation G380R in fibroblast growth factor receptor 3 uncouples ligand-mediated receptor activation from down-regulation, *Mol Cell Biol* 20, 516-522.

133. Monsonego-Ornan, E., Adar, R., Rom, E., and Yayon, A. (2002) FGF receptors ubiquitylation: dependence on tyrosine kinase activity and role in downregulation, *FEBS Lett* 528, 83-89.

134. Li, E., and Hristova, K. (2006) Role of receptor tyrosine kinase transmembrane domains in cell signaling and human pathologies, *Biochemistry* 45, 6241-6251.

135. Sharpe, S., Barber, K. R., and Grant, C. W. (2000) Val(659)-->Glu mutation within the transmembrane domain of ErbB-2: effects measured by (2)H NMR in fluid phospholipid bilayers, *Biochemistry* 39, 6572-6580.

136. Weiner, D. B., Liu, J., Cohen, J. A., Williams, W. V., and Greene, M. I. (1989) A point mutation in the neu oncogene mimics ligand induction of receptor aggregation, *Nature* 339, 230-231.

137. Tischer, E., and Cordell, B. (1996) Beta-amyloid precursor protein. Location of transmembrane domain and specificity of gamma-secretase cleavage, *J Biol Chem* 271, 21914-21919.

138. Lichtenthaler, S. F., Beher, D., Grimm, H. S., Wang, R., Shearman, M. S., Masters, C. L., and Beyreuther, K. (2002) The intramembrane cleavage site of the amyloid precursor protein depends on the length of its transmembrane domain, *Proc Natl Acad Sci U S A* 99, 1365-1370.

139. Citri, A., and Yarden, Y. (2006) EGF-ERBB signalling: towards the systems level, *Nat Rev Mol Cell Biol* 7, 505-516.

140. Marmor, M. D., Skaria, K. B., and Yarden, Y. (2004) Signal transduction and oncogenesis by ErbB/HER receptors, *Int J Radiat Oncol Biol Phys* 58, 903-913.

141. Olayioye, M. A., Neve, R. M., Lane, H. A., and Hynes, N. E. (2000) The ErbB signaling network: receptor heterodimerization in development and cancer, *Embo J* 19, 3159-3167.

142. Burgess, A. W., Cho, H. S., Eigenbrot, C., Ferguson, K. M., Garrett, T. P., Leahy, D. J., Lemmon, M. A., Sliwkowski, M. X., Ward, C. W., and Yokoyama, S. (2003) An open-and-shut case? Recent insights into the activation of EGF/ErbB receptors, *Mol Cell* 12, 541-552.

143. Schlessinger, J. (2000) Cell signaling by receptor tyrosine kinases, *Cell* 103, 211-225.

144. Fantl, W. J., Johnson, D. E., and Williams, L. T. (1993) Signalling by receptor tyrosine kinases, *Annu Rev Biochem* 62, 453-481.

145. van der Geer, P., Hunter, T., and Lindberg, R. A. (1994) Receptor protein-tyrosine kinases and their signal transduction pathways, *Annu Rev Cell Biol* 10, 251-337.

146. Blume-Jensen, P., and Hunter, T. (2001) Oncogenic kinase signalling, *Nature* 411, 355-365.

147. Robertson, S. C., Tynan, J. A., and Donoghue, D. J. (2000) RTK mutations and human syndromes: when good receptors turn bad, *Trends Genet* 16, 265-271.

148. Wang, Q., Villeneuve, G., and Wang, Z. (2005) Control of epidermal growth factor receptor endocytosis by receptor dimerization, rather than receptor kinase activation, *EMBO Rep* 6, 942-948.

149. Marmor, M. D., and Yarden, Y. (2004) Role of protein ubiquitylation in regulating endocytosis of receptor tyrosine kinases, *Oncogene* 23, 2057-2070.

150. Herbst, J. J., Opresko, L. K., Walsh, B. J., Lauffenburger, D. A., and Wiley, H. S. (1994) Regulation of postendocytic trafficking of the epidermal growth factor receptor through endosomal retention, *J Biol Chem* 269, 12865-12873.

151. Honegger, A. M., Dull, T. J., Felder, S., Van Obberghen, E., Bellot, F., Szapary, D., Schmidt, A., Ullrich, A., and Schlessinger, J. (1987) Point mutation at the ATP binding site of EGF receptor abolishes protein-tyrosine kinase activity and alters cellular routing, *Cell* 51, 199-209.

152. Gadella, T. W., Jr., and Jovin, T. M. (1995) Oligomerization of epidermal growth factor receptors on A431 cells studied by time-resolved fluorescence imaging microscopy. A stereochemical model for tyrosine kinase receptor activation, *J Cell Biol* 129, 1543-1558.

153. Lemmon, M. A., Bu, Z., Ladbury, J. E., Zhou, M., Pinchasi, D., Lax, I., Engelman, D. M., and Schlessinger, J. (1997) Two EGF molecules contribute additively to stabilization of the EGFR dimer, *Embo J* 16, 281-294.

154. Moriki, T., Maruyama, H., and Maruyama, I. N. (2001) Activation of preformed EGF receptor dimers by ligand-induced rotation of the transmembrane domain, *J Mol Biol* 311, 1011-1026.

155. Sako, Y., Minoghchi, S., and Yanagida, T. (2000) Single-molecule imaging of EGFR signalling on the surface of living cells, *Nat Cell Biol* 2, 168-172.

156. Guy, P. M., Platko, J. V., Cantley, L. C., Cerione, R. A., and Carraway, K. L., 3rd. (1994) Insect cell-expressed p180erbB3 possesses an impaired tyrosine kinase activity, *Proc Natl Acad Sci U S A* 91, 8132-8136.

157. Klapper, L. N., Glathe, S., Vaisman, N., Hynes, N. E., Andrews, G. C., Sela, M., and Yarden, Y. (1999) The ErbB-2/HER2 oncoprotein of human carcinomas may function solely as a shared coreceptor for multiple stroma-derived growth factors, *Proc Natl Acad Sci U S A* 96, 4995-5000.

158. Beerli, R. R., Graus-Porta, D., Woods-Cook, K., Chen, X., Yarden, Y., and Hynes, N. E. (1995) Neu differentiation factor activation of ErbB-3 and ErbB-4 is cell specific and displays a differential requirement for ErbB-2, *Mol Cell Biol* 15, 6496-6505.

159. Graus-Porta, D., Beerli, R. R., Daly, J. M., and Hynes, N. E. (1997) ErbB-2, the preferred heterodimerization partner of all ErbB receptors, is a mediator of lateral signaling, *Embo J* 16, 1647-1655.

160. Tzahar, E., Waterman, H., Chen, X., Levkowitz, G., Karunagaran, D., Lavi, S., Ratzkin, B. J., and Yarden, Y. (1996) A hierarchical network of interreceptor interactions determines signal transduction by Neu differentiation factor/neuregulin and epidermal growth factor, *Mol Cell Biol* 16, 5276-5287.

161. Garrett, T. P., McKern, N. M., Lou, M., Elleman, T. C., Adams, T. E., Lovrecz, G. O., Kofler, M., Jorissen, R. N., Nice, E. C., Burgess, A. W., and Ward, C. W. (2003) The crystal structure of a truncated ErbB2 ectodomain reveals an active conformation, poised to interact with other ErbB receptors, *Mol Cell* 11, 495-505.

162. Lenferink, A. E., Pinkas-Kramarski, R., van de Poll, M. L., van Vugt, M. J., Klapper, L. N., Tzahar, E., Waterman, H., Sela, M., van Zoelen, E. J., and Yarden, Y. (1998) Differential endocytic routing of homo- and hetero-dimeric ErbB tyrosine kinases confers signaling superiority to receptor heterodimers, *Embo J* 17, 3385-3397.

163. Worthylake, R., Opresko, L. K., and Wiley, H. S. (1999) ErbB-2 amplification inhibits down-regulation and induces constitutive activation of both ErbB-2 and epidermal growth factor receptors, *J Biol Chem* 274, 8865-8874.

164. Bargmann, C. I., Hung, M. C., and Weinberg, R. A. (1986) Multiple independent activations of the neu oncogene by a point mutation altering the transmembrane domain of p185, *Cell* 45, 649-657.

165. Bargmann, C. I., and Weinberg, R. A. (1988) Oncogenic activation of the neu-

encoded receptor protein by point mutation and deletion, *Embo J* 7, 2043-2052.

166. Gullick, W. J., Bottomley, A. C., Lofts, F. J., Doak, D. G., Mulvey, D., Newman, R., Crumpton, M. J., Sternberg, M. J., and Campbell, I. D. (1992) Three dimensional structure of the transmembrane region of the proto-oncogenic and oncogenic forms of the neu protein, *Embo J* 11, 43-48.
167. Mendrola, J. M., Berger, M. B., King, M. C., and Lemmon, M. A. (2002) The single transmembrane domains of ErbB receptors self-associate in cell membranes, *J Biol Chem* 277, 4704-4712.
168. Burke, C. L., Lemmon, M. A., Coren, B. A., Engelman, D. M., and Stern, D. F. (1997) Dimerization of the p185neu transmembrane domain is necessary but not sufficient for transformation, *Oncogene* 14, 687-696.
169. Beevers, A. J., and Kukol, A. (2006) The transmembrane domain of the oncogenic mutant ErbB-2 receptor: a structure obtained from site-specific infrared dichroism and molecular dynamics, *J Mol Biol* 361, 945-953.
170. Samna Soumana, O., Aller, P., Garnier, N., and Genest, M. (2005) Transmembrane peptides from tyrosine kinase receptor. Mutation-related behavior in a lipid bilayer investigated by molecular dynamics simulations, *J Biomol Struct Dyn* 23, 91-100.
171. Fleishman, S. J., Schlessinger, J., and Ben-Tal, N. (2002) A putative molecular-activation switch in the transmembrane domain of erbB2, *Proc Natl Acad Sci U S A* 99, 15937-15940.
172. Sternberg, M. J., and Gullick, W. J. (1989) Neu receptor dimerization, *Nature* 339, 587.
173. Sternberg, M. J., and Gullick, W. J. (1990) A sequence motif in the transmembrane region of growth factor receptors with tyrosine kinase activity mediates dimerization, *Protein Eng* 3, 245-248.
174. McLaughlin, S., Smith, S. O., Hayman, M. J., and Murray, D. (2005) An electrostatic engine model for autoinhibition and activation of the epidermal growth factor receptor (EGFR/ErbB) family, *J Gen Physiol* 126, 41-53.
175. Yamada, K., Carpentier, J. L., Cheatham, B., Goncalves, E., Shoelson, S. E., and Kahn, C. R. (1995) Role of the transmembrane domain and flanking amino acids

in internalization and down-regulation of the insulin receptor, *J Biol Chem* 270, 3115-3122.

176. Paul, A. V. (2002) Possible unifying mechanism of picornavirus genome replication, *In molecular Biology of picornaviruses, Eds. Semler,B. L., and Wimmer, E.* , ASM Press, Washington, DC, 227-246.

177. Bienz, K., Egger, D., and Pasamontes, L. (1987) Association of polioviral proteins of the P2 genomic region with the viral replication complex and virus-induced membrane synthesis as visualized by electron microscopic immunocytochemistry and autoradiography, *Virology* 160, 220-226.

178. Egger, D., Gosert, R., and Bienz, K. (2002) Role of cellular structures in viral RNA replication., *In Molecular Biology of Piocrnaviruses, Eds. B. L. Semler and Wimmer, E.*, ASM Press, Washington DC, 20036-22904.

179. Schlegel, A., Giddings, T. H., Jr., Ladinsky, M. S., and Kirkegaard, K. (1996) Cellular origin and ultrastructure of membranes induced during poliovirus infection, *J Virol* 70, 6576-6588.

180. Jackson, W. T., Giddings, T. H., Jr., Taylor, M. P., Mulinyawe, S., Rabinovitch, M., Kopito, R. R., and Kirkegaard, K. (2005) Subversion of cellular autophagosomal machinery by RNA viruses, *PLoS Biol* 3, e156.

181. Bienz, K., Egger, D., Pfister, T., and Troxler, M. (1992) Structural and functional characterization of the poliovirus replication complex, *J Virol* 66, 2740-2747.

182. Carrasco, L., Guinea, R., Irurzun, A., and Barco, A. (2002) Effects of viral replication on cellular membrane metabolism and function, *In molecular Biology of picornaviruses, Eds. Semler,B. L., and Wimmer, E.*, ASM Press, Washington, DC, 20036-22904.

183. Lyle, J. M., Clewell, A., Richmond, K., Richards, O. C., Hope, D. A., Schultz, S. C., and Kirkegaard, K. (2002) Similar structural basis for membrane localization and protein priming by an RNA-dependent RNA polymerase, *J Biol Chem* 277, 16324-16331.

184. Xiang, W., Cuconati, A., Hope, D., Kirkegaard, K., and Wimmer, E. (1998) Complete protein linkage map of poliovirus P3 proteins: interaction of polymerase 3Dpol with VPg and with genetic variants of 3AB, *J Virol* 72, 6732-

6741.

185. Towner, J. S., Ho, T. V., and Semler, B. L. (1996) Determinants of membrane association for poliovirus protein 3AB, *J Biol Chem* 271, 26810-26818.

186. Hope, D. A., Diamond, S. E., and Kirkegaard, K. (1997) Genetic dissection of interaction between poliovirus 3D polymerase and viral protein 3AB, *J Virol* 71, 9490-9498.

187. Strauss, D. M., Glustrom, L. W., and Wuttke, D. S. (2003) Towards an understanding of the poliovirus replication complex: the solution structure of the soluble domain of the poliovirus 3A protein, *J Mol Biol* 330, 225-234.

188. Harris, K. S., Xiang, W., Alexander, L., Lane, W. S., Paul, A. V., and Wimmer, E. (1994) Interaction of poliovirus polypeptide 3CDpro with the 5' and 3' termini of the poliovirus genome. Identification of viral and cellular cofactors needed for efficient binding, *J Biol Chem* 269, 27004-27014.

189. Paul, A. V., Cao, X., Harris, K. S., Lama, J., and Wimmer, E. (1994) Studies with poliovirus polymerase 3Dpol. Stimulation of poly(U) synthesis in vitro by purified poliovirus protein 3AB, *J Biol Chem* 269, 29173-29181.

190. Xiang, W., Harris, K. S., Alexander, L., and Wimmer, E. (1995) Interaction between the 5'-terminal cloverleaf and 3AB/3CDpro of poliovirus is essential for RNA replication, *J Virol* 69, 3658-3667.

191. Lama, J., Paul, A. V., Harris, K. S., and Wimmer, E. (1994) Properties of purified recombinant poliovirus protein 3aB as substrate for viral proteinases and as co-factor for RNA polymerase 3Dpol, *J Biol Chem* 269, 66-70.

192. Plotch, S. J., and Palant, O. (1995) Poliovirus protein 3AB forms a complex with and stimulates the activity of the viral RNA polymerase, 3Dpol, *J Virol* 69, 7169-7179.

193. Richards, O. C., and Ehrenfeld, E. (1998) Effects of poliovirus 3AB protein on 3D polymerase-catalyzed reaction, *J Biol Chem* 273, 12832-12840.

194. Rodriguez-Wells, V., Plotch, S. J., and DeStefano, J. J. (2001) Primer-dependent synthesis by poliovirus RNA-dependent RNA polymerase (3D(pol)), *Nucleic Acids Res* 29, 2715-2724.

195. Molla, A., Harris, K. S., Paul, A. V., Shin, S. H., Mugavero, J., and Wimmer, E.

(1994) Stimulation of poliovirus proteinase 3Cpro-related proteolysis by the genome-linked protein VPg and its precursor 3AB, *J Biol Chem* 269, 27015-27020.

196. Datta, U., and Dasgupta, A. (1994) Expression and subcellular localization of poliovirus VPg-precursor protein 3AB in eukaryotic cells: evidence for glycosylation in vitro, *J Virol* 68, 4468-4477.
197. Choe, S. S., and Kirkegaard, K. (2004) Intracellular topology and epitope shielding of poliovirus 3A protein, *J Virol* 78, 5973-5982.
198. Giachetti, C., Hwang, S. S., and Semler, B. L. (1992) cis-acting lesions targeted to the hydrophobic domain of a poliovirus membrane protein involved in RNA replication, *J Virol* 66, 6045-6057.
199. Heinz, B. A., and Vance, L. M. (1996) Sequence determinants of 3A-mediated resistance to enviroxime in rhinoviruses and enteroviruses, *J Virol* 70, 4854-4857.
200. Belov, G. A., Fogg, M. H., and Ehrenfeld, E. (2005) Poliovirus proteins induce membrane association of GTPase ADP-ribosylation factor, *J Virol* 79, 7207-7216.
201. Dodd, D. A., Giddings, T. H., Jr., and Kirkegaard, K. (2001) Poliovirus 3A protein limits interleukin-6 (IL-6), IL-8, and beta interferon secretion during viral infection, *J Virol* 75, 8158-8165.
202. Doedens, J. R., Giddings, T. H., Jr., and Kirkegaard, K. (1997) Inhibition of endoplasmic reticulum-to-Golgi traffic by poliovirus protein 3A: genetic and ultrastructural analysis, *J Virol* 71, 9054-9064.
203. Doedens, J. R., and Kirkegaard, K. (1995) Inhibition of cellular protein secretion by poliovirus proteins 2B and 3A, *Embo J* 14, 894-907.
204. Teterina, N. L., Levenson, E., Rinaudo, M. S., Egger, D., Bienz, K., Gorbalenya, A. E., and Ehrenfeld, E. (2006) Evidence for functional protein interactions required for poliovirus RNA replication, *J Virol* 80, 5327-5337.
205. Teterina, N. L., Rinaudo, M. S., and Ehrenfeld, E. (2003) Strand-specific RNA synthesis defects in a poliovirus with a mutation in protein 3A, *J Virol* 77, 12679-12691.
206. Lee, Y. F., Nomoto, A., Detjen, B. M., and Wimmer, E. (1977) A protein covalently linked to poliovirus genome RNA, *Proc Natl Acad Sci U S A* 74, 59-

63.

207. Paul, A. V., van Boom, J. H., Filippov, D., and Wimmer, E. (1998) Protein-primed RNA synthesis by purified poliovirus RNA polymerase, *Nature* 393, 280-284.

208. Paul, A. V., Rieder, E., Kim, D. W., van Boom, J. H., and Wimmer, E. (2000) Identification of an RNA hairpin in poliovirus RNA that serves as the primary template in the in vitro uridylylation of VPg, *J Virol* 74, 10359-10370.

209. Murray, K. E., and Barton, D. J. (2003) Poliovirus CRE-dependent VPg uridylylation is required for positive-strand RNA synthesis but not for negative-strand RNA synthesis, *J Virol* 77, 4739-4750.

210. van Ooij, M. J., Vogt, D. A., Paul, A., Castro, C., Kuijpers, J., van Kuppeveld, F. J., Cameron, C. E., Wimmer, E., Andino, R., and Melchers, W. J. (2006) Structural and functional characterization of the coxsackievirus B3 CRE(2C): role of CRE(2C) in negative- and positive-strand RNA synthesis, *J Gen Virol* 87, 103-113.

211. Fogg, M. H., Teterina, N. L., and Ehrenfeld, E. (2003) Membrane requirements for uridylylation of the poliovirus VPg protein and viral RNA synthesis in vitro, *J Virol* 77, 11408-11416.

212. Takeda, N., Kuhn, R. J., Yang, C. F., Takegami, T., and Wimmer, E. (1986) Initiation of poliovirus plus-strand RNA synthesis in a membrane complex of infected HeLa cells, *J Virol* 60, 43-53.

213. Molla, A., Paul, A. V., and Wimmer, E. (1991) Cell-free, de novo synthesis of poliovirus, *Science* 254, 1647-1651.

214. Lewis, B. A., and Engelman, D. M. (1983) Lipid bilayer thickness varies linearly with acyl chain length in fluid phosphatidylcholine vesicles, *J Mol Biol* 166, 211-217.

215. Lama, J., Sanz, M. A., and Carrasco, L. (1998) Genetic analysis of poliovirus protein 3A: characterization of a non-cytopathic mutant virus defective in killing Vero cells, *J Gen Virol* 79 (Pt 8), 1911-1921.

216. Towner, J. S., Mazanet, M. M., and Semler, B. L. (1998) Rescue of defective poliovirus RNA replication by 3AB-containing precursor polyproteins, *J Virol* 72,

7191-7200.

217. Towner, J. S., Brown, D. M., Nguyen, J. H., and Semler, B. L. (2003) Functional conservation of the hydrophobic domain of polypeptide 3AB between human rhinovirus and poliovirus, *Virology* 314, 432-442.

218. Dailey, H. A., and Strittmatter, P. (1981) Orientation of the carboxyl and NH2 termini of the membrane-binding segment of cytochrome b5 on the same side of phospholipid bilayers, *J Biol Chem* 256, 3951-3955.

219. Krajewska, W. M., and Maslowska, I. (2004) Caveolins: structure and function in signal transduction, *Cell Mol Biol Lett* 9, 195-220.

220. London, E. (1992) Diphtheria toxin: membrane interaction and membrane translocation, *Biochim Biophys Acta* 1113, 25-51.

221. Zhang, S., Finkelstein, A., and Collier, R. J. (2004) Evidence that translocation of anthrax toxin's lethal factor is initiated by entry of its N terminus into the protective antigen channel, *Proc Natl Acad Sci U S A* 101, 16756-16761.

222. Ivashkina, N., Wolk, B., Lohmann, V., Bartenschlager, R., Blum, H. E., Penin, F., and Moradpour, D. (2002) The hepatitis C virus RNA-dependent RNA polymerase membrane insertion sequence is a transmembrane segment, *J Virol* 76, 13088-13093.

223. Lee, H., Liu, Y., Mejia, E., Paul, A. V., and Wimmer, E. (2006) The C-terminal hydrophobic domain of hepatitis C virus RNA polymerase NS5B can be replaced with a heterologous domain of poliovirus protein 3A, *J Virol* 80, 11343-11354.

224. de Jong, A. S., Melchers, W. J., Glaudemans, D. H., Willems, P. H., and van Kuppeveld, F. J. (2004) Mutational analysis of different regions in the coxsackievirus 2B protein: requirements for homo-multimerization, membrane permeabilization, subcellular localization, and virus replication, *J Biol Chem* 279, 19924-19935.

225. Suhy, D. A., Giddings, T. H., Jr., and Kirkegaard, K. (2000) Remodeling the endoplasmic reticulum by poliovirus infection and by individual viral proteins: an autophagy-like origin for virus-induced vesicles, *J Virol* 74, 8953-8965.

226. Liu, W., Crocker, E., Siminovitch, D. J., and Smith, S. O. (2003) Role of side-chain conformational entropy in transmembrane helix dimerization of glycophorin

A, *Biophys J* 84, 1263-1271.

227. Hudziak, R. M., Lewis, G. D., Shalaby, M. R., Eessalu, T. E., Aggarwal, B. B., Ullrich, A., and Shepard, H. M. (1988) Amplified expression of the HER2/ERBB2 oncogene induces resistance to tumor necrosis factor alpha in NIH 3T3 cells, *Proc Natl Acad Sci U S A* 85, 5102-5106.